CHALMERS

A numerical study on mass displacements from piling in natural clay

JONATAN ISAKSSON

Department of Architecture and Civil Engineering
Division of Geology and Geotechnics
CHALMERS UNIVERSITY OF TECHNOLOGY
Göteborg, Sweden 2022

TECHNICAL REPORT FOR MID-TERM SEMINAR

A numerical study on mass displacements from piling in natural clay

JONATAN ISAKSSON

Department of Architecture and Civil Engineering
Division of Geology and Geotechnics
CHALMERS UNIVERSITY OF TECHNOLOGY

Göteborg, Sweden 2022

A numerical study on mass displacements from piling in natural clay

JONATAN ISAKSSON

Department of Architecture and Civil Engineering
Division of Geology and Geotechnics
Chalmers University of Technology
SE-412 96 Göteborg
Sweden
Telephone: +46 (0)31-772 1000

Chalmers Reproservice
Göteborg, Sweden 2022

A numerical study on mass displacements from piling in natural clay

TECHNICAL REPORT FOR MID-TERM SEMINAR

JONATAN ISAKSSON
Department of Architecture and Civil Engineering
Division of Geology and Geotechnics
Chalmers University of Technology

ABSTRACT

Densification of urban areas is a global trend. Since many of the worlds cities are built on soils with poor engineering properties, *e.g.* soft natural clay, the urban developments increases the demand of efficient deep foundations that are capable of supporting increasingly larger loads. The installation of deep foundations using displacement piles into clay leads to disturbance which need to be quantified to prevent damage on adjacent structures.

This work presents a coupled Eulerian numerical framework for the simulation of pile installation into natural soft clay. Furthermore, an advanced effective stress based constitutive model was implemented. The most important factor governing the magnitude of displaced soil volume is the volume of the installed pile. After installation, dissipation of excess porewater pressures leads to volumetric contraction in the soil. The displacements during this phase are in the reversed direction compared to the initial outward movement during installation. Incorporating the anisotropy and sensitivity of the clay in the analysis leads to increased displacements closer to the pile during penetration and larger reversed displacement trajectories in the subsequent porewater pressure equalisation stage. The overconsolidation ratio, elastic and plastic stiffness properties and the critical state friction angle are shown to be the most influential, both directly after installation and after equalisation of the excess porewater pressures.

The differences between the mass displacements predicted from full vertical penetration and numerical horizontal cavity expansion, show that the far field ($>10R$) displacement pattern are similar, while the displacement path of soil closer to the pile are not fully captured using horizontal cavity expansion. The Shallow Strain Path Method (SSPM) is shown to predict similar deformations as the Finite Element calculations using a failure criterion.

For the investigated normalised penetration rates in natural soft clay the emerging response from the coupled analyses indicated near constant volume conditions. Hence, any simplified method acknowledging this condition will predict displacement in a similar order of magnitude as the advanced method. However, an effective stress based model that captures the response of the natural clay is required if the magnitude of mass displacements during and after the porewater equalisation phase is of interest.

Keywords: Natural soft clay, displacement piles, pile installation, mass displacement, finite element analysis, large deformations.

ACKNOWLEDGEMENTS

The financial support from SBUF (Development fund of the Swedish construction industry, grant 13614), BIG (Better Interaction in Geotechnics), grant A2019-19, from the Swedish Transport Administration, NCC AB and Chalmers University are greatly acknowledged.

MID-TERM REPORT

This report contains the following appended publications:

Paper A J. Isaksson et al. (2022). "Simulation of CPT penetration in sensitive clay". In: *Cone Penetration Testing 2022 (1st ed.)* Ed. by G. Gottardi and L. Tonni. CRC Press, pp. 480–485. DOI: https://doi.org/10.1201/9781003308829

CONTENTS

Abstract i

Acknowledgements i

Mid-term report iii

Contents v

1 Introduction 7
1.1 Background . . . 7
1.2 Aim . . . 8
1.3 Objectives . . . 8
1.4 Limitations . . . 8

2 Pile installation in natural soft clays 9
2.1 Pile cycle . . . 9
2.2 Experimental observations on mass displacements from pile installation - physical model test . . . 12
2.3 Experimental observations on mass displacements from pile installation - field studies 13
2.3.1 Single pile . . . 16
2.3.2 Pile groups . . . 18
2.3.3 Displacement from piling in Gothenburg . . . 21
2.4 Modelling pile installation . . . 21
2.4.1 Cavity Expansion Method . . . 21
2.4.2 Shallow Strain Path Method . . . 22
2.4.3 Finite Element Analysis . . . 25

3 Modelling mass displacement 27
3.1 Eulerian pile penetration . . . 27
3.1.1 Fixed pile . . . 28
3.1.2 Moving pile . . . 29
3.2 Constitutive model . . . 30
3.3 Verification . . . 31
3.4 Modelling method . . . 31
3.4.1 Drainage conditions . . . 33
3.4.2 CPT in natural clay . . . 35
3.5 Experimental design . . . 39

4 Numerical study on mass displacements in natural clay 41
4.1 Reference case . . . 41
4.2 Displacement paths . . . 43
4.3 Inclinometers . . . 43
4.4 Bellowhose . . . 47

4.5 Movement in a horizontal cross section 47
4.6 Key results 47

5 Influence of soil properties on the mass displacement due to piling in natural soft clays 51
5.1 Displacement paths 51
5.2 Inclinometers 51
5.3 Bellowhose 55
5.4 Horizontal cross section 55
5.5 Remaining displacement after consolidation 55
5.6 Displaced soil volume 60
5.7 Sensitivity study - Design of experiments 61
5.8 Key results 63

6 Benchmark methods for predicting mass displacements from piling 65
6.1 Displacement paths 66
6.2 Inclinometers 66
6.3 Bellowhose 66
6.4 Movement in horizontal cross section 70
6.5 Consolidation displacement 70
6.6 Key results 74

7 Conclusions & recommendations 77
7.1 Conclusions 77
7.2 Recommendations for upcoming studies 79

References 79

I Appended Paper A 85

List of Figures

2.1 The pile cycle, different stages in the service life of a pile. Adopted from Randolph and Gouvernec (2011) 10

2.2 Normalised displacement paths due to the installation of a pile with radius R and length equal o $40R$ for targets located at a depth of $19R$. From Lehane and Gill (2004). 14

2.3 Displacements due to the installation of a pile with radius R and length equal to $10R$ into clay. Displacement vectors (a) were used to derive the horizontal (b) and vertical (c) normalised displacements contours due to the pile installation. Negative values indicates an upward movement. From Ni et al. (2010). 15

2.4 Vertical displacements due to pile installation measured at a shallow 0.5 m (a) and a deep2.2 m (b) horizontal cross section. From Cooke et al. (1979). 16

2.5 Normalised heave volume at different depth of pile penetration. The displaced soil volume was calculated from the shallow vertical displacements presented in Figure 2.4 by assuming an axisymmetric displacement field. From Cooke et al. (1979). 17

2.6 Radial displacements due to the installation of a solid pile with a radius R of 305 mm and subsequent dissipation of excess pore pressures. The inclinometers is located at $3R$ (B-4), $4R$ (B-5) and $6.5R$ (B-6) pile radii from pile wall. From Pestana et al. (2002). 18

2.7 Displacements due to the installation of a group of end-bearing solid concrete piles. A total of 116 piles with a radius of 150 mm was driven within an excavated area. From Bozozuk et al. (1978). 20

2.8 Displacement due to the expansion of a cylindrical cavity with an incompressible pile. From Randolph et al. (1979) 22

2.9 Conceptual model of the Shallow Strain Path Methods used to simulate the penetration of a pile into a half space with a stress-free surface. From Sagaseta et al. (1997) 24

3.1 *fixed pile*method. Boundary conditions between the soil and the pile can either be fixed in the normal direction or fully fixed. 28

3.2 Moving pile method. 29

3.3 SCLAY1S yield surface in triaxial stress space. 31

3.4 Vertical reaction force on the CPT tip from simulations using the *fixed pile* method with two different ways of applying BC and the *moving pile* method. 32

3.5 Cone tip resistance from simulations using the *fixed pile* method with two different ways of applying BC and the *moving pile* method. 33

3.6 Normalised cone resistance as function of normalised penetration rate. Comparison between results from this study and Monforte et al. (2021) is included to indicate the effect of interface properties on the CPTu response. From Isaksson et al. (2022). 35

3.7 Normalised excess porewater pressure as function of normalised penetration rate. Comparison between results from this study and Mahmoodzadeh and Randolph (2014) and DeJong and Randolph (2012). Results from Monforte et al. (2021) are included to indicate the effect of interface properties on the CPTu response. From Isaksson et al. (2022). 35
3.8 The effect on CPTu response from changing the consolidation coefficient c_v; overconsolidation ratio OCR; sensitivity S_t and considering fabric anisotropy α in the characterisation chart for CPTu proposed by Robertson (1990). From Isaksson et al. (2022). 37
3.9 The effect on CPTu response from changing the consolidation coefficient c_v; overconsolidation ratio OCR; sensitivity S_t and considering fabric anisotropy α in the characterisation chart for CPTu proposed by Schneider et al. (2008). From Isaksson et al. (2022). 38
4.1 Numerical model used to model pile penetration into Utby Clay. 43
4.2 Displacement paths for shallow (-1R) and deep (-19R) post points due to pile installation and subsequent dissipation of pore pressures at different radial coordinate (1.15, 1.5, 3, 5, 10) R. 44
4.3 Evolving radial displacements from pile installation and subsequent consolidation at four inclinometer locations (vertical cross sections) located at an initial radial coordinate of 3 R, 10 R, 20 R, and 40 R. 46
4.4 Evolving vertical displacement from pile installation and subsequent consolidation at four vertical cross sections located at a radial coordinate of 10R, 20R, 30R, and 40R. 48
4.5 Evolving vertical (a) and horizontal (b) displacements from pile driving and subsequent consolidation in a shallow (-R) horizontal cross section. 49
4.6 Evolving (a) vertical- and (b) radial displacements from pile driving and subsequent consolidation in a deep (-19R) horizontal cross section. 50
5.1 Shallow displacement in the soil at a depth of R, normalised with the pile radius R, after installation and consolidation for an isotropic clay, an anisotropic clay and a sensitive anisotropic clay. 52
5.2 Deep displacement in the soil at a depth of 19R, normalised with the pile radius R, after installation and consolidation for an isotropic clay, an anisotropic clay and a sensitive anisotropic clay. 53
5.3 Radial displacement from pile installation and subsequent consolidation for four inclinometers (vertical cross sections) located at a radial distance of respectively 3R, 10R, 20R, and 40R from the pile for an isotropic clay, an anisotropic clay and a sensitive anisotropic clay. 54
5.4 Vertical displacement from pile driving and subsequent consolidation in four vertical cross sections located at a radial coordinate of 3R, 10R, 20R, and 40R for an isotropic clay, an anisotropic clay and a sensitive anisotropic clay. 56
5.5 Evolving vertical (a) and horizontal (b) displacements from pile driving and subsequent consolidation in a shallow (-R) horizontal cross section. 57
5.6 Evolving vertical (a) and horizontal (b) displacements from pile driving and subsequent consolidation in a deep (-19R) horizontal cross section. 58

5.7 Remaining radial and vertical displacement after consolidation in vertical cross sections. Displacement after consolidation is normalised with the displacement after installation 59
5.8 Relative effect of parameters on the mass displacement from piling in an anisotropic sensitive clay. 63
5.9 Relative effect of parameters on the mass displacement from piling in an anisotropic sensitive clay. 64
6.1 Comparision of displacement paths for shallow soil at depth $1R$ below the surface, after installation (light) and consolidation (dark) for a sensitive anisotropic clay using vertical penetration (v) and horizontal expansion (h) compared to SSPM and CEM. 67
6.2 Comparision of displacement paths for deep soil at depth $19R$ below the surface, after installation (dark) and consolidation (light) for a sensitive anisotropic clay using vertical penetration (v) and horizontal expansion (h) compared to SSPM and CEM. 68
6.3 Comparision of horizontal displacement from pile installation for four vertical cross sections located at a radial coordinate of $3R$, $10R$, $20R$, and $40R$ for a sensitive anisotropic clay (St aniso) for vertical penetration (V) and horizontal expansion (H). Results from a linear elastic (LE H) and a linear elastic perfectly plastic analysis (MC H) as well as CEM and SSPM. 69
6.4 Comparison of vertical displacements from pile installation for four vertical cross sections located at a radial coordinate of $3R$, $10R$, $20R$, and $40R$ for a sensitive anisotropic clay (St aniso) for vertical penetration (V) and horizontal expansion (H). Results from a linear elastic (LE H) and a linear elastic perfectly plastic analysis (MC H) as well as the CEM and SSPM method are included. 71
6.5 Comparision of evolving vertical (a) and horizontal (b) displacements from pile installation and subsequent consolidation in a shallow ($-R$) horizontal cross section. 72
6.6 Evolving vertical (a) and horizontal (b) displacements from pile installation and subsequent consolidation in a deep ($-19R$) horizontal cross section. 73
6.7 Comparison of vertical displacement from pile installation four vertical cross sections located at a radial coordinate of $3R$, $10R$, $20R$, and $40R$ for a sensitive anisotropic clay (St aniso) for vertical penetration (V) and horizontal expansion (H). 74
6.8 Comparison of vertical displacement from pile installation four vertical cross sections located at a radial coordinate of $3R$, $10R$, $20R$, and $40R$ for a sensitive anisotropic clay (St aniso) for vertical penetration (V) and horizontal expansion (H). 75
6.9 Remaining displacement after consolidation for vertical cross sections. Displacement after consolidation is normalised with the displacement after installation for radial displacement (a) and vertical displacement (b). 76

List of Tables

3.1 Simulated conefactor for different values for the rigidity index Ir compared to the range from literature (Liyanapathirana 2009). 33
3.2 Model parameters used to investigate the effect of drainage conditions on the CPTu response. 34
3.3 Parameters used for investigation of the CPTu response in soft clays. 36
4.1 Soil characteristics of the Utby clay: wet density ρ, water content at plastic limit w_p, at liquid limit w_L, plasticity index PI sensitivity S_t and shear strength form fall cone test τ_{fu}. 42
4.2 Model parameters used for the coupled simulation of pile installation into the Utby clay using the SCLAY1S model. 45
5.1 Normalised radial coordinate of where the soil volume passing through a shallow vertical cross section, at depth R, corresponds to 25% and 50% of the total installed pile volume. The total volume of soil that is displaced through the shallow vertical cross section after installation $V_{s,i}$ and consolidation $V_{s,c}$ is also included. Both volumes are normalised with the total pile volume below the cross section V_{pile}. . 60
5.2 Total soil volume displaced through a series of inclinometeres (vertical cross sections). Volumes are normalised with the total installed pile volume, V_{pile}. The results are for each cross section presented both after installation (I) and after consolidation (C). 61
5.3 Range of parameters used in the two level fractional factorial sensitivity analysis for the modelling of pile installation into a sensitive anisotropic clay. 61
5.4 Table of contrast presenting the combination of parameters used for the 16 analyses needed for the two level fractional factorial experimental design 2^{8-4}_{IV} sensitivity analysis. 62
6.1 Overview of different modelling methods to predict the mass- displacements from pile installation into soft clay. 65

1 Introduction

1.1 Background

Population growth is driving more efficient use of the available space in urban areas around the world, inspiring the Civil Engineering community to meet increasing demands on larger building sizes and loads, the utilisation of underground space and the development of residential and commercial areas on less competent ground, in terms of engineering properties. A typical example of this process is the city of Gothenburg in the southwestern part of Sweden, where recent developments that include but are not limited to, the construction of a underground railway tunnel crosses both rock and soft sensitive clay deposits, as well as extensive developments along the Göta Riverbank including a new bridge and the construction of the soon to be tallest building in Sweden (Göteborgs Stad 2022). A major part of the city development is performed on deep deposits of soft sensitive clay leading to the need of extensive deep foundations for practically every new Civil Engineering project. In this solution piles are transferring structural loads from the structure on the surface down to more competent underlying soil or bedrock. Long and slender displacement piles made out of concrete are the most commonly used pile type in the region (Pålkommisionen 2022), due to the low cost and ease of installation in the clay deposits. The downside of the ubiquitous use of displacement piles in urban areas is the impact on the surroundings, *i.e.* problems with the foundations of existing nearby buildings might arise.

Displacement piles are installed in the ground by penetrating the pile from surface level downwards by applying a static (jacked) or dynamic (driven) load on the pile head. As the pile length embedded in the soil gradually increases, the soil needs to accommodate the extra volume of the pile. From a kinematics point of view, to accompany the introduced pile volume, the soil undergoes a combination of displacements (translation, rotation) and deformation (strain). In addition to the mechanical properties of the soil, the presence of groundwater in the pore space enclosed by the grains, and the drainage conditions is controlling this process. Commonly, soils with low hydraulic conductivity k, *e.g.* natural soft clays with $k = 1 \times 10^{-10}\,\mathrm{m\,s^{-1}}$ to $1 \times 10^{-8}\,\mathrm{m\,s^{-1}}$, exhibit an undrained response under constant volume during fast loading, due to the fact that groundwater is trapped inside the pore spaces of the soil hence preventing any volumetric deformation to occur in the soil. As a result, additional porewater pressures are generated, *i.e.* the increment in total stress from pile penetration is transferred to the porewater. The total stress increment is (almost) directly transferred to the solid grains (increment of effective stress), in case the loading period (rate) is relatively long (small) compared to the time required to dissipate any excess porewater pressures. The increment of effective stress governs the magnitude of deformations, either directly during penetration, *i.e.* in sand that has a large hydraulic conductivity, or in the equalisation period after pile installation (pile setup in clay). The relation between the loading rate, hydro-mechanical properties of the soil and drainage length in the soil deposit, is governing the combined response of deformation and (mass) displacement due to installation of displacement piles.

The ability to predict the magnitude and extent of mass displacements and disturbance from piling activities is essential for avoiding and/or mitigating potential damage to existing structures near the piling works and help prevent delays in production due to measurements of (un)expected excessive movement. The latter is an increasing issue with construction activities in an urban

environment. A number of numerical approaches for piling induced displacement and disturbance have been developed, ranging from pure empirical relations to advanced numerical analysis. Each method is based on a different set of assumptions and simplifications, as well as considering different aspects of the actual processes observed in the field.

1.2 Aim

This study aims to investigate the opportunities and limitations of different numerical approaches for modelling the disturbance and mass displacement from piling in natural (sensitive) clay. An advanced numerical model will be utilised to complement experimental evidence, in absence of a complete and consistent dataset on mass displacement from sites around Gothenburg. Consequently, the primary focus will be on investigating the governing processes in the soil that influence the magnitude and extent of mass displacement.

1.3 Objectives

- Develop a reference model. A numerical framework for large deformations with a coupled soil and groundwater formulation will be used together with advanced effective stress based constitutive models for natural soft clay.
- Identify the most important factors in the soil that governs the mass displacement from piling at the time of installation and after consolidation.
- Benchmark commonly used methods for the assessment of mass displacement from the installation of a pile in clay.

1.4 Limitations

This study focuses on the mass displacements in the soil, natural soft clay, due to the installation of a displacement pile. Although the impact of the effective stress and pore pressures is included in the numerical model the results will not be discussed in detail.

2 Pile installation in natural soft clays

A pile is a long slender object installed into the soil with the purpose to transfer loads from the superstructure to soil layers at larger depths that have superior engineering properties, *i.e.* strength and stiffness. Loads are commonly applied on the pile head and transferred downwards along the pile. The resistance of a pile arises from shaft friction along the perimeter of the pile and resistance at the pile base. Starting from the first prehistoric short wooden piles installed along riverbanks to support simple houses, piles are nowadays found in a variety of materials, sizes and shapes. The pile type of interest in this research is the displacement pile that is prefabricated in a factory before being brought to the site to be installed. In soft soils the displacements piles typically are driven into the ground.

2.1 Pile cycle

A complex system of interaction between the pile and the supporting soil is created during pile installation, and is active as long as the pile is embedded in the soil. Randolph and Gouvernec (2011) propose a separation of the analysis of piling and pile capacity into a number of stages. Each of the stages can then be investigated separately to facilitate an increased understanding of the system within a rational framework.

Figure 2.1 presents the four stages that together form the pile cycle. Although the division allows for the stages to be investigated separately, a strong dependency on the previous stages is present. The *in-situ* stage focuses on the soil at the site prior to the installation of the pile. The *installation* of the pile will affect the stress distribution in the soil surrounding the pile, leading to a new stress state in the soil. The new total stress state in the soil after pile installation is a combination of the effective stresses in the soil and a change in the porewater pressure. During the *equalisation* stage the excess porewater pressures are dissipating, and a number of intermediate stress states are found until a new equilibrium, where all excess porewater pressures from installation are dissipated, is reached. The final stage is the *loading* of the pile, where the working load is applied to the pile head and transferred to the soil surrounding the pile. The following Sections will elaborate the pile cycle, focusing on the installation, and subsequent dissipation of porewater pressures generated during installation of a displacement pile into a natural soft clay. A large number of studies have been conducted on the effect of pile installation in natural soft clay and is summarised by for example Jardine and Potts (1988), Pestana et al. (2002) and Karlsrud (2012).

Installation

The installation of a displacement pile into a natural soft clay will lead to displacements in the soil to facilitate the advancing pile. Due to these (non-uniform) displacements, the soil is distorted and the state and stresses in the soil changed, *i.e.* the soil is disturbed. As the pile behaviour is mostly governed by the soil response in the vicinity of the pile, this new disturbed state needs to be incorporated in the following stages in the pile cycle.

Karlsrud (2012) presents results from a field test in Lierstranda where the overconsolidation ratio (OCR) of the soft clay is decreasing from 2.3 at the top to about 1.15 in the bottom of the deposit. The ratio of excess porewater pressures over vertical effective stress $\Delta u/\sigma'_{v0}$ was shown

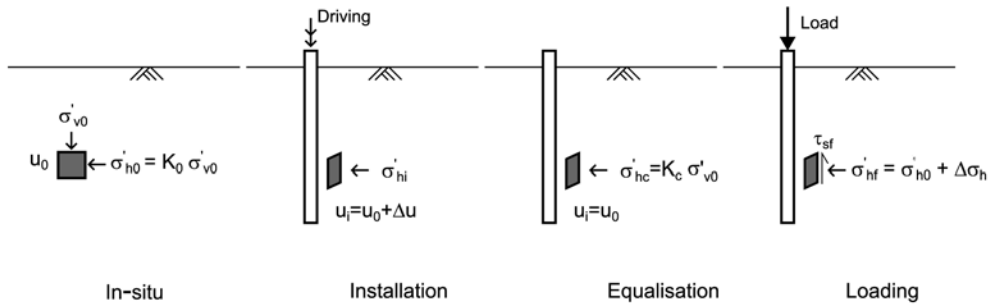

Figure 2.1: *The pile cycle, different stages in the service life of a pile. Adopted from Randolph and Gouvernec (2011)*

to decrease from the top the bottom of the deposit following the change in OCR. A ratio $\Delta u/\sigma'_{v0}$ of 2.0-2.4 is found by Azzouz and Morrison (1981) in a deep deposit of Boston blue clay (BBC) with an OCR of 1.2. In addition, the tests indicates that the increase in the horizontal total stress acting on the pile is totally attributed to the increase in the porewater pressure. The radial effective stress after installation was even found to decrease compared to the in-situ value in the soil. Roy et al. (1981) measured the emerging porewater pressures from pile iinstallation in addition to the measurements on the pile shaft. The ratio $\Delta u/\sigma'_{v0}$ decreased from around 2.25 at the pile shaft to about 0.93 $4D$ away from the pile and 0.3 at a distance of $8D$ from the pile. In situ vane tests were also conducted at the site, and showed a reduced shear strength very close to the pile, corresponding to about 60-75% of the in-situ tests results. At a distance of about $3D$, the measured shear strength, measured with the field vane test, was similar before and immediately after the installation of the pile. Massarsch (1976) and Bozozuk et al. (1978) report a similar decrease of undrained shear strength of respectively 15-30% and 15-50% immediately after pile driving in clay.

Lehane and Jardine (1994) presents the results from pile tests conducted at three different sites with an OCR of 1.5 in Bothkennar, 6 in Cowden and 30 in London, highlighting the difference in behaviour for different OCR of the natural clay. Due to the large OCR, both the Cowden clay and the London clay will dilate when loaded. Hence, on those sites a decrease in the porewater pressures during installation was measured in the clay near the pile tip. When the penetration was stopped, the porewater pressures quickly rose indicating that the porewater pressures slightly away from the pile shaft increased and were equalising towards the pile. In contrast, the only slightly overconsolidated Bothkennar clay showed a positive increase in porewater pressure at all times during the installation of the pile. The Bothkennar test results are supporting the findings of previous studies in clays with a low OCR that the radial effective stress is decreasing due to the pile installation. In contrast, an increase in the radial effective stress was measured in the London and Cowden again showing the impact of the dilatant behaviour.

Equalisation

The equalisation of the excess porewater pressures in the soil is the main driver in the set-up stage of the pile cycle. As the excess porewater pressures are present along the full length of the pile, the main direction of the equalising flow will be in the radial direction of the pile. The measurements of the porewater pressures in the soil at different radial distances from the pile by Roy et al. (1981), show that an initial increase in porewater pressure is occurring at some distance from the pile, supporting that the porewater pressures are mainly equalising in the radial direction. The large difference found between the excess porewater pressures close to the pile and further away from the pile immediately after pile driving is decreasing with time. During that stage the effective stress increases and deformations in the soil occur. The vane shear strength measured in the soil after full equalisation of the pore pressures show a similar strength as before pile installation, indicating that the strength reduction immediately after installation is limited and the strength is regained during the consolidation stage, which is also supported by the findings of Bozozuk et al. (1978).

Hunt et al. (2000) presented laboratory tests on clay samples extracted from the same site before and after the installation of a pile. The index tests related to the density and water content of the soil indicate that the soil sample, extracted after pile installation, has a higher density and a lower water content compared to the soil samples taken before pile installation, indicating a contraction due to the pile installation and subsequent dissipation of excess porewater pressures. Undrained triaxial tests sheared in compression were also performed, and these showed a small increase in the undrained shear strength for post pile samples. However, the ductility of the soil had increased dramatically, and the axial strain associated with the maximum shear stress increased from 1-3 % in the pre-pile samples to about 8-9 % in the post pile samples. The results from CRS tests showed that the the post pile samples have a much more gradual transition, when moving from a overconsolidated stress state to a normally consolidated stress state, indicating a reduction of the importance of stress history, *i.e.* no clearly discernable pre-consolidation pressure, due to remoulding of the soil during installation.

Karlsrud (2012) extracted a block sample extending from the pile shaft to a distance of about $5D$. The shear strain of the soil was derived form the distorted layering of the clay, and exceeded 100% close to the pile and was approaching zero at a distance of $1D$ from the pile. Within a zone extending about $0.1D$ from the pile wall, the original structure of the soil is impossible to detect. The water content in the clay close to the shaft was 16-17% lower than in the surrounding soil indicating a compression of the soil after the consolidation of the excess porewater pressures. At a distance of about $1D$, the water content in the soil was approaching the water content in the surrounding soil. Fall cone tests conducted on the block samples showed a very high shear strength in the soil very close to the shaft, while the undrained strength at an intermediate distance of about $1/3D$ was somewhat lower than the in-situ undrained shear strength.

Lehane and Jardine (1994) presented the reduction of the radial total stress after installation due to consolidation in the Bothkennar clay, Coweden till and London clay. The reduction was largest in the Bothkennar clay with low OCR, and the final total radial stress only corresponded to about 45% of the value immediately after consolidation. The two other sites showed a similar reduction to about 80% of the stress immediately after consolidation. Radial effective stresses were reported to increase from a low value found in both clays a few minutes after pile installation, corresponding to about 45 % of the value after full equalisation. However the London clay showed a reduction of effective radial stress after installation compared to the value after equalisation. The

ratio of the effective radial stress at the pile shaft to the in-situ vertical effective stress $\sigma'_{hc}/\sigma'_{v0}$ is shown to increase by OCR from about 1.2 ($OCR = 1.5$) in Bothkennar to 4 (OCR 6) at Cowden to 12 (OCR 12) in London. Karlsrud (2012) found a range in the $\sigma'_{hc}/\sigma'_{v0}$ between 0.2 and 1.3, and an increase in the ratio with an increase in the plasticity index of the clay.

Pile loading

The loading stage of a pile starts after the equalisation phase, when sufficient strength is recovered Randolph and Gouvernec (2011). The loading in the pile induces a relative displacement between the soil and the pile shaft. As this displacement occurs, a shear stress $\tau_{sf} = \sigma'_{hf} tan(\delta)$ mobilises between the soil and the pile. The magnitude of the shear stress depends on the horizontal effective stress at the pile shaft σ'_{hf}, after equalisation, and the interface friction angle δ between the soil and the clay. This shear stress will act in the opposite direction from the movement, and will result in shear strains in the soil that reduce with increasing distance from the pile-soil interface.

A displacement typically around 0.5-1% of the pile diameter is required to mobilise the full interface friction, followed by a reduction of the interface friction due to continuous straining in between the soil and the pile. Due to the axial compression of a loaded pile, *i.e.* elastic shortening of the pile, the shear strains on the pile - soil interface will be non-uniform. The shear strain will be larger closer to the applied load at the pile head, resulting in shear stress beyond the peak strength, whereas towards the pile base smaller shear strain, hence shear stress below the peak strength, are mobilised. A stress rotation will also occur when the shear stress is mobilised leading to a horizontal stress at failure σ'_{hf} different than the horizontal stress after consolidation σ'_{hc}.

The stress at the pile-soil interface at failure is often related to the undrained shear strength using a total stress approach by $\tau_{sf} = \alpha s_u$ or the in-situ vertical effective stress by $\tau_{sf} = \beta \sigma'_{v0}$. These two approaches allow for a simplified estimation of the shear stress at the interface. Both of these approaches are simplifications of the reality, where the combined effect of stress change and disturbance due to installation and loading is combined into the α and β, respectively.

2.2 Experimental observations on mass displacements from pile installation - physical model test

Lehane and Gill (2004) performed a laboratory study where a pile was installed in an artificial transparent clay like soil under undrained conditions, while tracking the displacements. The pile radius in the experiment was equal to R = 6.35 mm and the displacements was tracked by embedding black beads with a radius of 1 mm). A series of targets were placed at a vertical distance equal to about $18R$ from the surface corresponding to about half the final pile penetration depth.

The resulting displacements normalised with R for the targets are presented in Figure 2.2. The ratio h/R denotes the normalised vertical distance from the pile head to the target where a negative value indicate that the pile head is above the target. Targets at all locations show a radial displacement away from the pile, and the displacement is decreasing with the initial distance from the pile. All targets show an initial vertical downward movement. When the penetration continued passing the vertical location of the target, an upward movement larger in magnitude than the initial downward movement is found for soil at a distance from the pile. The additional movement due to continuous pile penetration deeper than h/r = 5 below the measurement position is limited.

In contrast, the upward movement for targets close to the pile is smaller in magnitude than the downward movement. The final normalised displacement profile was also compared to the results from two other lab tests reported in the literature (Francescon 1983; Gue 1984) and one field test (Cooke et al. 1979) where all of the tests showed good agreement.

Ni et al. (2010) present the results from a laboratory test on the pile installation in a artificial material similar to many natural clays, although the strength is higher and stiffer in the artificial material. The movement within the soil was recorded using particle image velocimetry (PIV), and the resulting displacement vectors are presented in Figure 2.3. The distance from the pile to the edge of the container was about $12.5R$. The displacement vectors are used to derive the normalised horizontal and vertical displacement contours included in the picture. By investigating the heave at the surface and relating this to the installed pile volume, a volumetric reduction of the soil was found to be about 0.3 - 0.4%, *i.e.* practically constant volume displacement. A comparison was conducted with the vertical displacement contours presented by Lehane and Gill (2004) and the two studies show good agreement.

Massarsch (1976) conducted a laboratory test where 20 model piles were installed in a artificial clay in a 4x5 pattern with a distance of about 6 pile diameter between the individual piles with the edges of the box within 2 pile diameters from the nearest pile. By tracking of the vertical and horizontal deformations of the targets located at the surface of the soil, a displacement for the surface was recorded. The measured heaved soil volume is corresponding to the installed pile volume, indicating an undrained response in the clay. The measured radial displacements of previously installed piles are following the displacements of the surrounding soil and the previously installed piles are considered to have a negligible effect on the horizontal deformation pattern. A subsequent experiment was conducted when soil was extracted in the place of the piles. The measured soil heave together with the extracted soil volume corresponded well to the installed pile volume. The horizontal displacements were also reported to scale accordingly to the extracted volume.

2.3 Experimental observations on mass displacements from pile installation - field studies

The displacements due to pile installation have also been studied in field conditions. In contrast to the laboratory studies where the full displacement field can be monitored, the field studies are limited to the measurements of displacement in a few instrumented locations. The displacement is often tracked by the tracking of movement in measurement locations at the surface of the soil during the installation of the piles. In addition to the measurement on the surface, inclinometers and bellow-hoses have been frequently used to track the horizontal and vertical movements, respectively, towards the depth in a soil deposit due to the installation of multiple piles in clay.

First, the displacements measured in two field tests due to the installation of a single pile will be presented. Secondly, the total effect of the installation of pile groups will be described based on a number of reported studies. Lastly, a short summary of some published results of mass displacement due to pile installation in the Gothenburg region will be conducted.

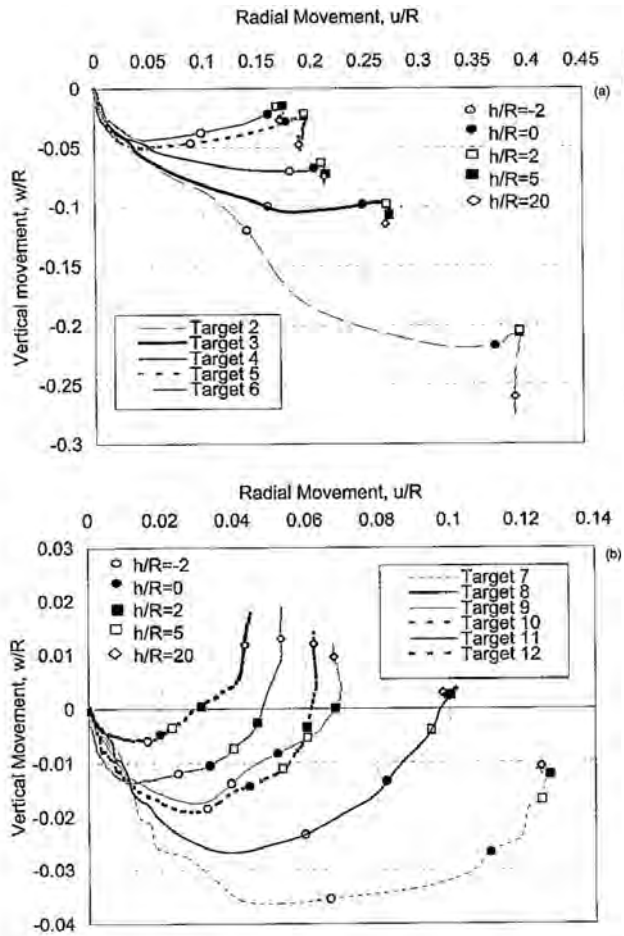

Target	r/R
1	0.77
2	1.17
3	1.58
4	1.84
5	1.99
6	2.24
7	3.25
8	4.65
9	6.73
10	7.41
11	8.94
12	11.39

Figure 2.2: *Normalised displacement paths due to the installation of a pile with radius* ***R*** *and length equal o* ***40R*** *for targets located at a depth of* ***19R****. From Lehane and Gill (2004).*

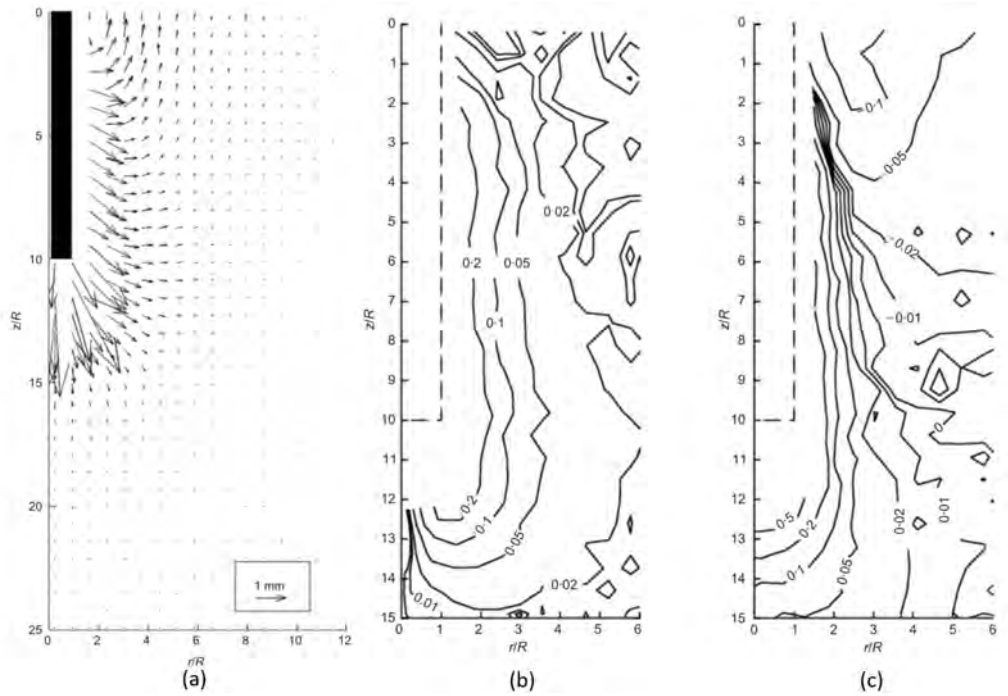

Figure 2.3: *Displacements due to the installation of a pile with radius* ***R*** *and length equal to* ***10R*** *into clay. Displacement vectors (a) were used to derive the horizontal (b) and vertical (c) normalised displacements contours due to the pile installation. Negative values indicates an upward movement. From Ni et al. (2010).*

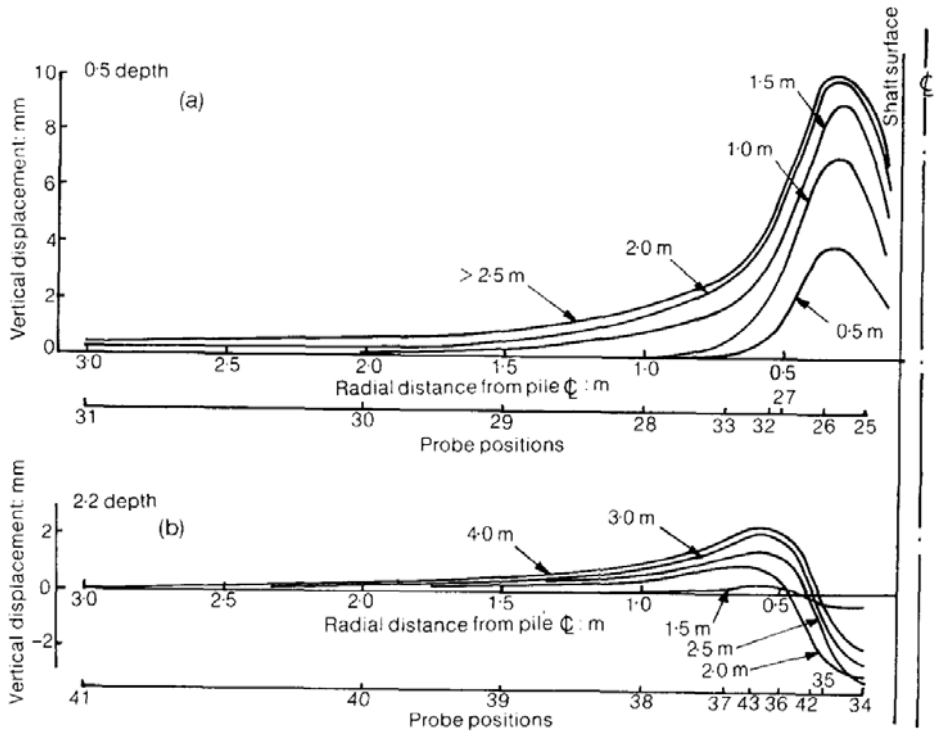

Figure 2.4: *Vertical displacements due to pile installation measured at a shallow* 0.5 m *(a) and a deep*2.2 m *(b) horizontal cross section. From Cooke et al. (1979).*

2.3.1 Single pile

The number of field tests conducted focusing on the displacements from the installation of a single pile into clay are limited. Two cases will be presented where the first was performed in London on the vertical displacements from pile installation as part of a wider study by Cooke et al. (1979) on the load displacement behaviour due to pile loading. The second case focuses on the radial displacements due to installation of a pile and subsequent consolidation of the pore pressures in San Francisco by Pestana et al. (2002).

Vertical displacement

The vertical displacements measured by Cooke et al. (1979) due to the installation of a cylindrical 5 m long pile with a radius R of 89 mm is presented in Figure 2.4 for two depths 0.5 m and 2.2 m, corresponding to a shallow depth equal to $7R$ and at a deeper location of $31R$.

A cross section is created from the measurement of vertical displacements at 9 discrete locations for each depth extending up to approximately 3 m or about $33R$ from the pile. First, it is obvious that the deformation pattern is different between the deep and the shallow locations, indicating an influence of the stress free surface of the soil deposit for more shallow soil. The soil at all shallow locations is experiencing an upward movement due to the installation of the pile. In contrast, the

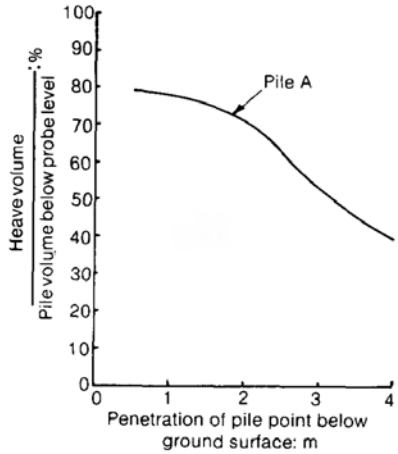

Figure 2.5: *Normalised heave volume at different depth of pile penetration. The displaced soil volume was calculated from the shallow vertical displacements presented in Figure 2.4 by assuming an axisymmetric displacement field. From Cooke et al. (1979).*

deeper soil close to the pile is experiencing a net downward movement, while the soil further away is showing an upward displacement also for the deeper lying soil. No additional vertical displacements were measured in either of the positions once the pile reached about 2 m below the position of the cross section. The magnitude of the displacements is decreasing non-linearly with the increased distance from the pile. The volume under the curves presented in Figure Cooke et al. (1979) is calculated considering axisymmetry, and thereafter normalised with the pile volume below the level of the probes at different penetration depths. The normalised heaved volume is presented in Figure 2.5 and is decreasing with the continuous penetration of the pile. This indicates that an considerable amount of the soil movement is occurring further away from the pile than the probe at a distance of 3 m from the pile. At the moment when the pile is being penetrated down to 3 m, the extent of the measurements is equal to the penetration depth and the normalised volume passing the cross section corresponds to 55% of the pile volume below the measurement position. Assuming a constant volume displacement of the soil due to the pile installation this indicate that 45% of the soil is displaced further away than a horizontal distance corresponding to one pile length away from the installed pile. Although the measured displacements at distance from the pile are very small, the corresponding soil volume in the axisymmetric calculation is considerable.

Horizontal displacement

Pestana et al. (2002) presents the horizontal displacements measured in three inclinometers after the installation of a cylindrical pile in clay with a radius of 0.305 m. The pile was pre-drilled through a fill layer of about 4 m before being driven into the clay referred to as Young Bay Mud. The displacements were measured by three inclinometers located at a distance corresponding to a mean distance over the full depth of the inclinometes of 3 (B-4), 4 (B-5) and 6.5 (B-6) pile radii from the installed pile wall. The radial displacements of the clay are increasing from the fill

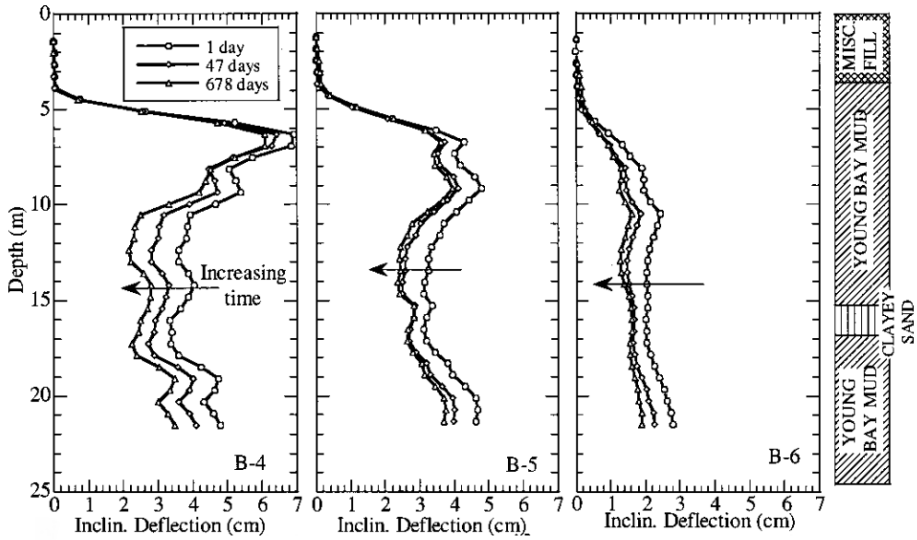

Figure 2.6: *Radial displacements due to the installation of a solid pile with a radius* R *of* 305 mm *and subsequent dissipation of excess pore pressures. The inclinometers is located at* $3R$ *(B-4),* $4R$ *(B-5) and* $6.5R$ *(B-6) pile radii from pile wall. From Pestana et al. (2002).*

layer for about 3 m corresponding to about 10 pile radii indicating a surface effect at the interface between clay and fill. The study focused on the link between the build up and dissipation of excess pore pressures and the corresponding deformations in the clay.

Horizontal displacements immediately after installation at an intermediate stage during the consolidation, and finally after the full dissipation of pore pressures had occurred, are presented in Figure 2.6. The outward radial displacement is largest immediately after pile installation and is decreasing with the increased radial distance from the pile. Due to the subsequent consolidation process, the initial radial outward displacement direction is reversed and the inclinometers show a movement towards the pile. The remaining deformation after consolidation corresponds to between 80% and 60% of the displacements immediately after consolidation, where the ratio of remaining deformations tend to decrease with the distance from the pile.

2.3.2 Pile groups

Displacements piles in natural clays are most often installed in groups and the accumulated mass displacement from multiple piles is therefore of a particular interest for engineers. A large number of case studies have been reported in the literature, while numerous unpublished measurements have been conducted as part of regular monitoring programmes during piling projects. First, the mass displacements from one specific pile group will be introduced followed by a discussion on various factors that might influence the resulting mass displacement from pile installation in natural clays.

The mass displacements due to the installation of 116 end bearing solid concrete piles with an (equivalent) radius of 150 mm is reported by Bozozuk et al. (1978). Initially, an excavation of

2.44 m was conducted before the piling operations started. Vertical and horizontal displacements were measured using bellow-hoses and inclinometers, respectively, and are presented in Figure 2.7. Both the vertical and horizontal displacements are found to be largest at the surface and decreasing with depth. With an increase in the distance from the pile group, the displacements are decreasing with a similar rate as for the single pile measurements shown in for example Figure 2.2.

Hagerty and Peck (1971) summarise conclusions from comparing the mass displacements due to the installation of pile groups from thirteen locations into various types of clay. Both sensitive and nonsensitive clays were included in the study. Generally, the study shows that the mass displacements from pile installation into clay is a process under constant volume conditions, as the installed pile volume corresponds well to the displaced soil volume which is also supported by Bozozuk et al. (1978), Massarsch (1976), Dugan and Freed (1984), Cooke et al. (1979), and Edstam (2011). However, the presence of sensitivity in the soil was shown to alter the pattern of mass displacement, with a tendency to give smaller displacement outside the pile group. The reason behind this is explained by a mechanism where the disturbed clay close to the pile appeared to be extruded along the shaft. In addition, the partial consolidation during the duration of the pile driving operations of the very soft remoulded clay reduced the magnitude of outward displacements. The study also shows that the presence of thin permeable and contractive layers in a clay deposit strongly decrease the measured heave at the site.

Dugan and Freed (1984) presents the conclusion from the measurements of nine case histories where pile groups were driven into the same soil deposit in the area of Boston and Cambridge, Massachusetts. As the soil conditions are similar at the studied sites, a homogeneous deep clay layer with piles driven into a underlying glacial till, the study focused on other possible factors influencing the displacement pattern. The study concluded that the vertical stress distribution in the soil surrounding the piling operations is influencing the pattern of mass displacement. Piling within an excavation leads to increased heave within the excavated area, and lower heave outside the excavation compared to piling conducted in an area with a level surface. Additionally, the heave measured in stationary buildings is significantly smaller than the measurements of the soil heave at the surface at neighbouring locations (green field conditions). The influence of the vertical stress on the displacement is also evident in sloping ground conditions, where the lateral displacements is larger towards the downward direction of the slope (Vytiniotis et al. 2018; Massarsch and Wersäll 2013). The case histories from Boston (Dugan and Freed 1984) also showed a considerable downward movement after the pile installation was ceased, which is attributed to the compression of the clay due to the dissipation of excess porewater pressures. The downward movement due to consolidation was similar, or even greater in magnitude as the initial heave from pile installation, and the authors suggest that the net movement due to pile installation can be approximated as zero.

Massarsch (1976) found similar trends for both the horizontal and vertical consolidation movement due to the installation a group of wooden piles to support a road embankment in Ursvik, close to Stockholm in Sweden. The piles were driven through a layer of clay into a supporting till layer. The initial deformations were outward (inclinometer) and upward (bellow-hose) away from the piling area. The build up of excess pore pressures due to the installation of the piles was also monitored. As the piling driving ceased, the movement in both vertical and horizontal directions was reversed, and a movement towards the pile group was monitored. After two years, the measured net vertical and horizontal deformation from piling and subsequent consolidation was shown to be approximately zero. However, the deformations from the pile penetrating till layers below was influencing the deformations for the Ursvik and Boston case studies.

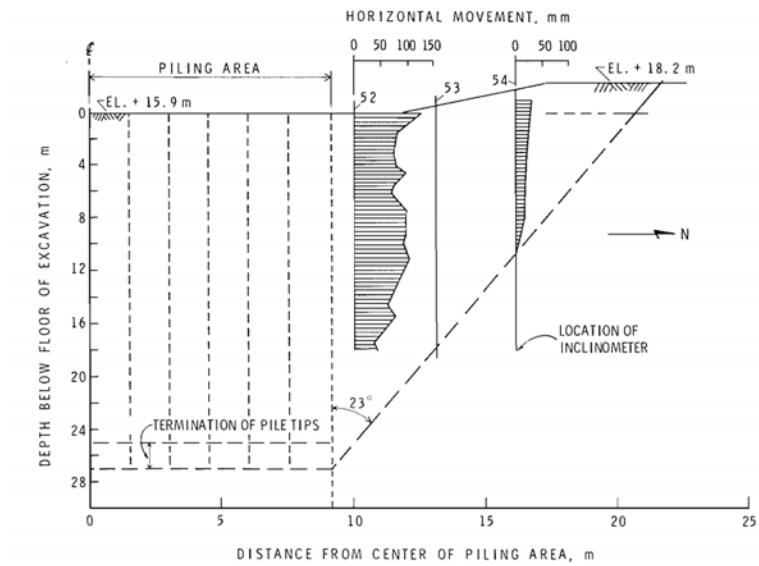

(a) *Horizontal displacement*

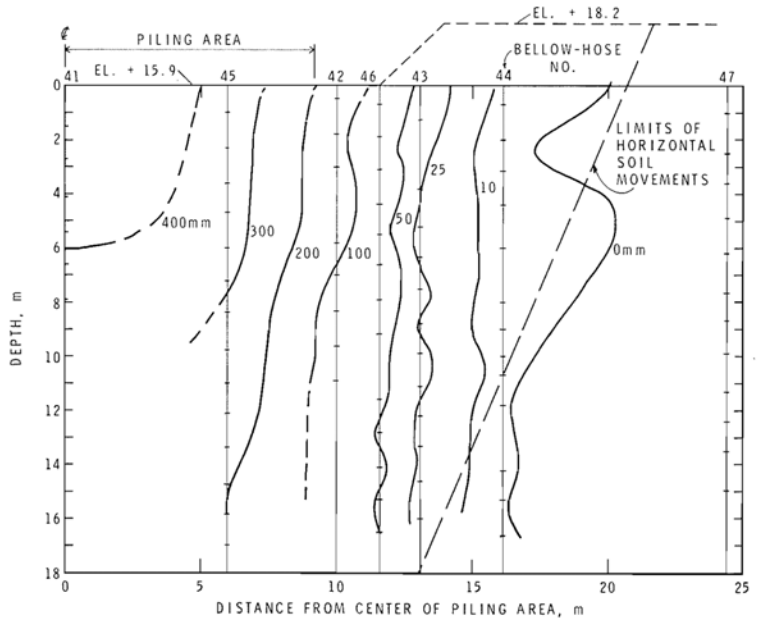

(b) *Vertical displacement*

Figure 2.7: *Displacements due to the installation of a group of end-bearing solid concrete piles. A total of 116 piles with a radius of* 150 mm *was driven within an excavated area. From Bozozuk et al. (1978).*

2.3.3 Displacement from piling in Gothenburg

This Section will present a few case studies on the mass displacement due to the installation of pile groups in Gothenburg, on the west coast of Sweden. Edstam (2011) presents measurements of the mass displacement due to the installation of a floating pile group in a deep clay deposit in Gothenburg, Sweden. The measurement was performed using multiple bellow-hose and inclinometer measurements in addition to the monitoring of surface points. The resulting mass displacement was shown to correspond well to the installed pile volume. The resulting direction of displacement was shown to be outwards and upwards from the pile. Both the vertical and horizontal displacement is shown to linearly decrease with depth, from the maximum value found close to the surface of the soil. The vertical displacements at the surface was shown to decrease with a factor just over two when the distance from the pile group is doubled. Considerable movement was detected at distances further than one pile length from the pile group.

Massarsch (1976) studied the displacement due to the installation of a large pile group in Bäckebol in Gothenburg, Sweden. The installation of the piles was performed in an excavated area. The excavation depth was not uniform within the area and measurements of the surface heave due to pile installation was shown to increase with the increased depth of excavation in an area. In addition, the evolution of vertical movement was measured with a bellow-hose for about 2 years after the installation of the piles. The initial vertical upwards movement was reversed during the consolidation time, and the net upward movement after 2 years corresponds to about half of the initial maximum upward movement.

Hall et al. (2020) present the measurements conducted due to the installation of two adjacent pile groups into clay, with an existing building in between the two piling sites. The study shows that the net horizontal displacement of the existing building was small due to the fact that piling was made simultaneously on the two sides of the building with equal magnitude of displacement but in opposite directions. In addition, the measurements show that the driving of piles into frictional layer underlying the clay lead to a reversed movement compared to the installation for both the radial and vertical movement due to the compaction of the frictional layer. A number of construction projects involving piling have been conducted close to an old steel bridge in the central part of Gothenburg (Trafikkontoret 2021). Measurements of the movement in the vicinity of and at the bridge due to these piling activities were monitored. The report emphasises that the problem of mass displacements due to piling is a problem reaching beyond the physical limits of each individual project, and that the combined effect should be analysed.

2.4 Modelling pile installation

2.4.1 Cavity Expansion Method

A wide range of practical problems can be modelled as a expanding or contracting spherical or cylindrical cavity in a solid material. The first use of the method in solid mechanics looked at metal indentation problems of a conical punch into copper (Bishop et al. 1945). By combining the expansion of a cavity with the constitutive response and boundary conditions of the containing solid, a set of equilibrium equations is formulated.

Yu (2000) summarised the history of the Cavity Expansion Method (CEM) in Geotechnics. The method has been applied to analyse problems such as the modelling of tunnelling, piling,

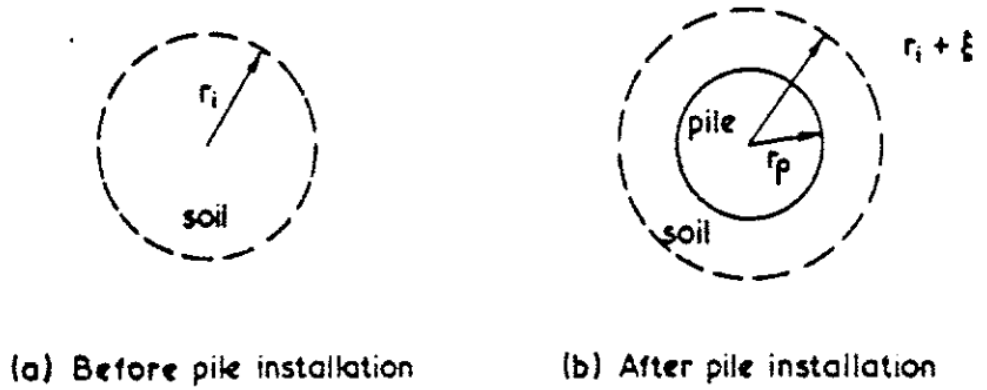

Figure 2.8: *Displacement due to the expansion of a cylindrical cavity with an incompressible pile. From Randolph et al. (1979)*

wellbore stability as well as the theoretical modelling of in-situ tests, such as pressuremeters and penetrometers. Randolph et al. (1979) suggest that the radial displacement due to pile installation in clays can be captured by the expansion of a infinitely long cylindrical cavity embedded in a continuum deforming under constant volume, *i.e.* undrained conditions. Based on the assumption of conservation of volume, a geometrical solution to the problem can be found.

Consider a volume of soil contained within a circle having the radius r_i, see Figure 2.8. Starting from the centre of the soil volume, a cylinder representing the pile is expanding with the radius r_p pushing the soil radially outwards. To accommodate for the expanding volume of the cylinder, the soil needs to displace radially ξ to conserve the initial volume of the soil. By setting the soil volume before and after the expansion of the pile, the following expression is obtained

$$r_i^2 = (r_i + \xi)^2 - r_p^2 \tag{2.1}$$

which can be rearranged to

$$\xi / r_p = ((r_i / r_p)^2 + 1)^{\frac{1}{2}} \tag{2.2}$$

Although this modelling approach neglects vertical movements, the method has been successfully used to capture the radial displacements from undrained pile installation. The results compare well with experimental data from model tests and in-situ measurements (Lehane and Gill 2004; Pestana et al. 2002; Massarsch and Wersäll 2013). The reported studies focused on the resulting displacement in the vicinity of the pile with a distance less than $20R$ from the pile group.

2.4.2 Shallow Strain Path Method

The Strain Path Method (SPM) was developed over a period of time at MIT, and is presented by Baligh (1985) as an alternative to the one dimensional CEM. The method is based on the assumption that a known velocity field is giving the strains in the soil. Subsequently, the strain field can be used to calculate the corresponding stress state by combining the known strain field

with a constitutive model and an initial stress state in the soil. Observation of soil deformations "far" below the surface caused by the deep undrained penetration of an object into saturated clay showed that the displacement seems to be independent of the mechanical properties and stress state in the soil. These observations lead to the assumption that the soil movement in a saturated clay can be estimated by assuming a incompressible isotropic and homogeneous soil material under isotropic stress.

SPM assumes a deep steady state solution, which disqualifies the method from being used to estimate displacements close to the stress free surface. Further developments were made to SPM by Sagaseta et al. (1997) introducing a Shallow Strain Path Method (SSPM) to incorporate the presence of a free surface of the problem. As it is not possible to treat the problem as a steady state solution, additional steps are required. Figure 2.9 shows the representation of the SSPM for a simple pile penetrating into an infinite half space where the final condition of a stress free surface on the top should be reached. The solution to achieve these conditions consists of three specific steps. Step 1 considers a point source discharging a volume (Q) in an infinite full space moving from the origin along the positive vertical axis to the desired depth of penetration with the velocity U. Step 2 adds a surface free from vertical stress by including a mirrored image sink (-Q) in the same infinite full space, with the magnitude equal to the source, while moving along the negative vertical axis. The combination leads to the cancellation of the vertical stress components at a plane perpendicular to the vertical axis as desired. To eliminate the shear stress from the surface, a distributed shear stress is applied equal in magnitude but in the opposite direction from the combined shear stress induced from the source and the image sink. The applied shear stress will give rise to a velocity field in the soil. Combining the velocity field arising from applied shear stress to the velocities from the point source and the image sink, the velocity field for the shallow penetration of a rigid pile into a homogeneous incompressible half space with a stress free surface is obtained.

Sagaseta and Whittle (2001) compared the predictions of the SSPM with data from a number of actual sites and laboratory tests, and showed that the method was able to predict movement from the installation of pile group, as well as the the evolving movement in soil due to the installation of a single pile. The surface heave was generally underestimated by the SSPM. The SSPM has further been successfully used to predict the evolving displacements in a clay like soil from undrained penetration in laboratory environment Lehane and Gill (2004) and Ni et al. (2010).

By superposition of the single pile displacement, the displacement from the installation of a pile group can be predicted. Several case studies where the measured field displacement has been compared to superposition of the SSPM single pile solution is reported. The impact of preaugering, *i.e.* removing soil in the place of the pile, can also be modelled by a "negative" pile representing the outtake of soil volume before the installation of a pile.

Rehkopf (2001) showed a good match between the SSPM predicted displacement and the measured displacement due to the installation of about 350 piles into clay including preaugering in East Boston. Three case studies reported from the Gothenburg area (Edstam 2011; Hall et al. 2020; Trafikkontoret 2021) also yielded a good comparison between the predicted and the measured displacements. Care should be taken when using SSPM, as the method is not able to predict the situations more complex than the a stress free plane surface in axisymmetric or plane strain situation.

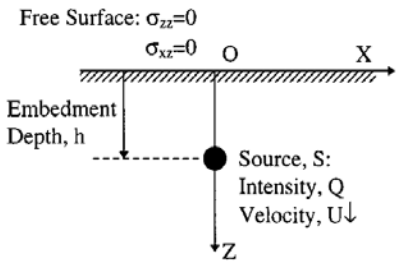

a) SSPM Representation of Shallow Penetration Problem

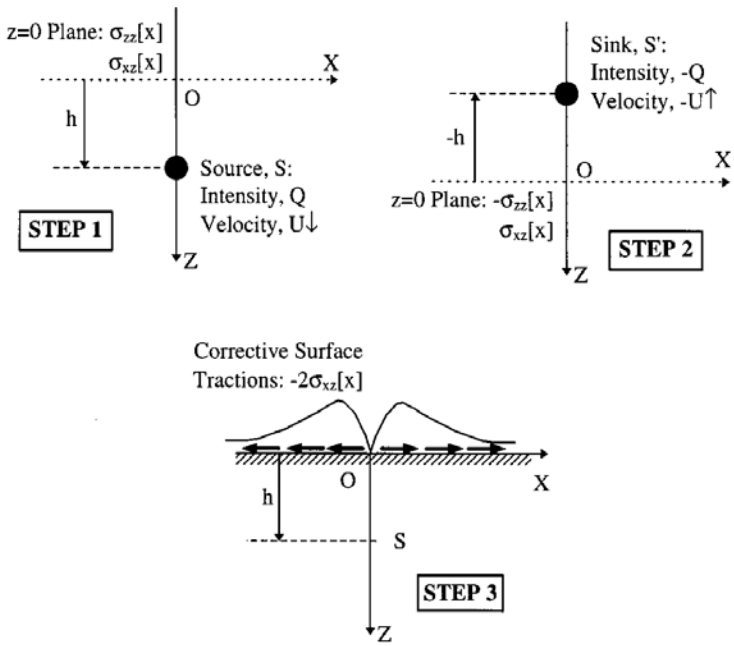

b) Equivalent Solution (Steps 1+2+3)

Figure 2.9: *Conceptual model of the Shallow Strain Path Methods used to simulate the penetration of a pile into a half space with a stress-free surface. From Sagaseta et al. (1997)*

2.4.3 Finite Element Analysis

Finite element modelling (FEM) of the penetration of a long slender object, such as a pile or the CPT, has been performed by several authors using different numerical approaches. The penetration of a long and slender object into soil is associated with large distortions of the calculation mesh that in the common Lagrangian numerical formulation is following the deformations of the soil. A common way of circumventing the problems related to these mesh distortions is to pre-embed the full length of the pile inside the FE mesh (Castro and Karstunen 2010; Sheil et al. 2015). The pile installation is then modelled by a horizontal expansion of the pre-embedded pile, corresponding to the pile geometry leading to acceptable mesh distortions. The horizontal expansion can be followed by a step of limited vertical penetration inducing shear at the pile shaft interface and mobilising the base resistance (Abu-Farsakh et al. 2015).

Another frequently used technique is to perform a limited number of calculation stages with a vertical penetration mechanism in a Lagrangian mesh, followed by a remeshing procedure adjusting the calculation mesh to be better shaped elements (Hu and Randolph 1998). Different approaches using a stationary Eulerian mesh can also be used where the material information is convected in between the elements (Pucker and Grabe 2012; van den Berg 1994). A special procedure where the displacement of the soil is decoupled from the independently deforming calculation mesh has also been used (Nazem et al. 2006).

Recently, a number of methods have been presented using material points (MPM or SPH) carrying material information through the numerical domain (Ceccato et al. 2016; Monforte et al. 2021; Bui et al. 2008). Most of theses studies focus on the dependency of the stress situation on the installation of the pile into different soil, and the impact on the deformations is more scarce.

Massarsch (1976) conducted a series of FE calculations on the resulting mass displacement due to the installation of a pile row by prescribing a horizontal movement at the boundary of the FE model. The study investigated the effect on the resulting displacement due to different values of shear strengths, K_0 values, and strength anisotropy using an incompressible soil. The study showed a significant difference in the resulting deformations, where a low K_0 will lead to larger radial deformations and smaller vertical deformation compared to a higher value of K_0. The presence of a high strength top layer, representing the dry crust of a natural clay, was shown to reduce the vertical deformations and to increase the horizontal deformations in the soil. Edstam (2011) simulated the displacements due to the installation of a pile group by using volume expansion of pre-embedded solid elements to represent the pile installation in a 3D FE-model. The pile group consisting of more than 50 piles was represented by 3 solid elements that was expanded to correspond to the total volume of the single piles. The soil was modelled as a linear elastic incompressible material, and the resulting displacements showed good comparison with displacements measured in the field.

The deformations due to the installation a stone column was modelled using a prescribed horizontal displacement of the axisymmetric boundary in a 2D FE model using the SCLAY1S constitutive model by Castro and Karstunen (2010). Vertical displacement upwards and outwards was detected after installation. The consolidation of excess pore pressures lead to a volumetric compression of the soil and corresponding downward vertical movement at the soil surface. The presence of sensitivity in the soil was shown to increase the downward movement due to consolidation, compared to the insensitive case.

Karlsson et al. (2019) combined SSPM method with a subsequent 2D FE model to study the

impact of pile installation on pile ageing, *i.e.* the increase in bearing capacity with time. The steady state results of the deformations calculated with SSPM were mapped to a 2D FE model, so that the dissipation of excess porewater pressures from installation as well as the creep with time could be quantified. The analyses used the Creep-SCLAY1S constitutive model. The average of the results of the SSPM for open ended and closed ended piles, using the plugging ratio, compared well with measured results from the field. Furthermore, the results indicate a clear link between the amount of disturbance and the subsequent re-gain in pile bearing capacity, where open-ended piles disturbed less and recovered faster towards the original undrained shear strength. However, it should be noted that for the reported simulations in sensitive clay the capacity only recovered slowly, as the softening from remoulding during pile installation counter acts the hardening from the equalisation stage.

3 Modelling mass displacement

3.1 Eulerian pile penetration

In Chapter 2.4, a number of possible numerical techniques for modelling the installation of a pile into soil were briefly discussed. This Chapter will describe the numerical method used in this study to model pile installation.

The numerical method relies on the combination of an Eulerian (E) material description for the soil and a quasi-Lagrangian description for the pile. The code used, Tochnog Professional Roddeman (2022), which has been used previously to model flow like landslides (Crosta et al. 2003; Crosta et al. 2015) as well as pile installation (Dijkstra et al. 2011). In contrast to commonly used Lagrangian or updated Lagrangian small strain FE-formulations, this method is able to consider the large deformations around the tip of an advancing cone or displacement pile without numerical convergence issues.

The Eulerian description is based on the method suggested by Huetink (1986) where each time step is divided into an initial Updated Lagrangian step followed by the convection of material (and its state) through a stationary mesh with the Streamline Upwind Petrov Galerkin method (SUPG). The Finite Element mesh is fixed, *i.e.* independent of the material deformations, throughout the analysis, however, each type step any change in the geometry, *e.g.* a second Lagrangian mesh or a geometry entity with prescribed boundary condition is continuously updated. A fully coupled numerical formulation with an effective stress based constitutive model is used to link the material deformations to the emerging porewater pressure and flow and vice versa. The hydraulic head in the system and the flow of porewater is solved for simultaneously with the mechanical problem for the ongoing pile penetration. Hence, for each element in the domain the drainage response will emerge from the hydraulic conductivity and penetration rate for the pile, as well as the drainage length to nearest open boundary. As a result, in addition to the undrained or drained penetration problem, intermediate drainage regimes spanning from undrained to drained response can be studied.

For an Eulerian mesh two different methods to model the installation of a pile into soil, have been proposed. Both rely on an Eulerian framework and an axisymmetric model domain. The two methods were previously proposed by Dijkstra et al. (2011) to model pile installation in sand using the same numerical framework. Although the two methods are based on the same FE formulation and constitutive model, they are fundamentally different in how the kinematics of the problem are introduced in the domain.

In the *fixed pile* method the problem is modelled as a stationary flow problem where the pile is fixed and the soil is flowing upwards in the domain. The pile geometry will affect the flow patterns in the soil, thus capturing the pile penetration mechanism. A steady state solution will eventually be reached for the specified geometry of the model.

A more intuitive way of modelling the penetration process is by the *moving pile* method, where pile installation is modelled by penetrating a pile object into an initially stationary soil. In this approach the geometry of the pile, and the boundary conditions prescribed on that entity, are gradually changed. As the pile is pushed further into the soil the solution at any given moment during the calculation will be showing the current geometry. Analogously to the modelling of a flat pile tip, another shape of the penetrating object can be used for both of these two methods.

3.1.1 Fixed pile

The *fixed pile* method is illustrated in Figure 3.1. The *fixed pile* method considers a pile with a

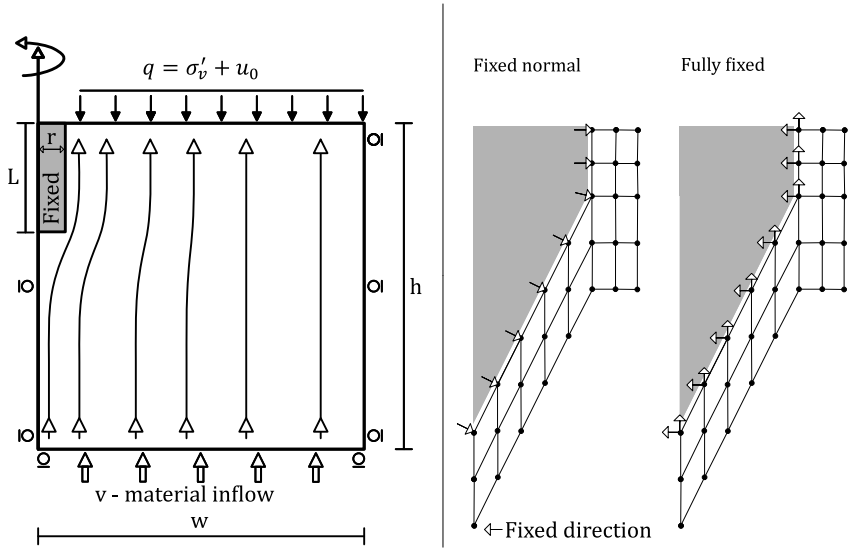

Figure 3.1: *fixed pilemethod. Boundary conditions between the soil and the pile can either be fixed in the normal direction or fully fixed.*

radius r that is initially embedded to the full penetration length L of the pile at the axisymmetric boundary in homogeneous soil. The geometry is kept constant throughout the complete analysis. The kinematics of the method are introduced by a vertical inflow v of soil at the bottom boundary of the domain. Pushing the soil already in the domain up and eventually out of the domain at the top boundary. As the soil is continuously flowing upwards, the stationary pile is affecting the flow pattern of the soil and the penetration mechanism of the pile installation is being captured. Eventually, a steady state is reached giving a solution to the problem for the specified geometry. Due to the flow of soil in the domain, the *fixed pile* method is limited to a homogeneous initial stress state in the soil. In the analysis, the soil can be modelled as a fluid, but more commonly an effective stress based constitutive model developed for soils is used. This initial stress state is prescribed though the domain, and in equilibrium in between the vertical force q applied as a boundary condition at the top of the domain and the inflow. Soil entering the domain through the bottom boundary is given the initial stress state throughout the calculation.

Numerically, the pile is included by adjusting the geometry of the axisymmetric boundary to the shape of the pile, though a pile material can also be added. Two different ways of applying the boundary conditions (BC) from the pile geometry on the soil will be used (Figure 3.1). The fully fixed BC is preventa all movement at the nodes in the soil that are connected to the pile. In contrast the fixed normal only prevents nodes from moving in the normal direction to the pile geometry. Below the pile, regular axisymmetric boundary conditions are used preventing horizontal displacements. Horizontal displacements are also set to zero at the right boundary.

3.1.2 Moving pile

The second method for modelling pile installation, the *moving pile* method is illustrated in 3.2. In contrast to the *fixed pile* method, the pile is initially modelled outside above the axisymmetric domain. A geometric entity, a quadrilateral with radius r, is defined to represent the pile initially outside the domain. Penetration is modelled by moving the bottom line of the quadrilateral, that represents the pile, downwards with a velocity v representing the penetration rate into the soil. As the pile geometry is continuously expanding downwards, a mapping at each time step is performed to check which of the nodes in the domain are at the location of the the pile geometry. All nodes within and on the boundary of the pile geometry will be given a vertical velocity equal to the penetration velocity of the pile, while the horizontal velocity is set to zero. This process will be repeated until the pile geometry has reached the final penetration depth L. Once all nodes of an element are associated with the pile geometry, the element can either be deleted or replaced by a material representing the pile. Both of these choices will lead to a completely rigid pile during the installation stage, *i.e.* all nodes have a prescribed velocity. In this modelling approach, all the steps inbetween the initial and final calculation step represent a valid solution for the specific geometry of the current time step.

At the left and right vertical boundaries horizontal displacements in the soil are fixed by prescribing a zero velocity. Initially, before the pile enters the domain the initial stress state of the model is set. In addition to the possibility of prescribing a homogeneous stress state in equilibrium with the vertical force q on the top boundary and the bottom boundary, as in the case of the *fixed pile* method, also a more natural gravity based stress distribution can be calculated in an initial step.

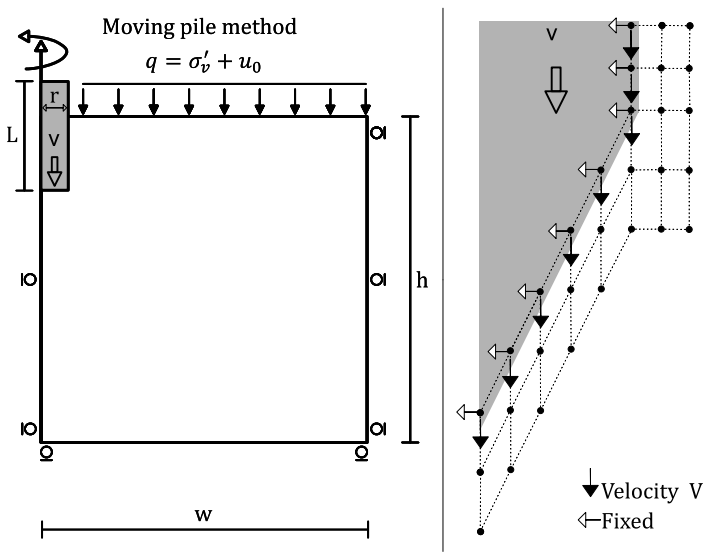

Figure 3.2: *Moving pile method.*

3.2 Constitutive model

SCLAY1S is an effective stress based constitutive model suitable to model the behaviour of lightly overconsolidated natural clays, as it is able to capture the evolving anisotropy and bonding present in these soils (Koskinen et al. 2002). In the following, the simplified formulation is presented, corresponding to the conditions in a typical triaxial test.

The model assumes an associated flow rule, and builds from the critical state framework, *i.e.* Modified Camclay (MCC), using an isotropic elastic behaviour with volumetric $d\epsilon_v^e$ and deviatoric $d\epsilon_d^e$ elastic strain increments identical to MCC.

$$d\epsilon_v^e = \frac{\kappa dp'}{vp'} \tag{3.1}$$

$$d\epsilon_d^e = \frac{dq}{3G'} \tag{3.2}$$

where κ is the unloading reloading index in the $\ln p' - v$ -space where v refers to the specific volume of the soil. The yield surface of the anisotropic and bonded SCLAY1S model is formulated using a sheared ellipse where α controls the inclination of the surface *i.e.* the plastic anisotropy of the soil, Figure 3.3.

$$f = (q - \alpha p')^2 - (M^2 - \alpha^2)(p'_m - p')p' = 0 \tag{3.3}$$

To capture the evolving anisotropy due to loading of the soil, a rotational hardening law is used where the change in anisotropy is related to the plastic volumetric ϵ_v^p and deviatoric strain ϵ_v^d by the stress ratio $\eta = q/p'$ and the rate parameters ω and ω_d.

$$d\alpha = \omega \left[\left(\frac{3\eta}{4} - \alpha \right) \langle d\epsilon_v^p \rangle + \omega_d \left(\frac{\eta}{3} - \alpha \right) |\epsilon_d^p| \right] \tag{3.4}$$

Bonding is incorporated by including an (imaginary) intrinsic yield surface, using the same shape and inclination as the yield surface of the soil and linked in size by the bonding parameter χ.

$$p'_m = (1 + \chi)p'_{mi} \tag{3.5}$$

Two additional hardening laws are included to control the size of the two yield surfaces. The increase in size of the intrinsic yield surface is linked to the volumetric plastic strains of the soil $d\epsilon_v^p$ using the intrinsic compression index λ_i (or λ in absence of bonding), similar to the hardening law used in MCC for a soil without bonding.

$$dp'_{mi} = \frac{vp'_{mi}}{\lambda_i - \kappa} d\epsilon_v^p \tag{3.6}$$

The change in relative difference in size, *i.e.* the bonding parameter χ, between the two surfaces is controlled by the third hardening law, linking the degradation of the bonding parameter to the absolute plastic strain increments

$$d\chi = -a\chi(|d\epsilon_v^p| + b|\epsilon_d^p|) \tag{3.7}$$

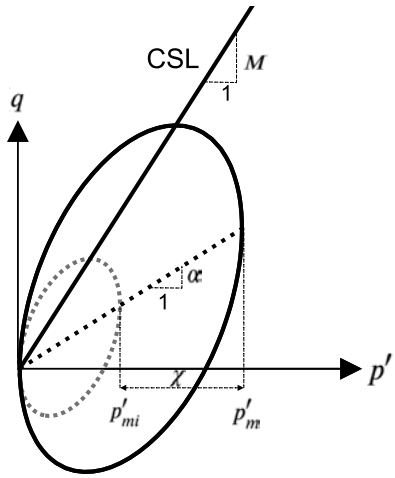

Figure 3.3: *SCLAY1S yield surface in triaxial stress space.*

where a and b are controlling the rate of degradation. Negative bonding, that might occur for very large strains in this analysis, is capped by the model to 0.

The SCLAY1S model is a hierarchical model leading to the possibility to use the model without the consideration of bonding (SCLAY1) and with an isotropic yield surface (MCC). Setting the bonding parameter $\chi = 0$ and replacing the intrinsic compression index λ_i with the compression index λ leads to the SCLAY1 model where $pm = pm_i$. Additionally, if α together with the associated rate parameter ω are set to zero, the model becomes identical to the MCC.

3.3 Verification

The numerical method used in this work was verified by looking at the CPT penetration into soil, essentially representing an instrumented mini pile. The CPT is preferred over the pile geometry to verify the modelling method due to the large amount of theoretical studies conducted on the CPT penetration, in addition to the extensive empirical research available on the relation between the soil properties and the CPT response (Robertson 1990; Schneider et al. 2008).

3.4 Modelling method

Initially, the *moving pile* method and the *fixed pile* method were used to model the CPT geometry penetrating into a soil with a homogeneous stress state and soil properties. A linear elastic perfectly plastic stress strain relation with the Tresca failure criterion was used to model the soil behaviour. A Poisson's ratio of $\nu = 0.49$ ensured a constant volume behaviour similar to the undrained response of saturated fine grained soils, such as clay. An uniform initial stress was set throughout the domain

with vertical stress σ_v =5 kPa and a lateral earth pressure coefficient K_0 equal to 1. For the first set of simulations a Young's modulus $E = 5960$ kPa combined with a shear strength s_u of 40 kPa was used with a rough interface formulation.

Figure 3.4 shows the resulting vertical reaction force on the tip of the CPT from the *moving pile* method and the *fixed pile* method using two different boundary conditions. The *moving pile* method and the *fixed pile* method with fully fixed boundaries show very similar results. However, the *fixed pile* method, where the movement was only prevented in the normal direction, shows a considerably lower reaction force. The explanation can be found by a closer look in Figure 3.1 on how the BC's are applied to the soil. The node located at the shoulder of the CPT, at r is in the formulation using a normal boundary condition allowed to move freely along the CPT. In contrast the fixed boundary condition is forcing the soil closest to the CPT, at r, to be stationary. Hence, the movement will occur in the node located one element width away from the pile geometry which results in a numerical radius extension. Since the model is axisymmetric, a rather small increase in the radius leads to large increase in area and corresponding vertical force. Figure 3.5 is instead showing the vertical pressure on the tip using an area of the CPT calculated with this numerical radius extension. The vertical pressure was found to be within 2% when comparing the two simulations.

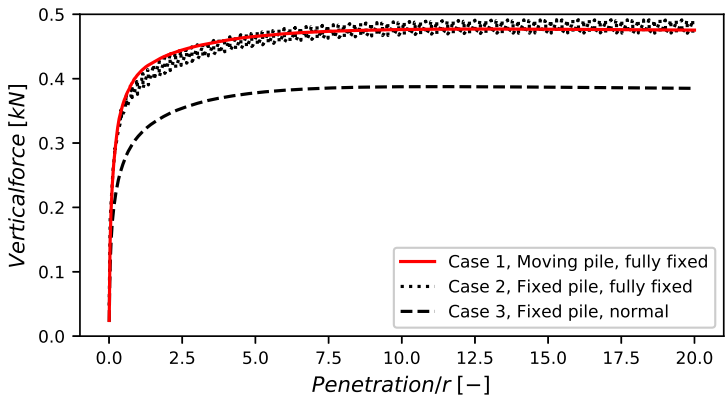

Figure 3.4: *Vertical reaction force on the CPT tip from simulations using the fixed pile method with two different ways of applying BC and the moving pile method.*

Furthermore, the numerical method was also compared to prior numerical studies from literature on the resulting cone resistance on a CPT tip penetrating into a Tresca material. The *fixed pile* method with fully fixed boundary conditions was used and the resulting cone factor was calculated from a series of simulations using different rigidity index $Ir = E/s_u$. The cone factor is calculated as the cone tip resistance over the undrained shear strength of the soil. All other model parameters are kept constant throughout the series of simulations. Table 3.1 shows the resulting cone factor for both smooth and rough contact formulation and is compared to a range of cone factors calculated by previous studies summarised in Liyanapathirana (2009). For the smooth interface formulation the result found is in the upper range of the literature, in contrast to the rough interface which is closer to the lower range found in literature. The results for both the smooth and rough interface from this study are showing a similar dependency on the rigidity index as the previous studies.

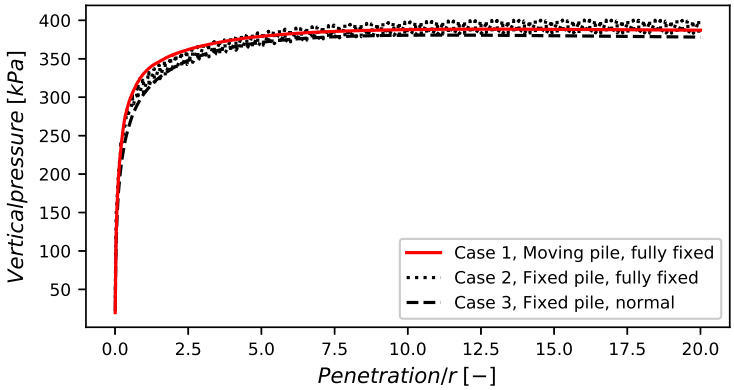

Figure 3.5: *Cone tip resistance from simulations using the fixed pile method with two different ways of applying BC and the moving pile method.*

Table 3.1: Simulated conefactor for different values for the rigidity index Ir compared to the range from literature (Liyanapathirana 2009).

Ir	Contact	This study	Previous studies
50	smooth	8.6	8.1 - 9.6
	rough	9.3	9.4 - 13.8
150	smooth	11.5	9.8 - 11.4
	rough	12.2	11.8 - 15.0
300	smooth	13.2	10.6 - 12.5
	rough	13.9	13.3 - 15.8
500	smooth	14.1	11.2 - 14.4
	rough	14.9	14.4 - 20.7

Hence, the proposed numerical framework was shown to give results in accordance to previous studies. In addition, the two proposed methods for modelling the pile installation gave similar response on the resulting tip resistance in the soil. As the *moving pile* method allows for a wider range of geotechnical applications *e.g.* linear increasing gravity loads, staged construction and intermediate calculation results, this method is preferred over the fixed pile method and was used in for the rest of the simulations in this work. Furthermore, the *moving pile* method can be expanded to study multiple piles in a group in a 3D calculation.

3.4.1 Drainage conditions

The results presented in this Section, and in Section 3.4.2, is a summary of the work presented in the appended Paper A (Isaksson et al. 2022) that investigates CPT penetration into natural clay using numerical modelling. The emerging drainage conditions arising from the coupled soil deformation and porewater pressure formulation was studied numerically. A series simulations of the Cone Penetration Test (CPT), or more precisely the piezocone (CPTu) that also registers excess porewater pressures, was performed using the MCC constitutive model and the *moving pile*

Table 3.2: Model parameters used to investigate the effect of drainage conditions on the CPTu response.

Symbol	Parameter	Value
σ'_v	Vertical effective stress [kPa]	109
u_0	Initial porewater pressure [kPa]	70
$K0$	Initial earth pressure koefficient [-]	0.61
OCR	Overconsolidation ratio [-]	1.02
e_0	Initial void ratio [-]	1.41
λ	Virgin compression index [-]	0.205
κ	Swelling/recompression index [-]	0.044
ν	Poisson's ratio	0.3
M	Slope of CSL line [-]	0.9

method. The full range of drainage conditions, ranging from undrained to drained, was covered, by varying the hydraulic conductivity k of the soil between $5.5 \times 10^{-3}\,\mathrm{m\,s^{-1}}$ and $1.1 \times 10^{-8}\,\mathrm{m\,s^{-1}}$. While the hydraulic conductivity was varied, all other model parameters were fixed using the values summarised in Table 3.2. Hence, any difference in response of the net cone resistance and the pore pressures can therefore solely be attributed to the change in drainage conditions. To quantify the drainage condition for each case, a dimensionless normalised penetration rate V was used:

$$V = \frac{vd}{c_v} \tag{3.8}$$

where v is the penetration rate, d is the diameter of the pile (or cone) and c_v is the vertical consolidation coefficient of the soil. The normalised penetration velocity enables a unified direct comparison to be made between the drainage conditions arising from different experimental set-ups or numerical simulations.

$$c_v = \frac{k_v(1 + e_0)\sigma'_{v0}}{\lambda\gamma_w} \tag{3.9}$$

The net cone resistance was normalised with the net cone resistance from the practically undrained condition (the simulation with the smallest hydraulic conductivity) and presented in Figure 3.6 at different normalised penetration rates V. Similarly, the excess porewater pressure emerging from the CPT penetration was normalised with the porewater pressures from the practically undrained condition and presented in Figure 3.7.

Two different alternatives for extracting the porewater pressures from the simulations were included. The first alternative extracts the pressure from a single element at the cone shoulder, while alternative 2 uses the mean value over the 4 closest elements on the shoulder. The results from this study were compared to the laboratory studies conducted by Mahmoodzadeh and Randolph (2014) and DeJong and Randolph (2012). Additionally, a comparison was made with numerical results from Monforte et al. (2021) where the interface friction was varied.

The drainage condition has a significant impact on the emerging net cone resistance, resulting in a 3.5 times higher resistance for the drained compared to the undrained simulation. As expected, the emerging excess porewater pressures decrease when lowering V (in this case due to a increase

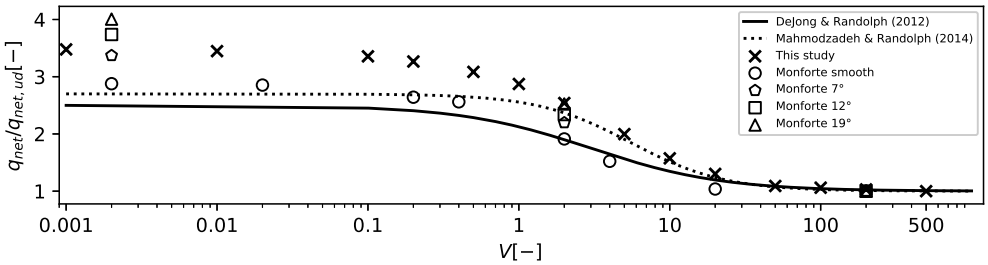

Figure 3.6: *Normalised cone resistance as function of normalised penetration rate. Comparison between results from this study and Monforte et al. (2021) is included to indicate the effect of interface properties on the CPTu response. From Isaksson et al. (2022).*

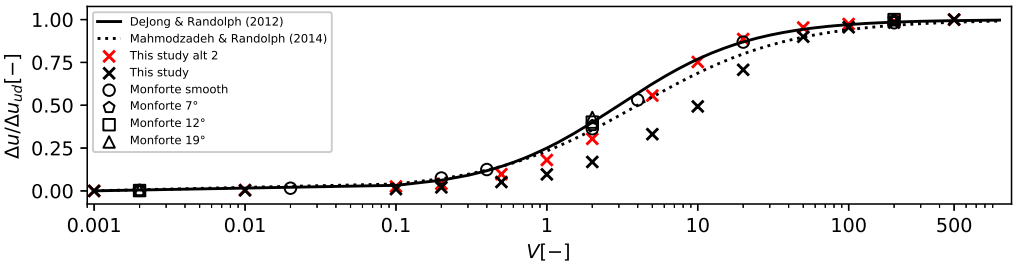

Figure 3.7: *Normalised excess porewater pressure as function of normalised penetration rate. Comparison between results from this study and Mahmoodzadeh and Randolph (2014) and DeJong and Randolph (2012). Results from Monforte et al. (2021) are included to indicate the effect of interface properties on the CPTu response. From Isaksson et al. (2022).*

in c_v). A practically undrained response is found for $V > 100$ while a practically drained response can be found for $V < 0.01$. In between these two limiting states, a transition with increasing excess porewater pressures and decreasing net cone resistance are found for increasing V. The general trend on drainage behaviour was captured well by the numerical model, when compared to the published laboratory and numerical studies.

3.4.2 CPT in natural clay

In addition to the emerging drainage response, the appended Paper A (Isaksson et al. 2022) also investigates the response of CPT for different clay characteristics. The full capabilities of the SCLAY1S constitutive model were used to capture the response of natural sensitive clays, and compared with the well established empirical charts between CPT response and soil properties. A normally consolidated reference state was calculated first for a modelled soil without initial bonding or anisotropy, using a normalised penetration rate of $V = 200$, *i.e.* practically undrained behaviour.

A series of simulations was then performed where the model parameters were sequentially altered, and the change in CPT response was monitored. First, the response from varying the OCR

Table 3.3: Parameters used for investigation of the CPTu response in soft clays.

Symbol	Parameter	Value
OCR	Overconsolidation ratio [-]	1.2, 1,5, 1,8
χ_0	Initial amount of bonding [-]	2, 5, 10, 20, 50
a	Rate of destructuration [-]	6
b	Rate of destructuration due to to deviator strain [-]	0.4
α_0	Initial anisotropy [-]	0.352
ω	Rate of rotation [-]	10
ω_d	Rate of rotation due to deviator strain [-]	0.374

between 1.02 and 1.8 was investigated. In addition, different degrees of sensitivity in the soil were investigated by varying the SCLAY1S state parameter χ_0 between 0 (no structure) and 50 (highly sensitive clay). The effect of fabric anisotropy was also studied by including an inclined yield surface evolving with deviatoric and volumetric strains. Table 3.3 presents the range of SCLAY1S parameters used in the study. Two common classification charts used to evaluate CPT penetration is used to present the results. Figure 3.8 shows the results in the chart originally proposed by Robertson (1990). The response is presented using the normalised porewater pressure parameter B_q and the normalised cone resistance Q_t

$$Q_t = \frac{q_{net}}{\sigma'_{v0}} \tag{3.10}$$

$$B_q = \frac{\Delta u}{q_{net}} \tag{3.11}$$

In addition to the new analyses, also the results from on the effect of drainage conditions (c_v), that were already presented in Section 3.4.1, are also included in the charts. The arrows annotate the data points corresponding to each model parameter, and are showing the direction of the normalised CPT response, when the value for the parameter is increased in the numerical analysis. Distinct trends for each parameter are clearly identified and are in good agreement with trends proposed by Robertson (1990), for both S_t and OCR.

The numerical results are also presented in the classification chart (Fig. 3.9) originally proposed by Schneider et al. (2008), which is based on Q_t and the excess porewater pressure (Δu) normalised with the initial vertical effective stress (σ'_{v0}). The impact of changing S_t, OCR and c_v indicates clear trends that are in good agreement with the response suggested by Schneider et al. (2008).

The effect of fabric anisotropy α only shows limited impact on the results. The results are only slightly changed, due to the lower Q_t and excess porewater pressures when compared to the isotropic model results. However, a strong influence of the increased *i.e.* sensitivity, is found where an increased sensitivity leads to a significantly decreased normalised cone resistance and only a small change in the excess porewater pressure. In contrast, the increasing OCR leads to an increase in both the normalised cone resistance and excess porewater pressures. The observed trends in the simulations from the OCR, drainage conditions (c_v) and brittleness (S_t) are in very good agreement with the trends proposed by Schneider et al. (2008) and Robertson (1990). This increases the confidence in the numerical method proposed.

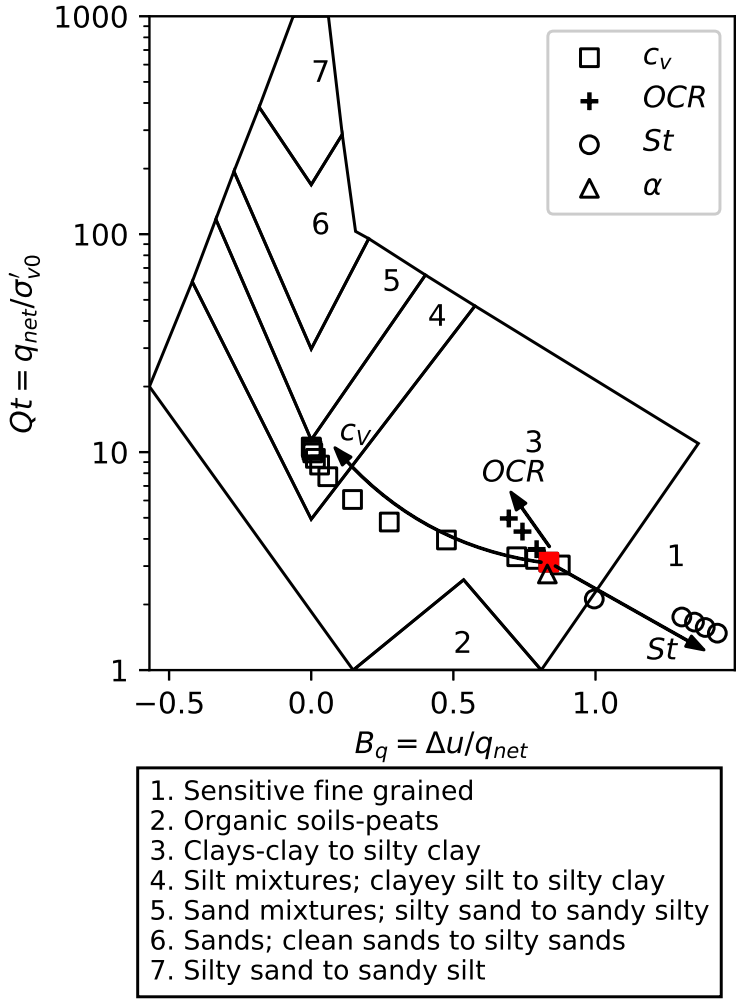

Figure 3.8: *The effect on CPTu response from changing the consolidation coefficient c_v; overconsolidation ratio OCR; sensitivity S_t and considering fabric anisotropy α in the characterisation chart for CPTu proposed by Robertson (1990). From Isaksson et al. (2022).*

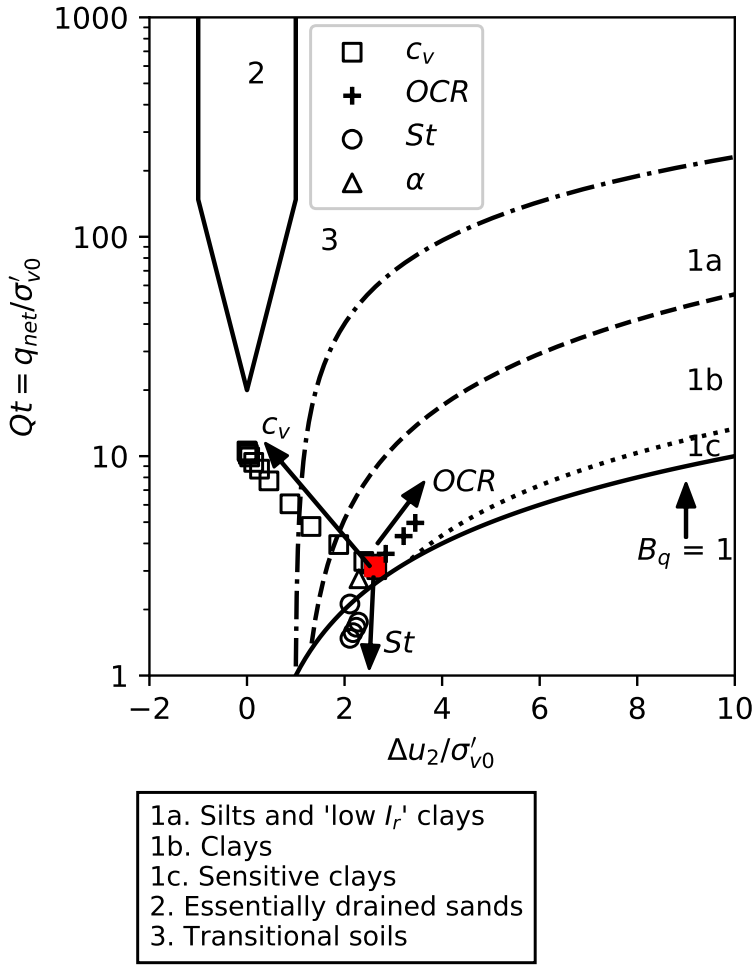

Figure 3.9: *The effect on CPTu response from changing the consolidation coefficient c_v; overconsolidation ratio OCR; sensitivity S_t and considering fabric anisotropy α in the characterisation chart for CPTu proposed by Schneider et al. (2008). From Isaksson et al. (2022).*

3.5 Experimental design

The amount of sampling and testing data available from a geotechnical site is very limited in comparison to the amount of soil in the ground at the site. In addition, as a soil deposit is formed by nature, some variability of the material is expected (Phoon and Kulhawy 1999). Uncertainties from the limited site investigation are inherited by the numerical idealisation performed when creating a numerical model. A number of methods exists to quantify the impact of the anticipated uncertainties and to highlight the most important factors governing the model response.

Experimental design is a concept using a systematic approach of conducting Sensitivity Analysis (SA), aiming to provide the maximum possible information from a limited number of experiments (Box and Draper 2006). Experiments herein are referred to as the realisation of a numerical simulation with a specific set of parameters. Experimental design using the two-level factorial design is a statistical method in which the factors are given a low (-) and a high (+) value leading to a total of 2^k possible realisations for the full set of parameter combinations.

The realisation of the full set gives information about the main effects related to the change of a single parameters, as well as all possible interaction effects between two or more parameters. However, by assuming that the higher order interaction effects are negligible compared to the lower order interaction effects and the main effects, only a fraction of the full set of possible experiments needs to be conducted. A fractional factorial design of resolution IV relies on the assumption that the interaction effects are small in comparison to the main effects. The main effects for the change in a single parameter will with this resolution not be confounded with any other main or two-factor effects.

Tahershamsi and Dijkstra (2022) conducted Global Sensitivity Analyses (GSA) using a numerical constant rate strain test (CRS) on the impact of the Creep-SCLAY1S parameters. The study highlights the importance of different parameters in the constitutive model at different temporal and spatial locations. The GSA was performed by means of Experimental design and the Sobol method to analyse the impact of different factors on the response of the CRS test. It was concluded that the effects of these factors changes at different temporal stages of the CRS test, which are corresponding to the elastic and plastic response of the numerical model. The rational framework developed for GSA was also used in the studies conducted in this work.

4 Numerical study on mass displacements in natural clay

This chapter presents the emerging displacements from the installation of a single displacement pile into a saturated natural soft clay in Utby, Gothenburg, using the results from a numerical analysis. A similar numerical framework as for the CPT described in Chapter 3 was used. The numerical model only approximates the true behaviour of a pile installed into clay. However, in absence of complete well documented datasets from field or laboratory studies, the model provides a best estimate of the resulting soil displacements during pile installation and subsequent consolidation.

4.1 Reference case

The numerical results presented in this chapter will be used as a reference case to evaluate the influence of anisotropy and bonding of natural clays on the resulting mass displacements from pile installation, and after subsequent consolidation. Additionally, the reference case is also used to investigate the capability of different modelling approaches to accurately describe the pile installation process for a natural sensitive clay that is anisotropic.

The results will be presented as the continuous displacement path for a distinct soil patch (think of it as a particle) in a similar approach as the experimental data that is presented in *e.g.* Lehane and Gill (2004). In addition, the displacements along a number of vertical cross sections corresponding to the commonly used *in situ* instrumentation using an inclinometer (horizontal movement) and a bellow-hose (vertical movement) will be presented.

Field measurements are most commonly performed on the ground surface, therefore the displacement along a shallow horizontal cross section at depth of $1R$ will also be presented. The latter results will be compared with the displacements along a deep horizontal cross section, to contrast shallow and deep displacement patterns. All displacements will be normalised with the pile radius R to extend the results to be applicable to any radius of the pile with the same slenderness ratio (L/R), this enables a more general interpretation of the results of this study.

The Utby test site is located east of of the city of Gothenburg on the west coast of Sweden. Previously, the site has been used for research on energy piles (Bergström et al. 2021) and sampling disturbance (Karlsson et al. 2016). In addition, test data from the site has also been used benchmark different constitutive soil models on a series of problems such as, *e.g.* embankments, cut excavations and cantilever wall problem (Karstunen and Amavasai 2017). The clay deposit in Utby is approximately 30 m deep and is supported by a 1 m to 3 m thick till layer on top of the bedrock. The soil properties determined from routine laboratory tests are presented in Table 4.1 and the results from a series of laboratory tests on the Utby clay can be found in Karlsson et al. (2016), including CRS test, IL test as well as anisotropically consolidated undrained triaxial tests sheared into compression and extension. Combined these tests allow for the calibration of all models used in this study.

The numerical modelling was performed using the fully coupled deformation and porewater pressure formulation in Tochnog Professional (Roddeman 2022) using the Moving Pile method using the Eulerian framework for large deformations, previously discussed in Chapter 3 The

Table 4.1: Soil characteristics of the Utby clay: wet density ρ, water content at plastic limit w_p, at liquid limit w_L, plasticity index PI sensitivity S_t and shear strength form fall cone test τ_{fu}.

Depth [m]	ρ t/m^3	w_p [%]	w_l [%]	PI [%]	S_t	τ_{fu} (kPa)
5	1.55	25	63	38	30	10
6	1.59	22	55	33	26	9
7	1.58	20	55	35	27	10
8	1.54	23	60	37	28	14
9	1.58	19	61	42	29	17

moving pile method is initially considering the pile to be out of the domain, and is gradually moved vertically into the domain along the symmetry axis. The left and right boundary are modelled as fixed, preventing any material displacements and groundwater flow, while the top boundary is modelled using a prescribed total vertical stress σ_v corresponding to the upper dry crust found in the Utby site, see Figure 4.1. Gravity is included in the analysis giving an increase in vertical stress with depth. Initial horizontal stresses follow from the vertical stress and the earth pressure coefficient K_0 equal to 0.6, similar to that assumed for Utby. The initial porewater pressures in the soil are set as a hydrostatic pressure with a phreatic level at the top of the domain. The pile is modelled with a radius R of 0.155 m and is being pushed towards a final depth corresponding to a pile length L of 40 R with a penetration rate v_{pen} of 0.155 m s^{-1}. Following the installation of the pile the system, porewater pressures are allowed to equlibrate (dissipation of excess porewater pressures), whilst recording the displacements in the soil while keeping the pile in place. The width w and height h of the domain are set equal to twice the pile length, 80 R.

The behaviour of the soft clay in Utby is modelled using the SCLAY1S constitutive model with the model parameters presented in 4.2. The SCLAY1S model parameters are taken as the parameters derived for the Creep-SCLAY1S model by Karstunen and Amavasai (2017) but excluding the parameters related to creep. To avoid convergence issues related to the coupled formulation, and the very low permeability of the natural clay, the hydraulic conductivity k had to be increased compared to the suggested value. Although the time of consolidation will need to be scaled accordingly to match the *in situ* conditions, the pile penetration will still be modelled under undrained conditions, *i.e.* in the analysis the normalised penetration rate V is $\approx$ 800, well above the 100 which is considered to fulfil penetration under fully undrained conditions (Schneider et al. 2007; Mahmoodzadeh et al. 2014).

The Eulerian formulation of the numerical framework has a fixed mesh and solves for the velocity field and displacements in an Eulerian reference frame. Hence, special consideration was therefore needed to get the Lagrangian displacements of the soil due to the pile installation. To get the displacements, 1614 discrete post points were defined in the domain. During the simulation, the post points were convected with the material flow using the velocity field in the domain. The position of a post point at any given time step can therefore be interpreted as the displaced position of a soil particle initially located at the original position of the respective post point. The displacements were tracked using a resolution for printing of 0.1 mm, although this seems to be sufficiently accurate, the accuracy seemed to be slightly on the low side for soil located further away from the pile. The effect on the analyses will be discussed later when presenting the results.

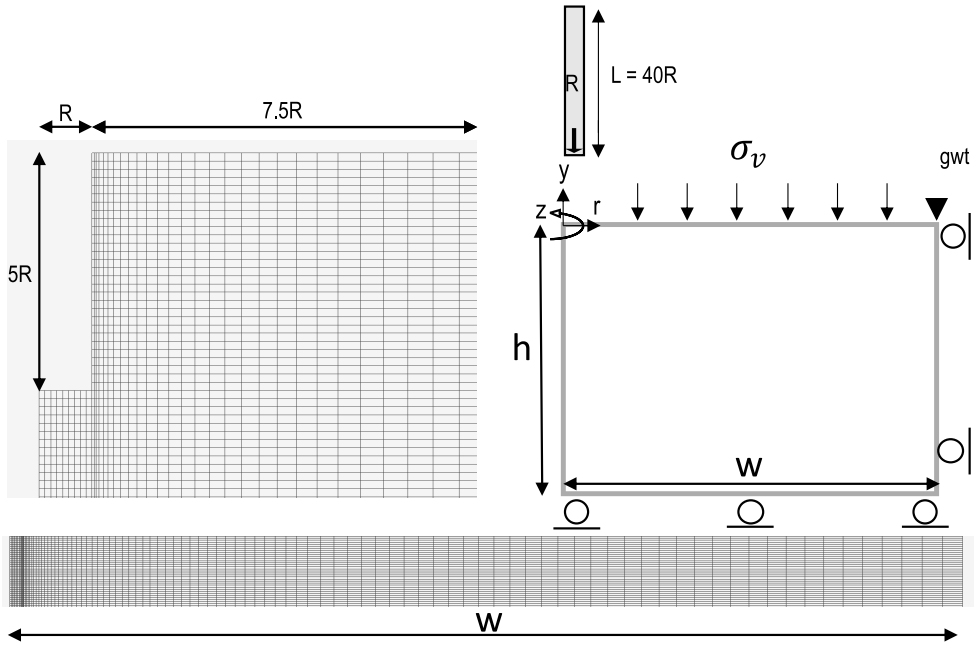

Figure 4.1: *Numerical model used to model pile penetration into Utby Clay.*

4.2 Displacement paths

Figure 4.2 presents the full displacement path from installation and consolidation for 10 post points in the clay close to the pile. Five of the points are located at a shallow depth of $1R$, whereas the remaining points are located further down at a depth of $19R$. It should be noted that the radial coordinate of the points is specified from the centre of the axisymmetric model, and the pile wall is located at a radial coordinate of $1R$. Hence, the point located at a radial coordinate of $1.5R$ has a distance equal to $0.5R$ from the pile wall. A clear difference in the displacement paths of shallow and deep soil is found, where the shallow soil at all radial distances is moved upwards, in contrast to the deeper soil where a downward movement is registered for soil located close to the pile. An upward movement is shown for the deep soil located further away from the pile. The radial movement is in the same outward direction for all of the measured points, with a tendency to be larger at the deeper location. Displacements due to the consolidation of the excess porewater pressures are in the opposite direction, inward and downward, to the direction of the installation movement.

4.3 Inclinometers

The horizontal displacements in the soil at 4 vertical cross sections (inclinometers) with respectively radial coordinates of 3 R, $10R$, $20R$ and $40R$ are presented in Figure 4.3. The displacements at

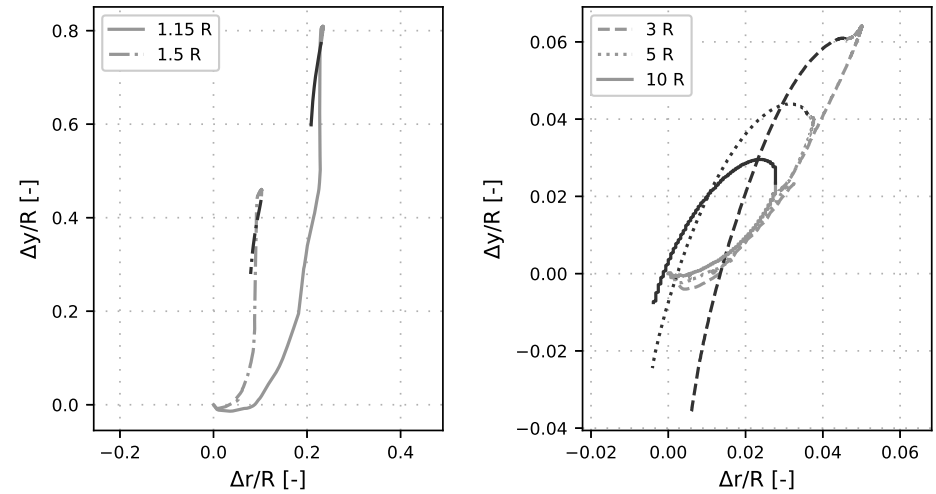

(a) *Shallow: -R*

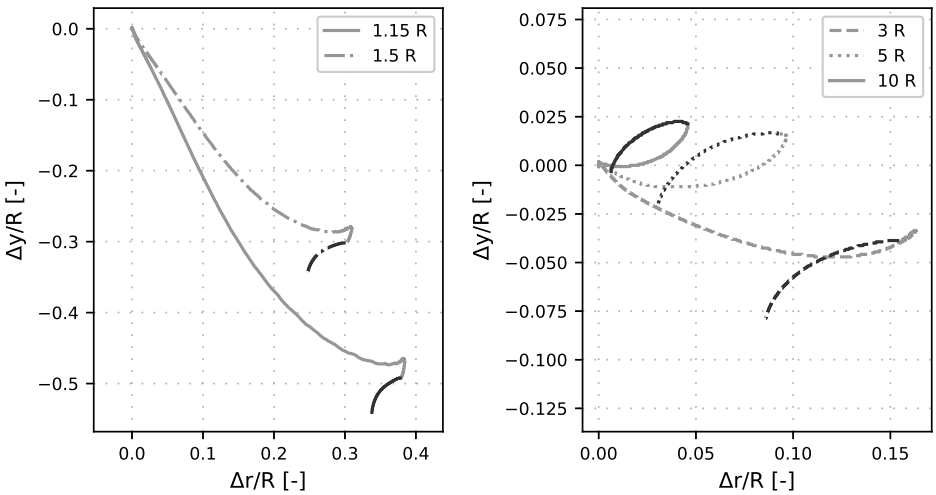

(b) *Deep: -19R*

Figure 4.2: *Displacement paths for shallow (-1**R**) and deep (-19**R**) post points due to pile installation and subsequent dissipation of pore pressures at different radial coordinate (1.15, 1.5, 3, 5, 10) **R**. Displacement paths are normalised with the pile radius **R**. Different colours are used to highlight the displacement from installation (light) and subsequent consolidation (dark).*

Table 4.2: Model parameters used for the coupled simulation of pile installation into the Utby clay using the SCLAY1S model.

Symbol	Parameter	Value
K_0	Initial lateral earth pressure coefficient [-]	0.6
OCR	Overconsolidation ratio [-]	1.45
k	Hydraulic conductivity [m/s]	6.67 e-6 (1 e-9)
σ_v	Vertical pressure	18 kPa
ρ	Density	1.6 t m^{-3}
e_0	Initial void ratio [-]	2.05
λ_i	Intrinsic compression index [-]	0.329
λ	Compression index [-]	0.903
κ	Swelling index [-]	0.061
ν	Poisson's ratio	0.2
M	Slope of CSL line [-]	1.56
α_0	Initial anisotropy [-]	0.63
ω	Rate of rotation [-]	30
ω_d	Rate of rotation due to deviator strain [-]	1.0
χ_0	Initial amount of bonding [-]	5
a	Rate of destructuration [-]	9
b	Rate of destructuration due to to deviator strain [-]	0.4

different penetration depths, *i.e.* $10R$, $20R$, $30R$ and $40R$, and after consolidation at the full depth are included to illustrate the evolving process. As previously stated, the resulting displacements and the vertical coordinate of the soil are normalised with the pile radius. The jagged appearance of the displacement profiles at larger distance from the pile, where the displacements magnitudes are in the order of millimeters), are affected by the 0.1 mm resolution in plotting the location of the post points.

By looking at the horizontal movement, it is evident that the pile penetration is continuously displacing an increasing amount of soil as the length of the pile in the soil is increased. Interestingly, the radial displacements close to the pile are not significantly affected by the continuous penetration of the pile after the pile base passes beyond the depth of the affected point. In contrast, the radial displacement further away from the pile are continuously increasing with increasing penetration depth at all depths. Furthermore, the shape of the displacement patterns is changing from appearing as an "S"-like shape close to the pile to a wedge that has decreasing displacement with depth further away form the pile. This transition in shape of the resulting displacement patterns seems to be occurring at a similar distance from the pile to where the continuous vertical penetration is not leading to further radial displacements. Following the initial outward movement during pile installation, an substantial inward movement due to consolidation is present at all radial locations.

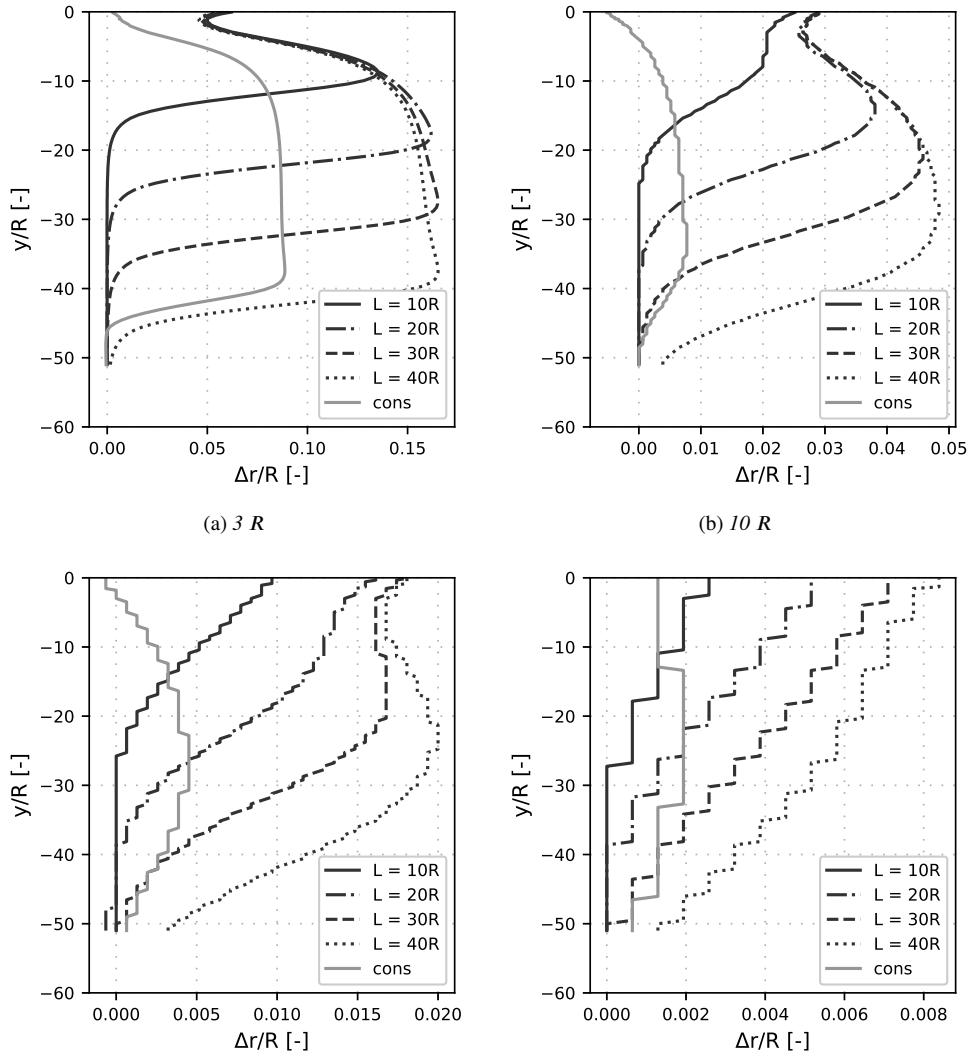

(a) *3 R*

(b) *10 R*

(c) *20 R*

(d) *40 R*

Figure 4.3: *Evolving radial displacements from pile installation and subsequent consolidation at four inclinometer locations (vertical cross sections) located at an initial radial coordinate of 3 R, 10 R, 20 R, and 40 R.*

4.4 Bellowhose

Vertical displacements in the same vertical cross sections (bellowhose) as previously used for the radial displacements is presented in Figure 4.4. As for the displacement path for individual particles, vertical displacement in the vicinity ($3R$) of the pile is strongly influenced by the vertical location. Soil within a vertical distance of $9R$ from the surface experience an heave, while deeper soil is pushed downwards. Similarly to the horizontal displacements, the vertical displacements close to the pile are not strongly influenced by further penetration below the soil depth. At a distance of $9R$ from the pile, the vertical movement is essentially upwards at all depths, except for small areas located below the current position of the pile. Further away from the pile, all movement is in the upward direction and is increasing at all depths with the continuous pile penetration. Vertical movement due to consolidation is predominately downwards at all distances from the pile except at locations very close to the tip of the pile where some heave occurring due to the consolidation.

4.5 Movement in a horizontal cross section

In addition to inclinometers and bellow-hoses, the displacements are presented along two horizontal lines, one shallow (Figure 4.5) and one deep (Figure 4.6) giving continuous displacement profiles at two depths between the horizontal cross sections. In addition to supporting trends previously discussed, some phenomena is appearing more clearly. Both the vertical and radial displacements are approximately halved when the distance from the pile is doubled. As previously indicated, but now appearing much clearer, is how the displacement close to the pile is almost unaffected by the continuous pile penetration in contrast to soil further away than about $9R$ from the pile, which is increasingly displaced in both the radial and vertical direction with increasing penetration. It is also worth noting that the movement of the shallow soil very close to the pile is downwards in contrast to the rest of the upwards displacing soil. A net downward displacement is found in the shallow cross section for soil located between $1R$ and about $20R$ from the pile after full consolidation.

4.6 Key results

The magnitude and extent of the displacements in the soil resulting from pile installation is strongly influenced by the radius of the pile and the length of the pile. The radius governs the deformation behaviour close to the pile while the penetration depth, *i.e.* embedded length of the pile, dominates the response at larger distances from the pile. The shape of the displacements in the vertical cross sections seem to be changing from a curve to a inclined straight line at a similar distance as for the transition from a displacement field most influenced by the radius instead of the pile length. The consolidation of excess porewater pressures leads to a reversed displacement trajectory when compared to the trajectories during pile installation. Consolidation displacements are significant, and might even lead to a net downward movement for soil close to the pile.

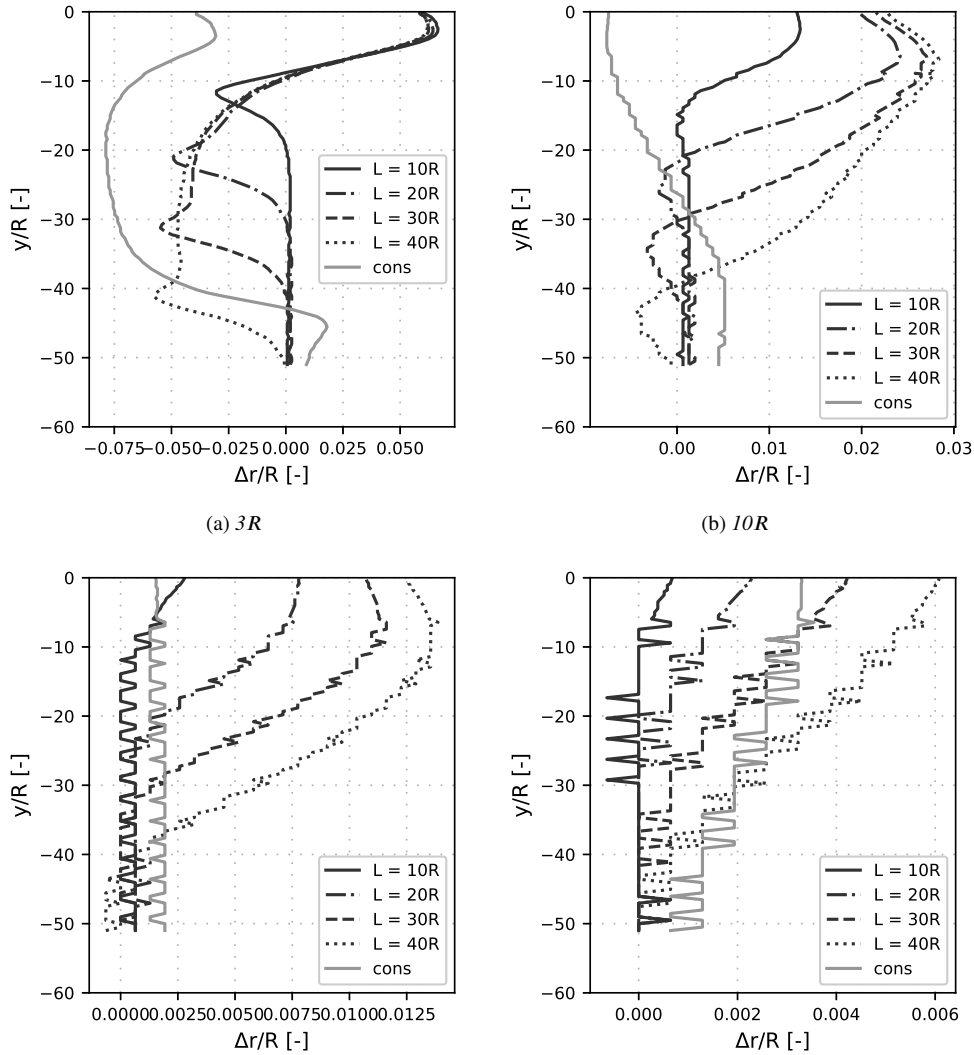

(a) *3R*

(b) *10R*

(c) *20R*

(d) *40R*

Figure 4.4: *Evolving vertical displacement from pile installation and subsequent consolidation at four vertical cross sections located at a radial coordinate of 10R, 20R, 30R, and 40R.*

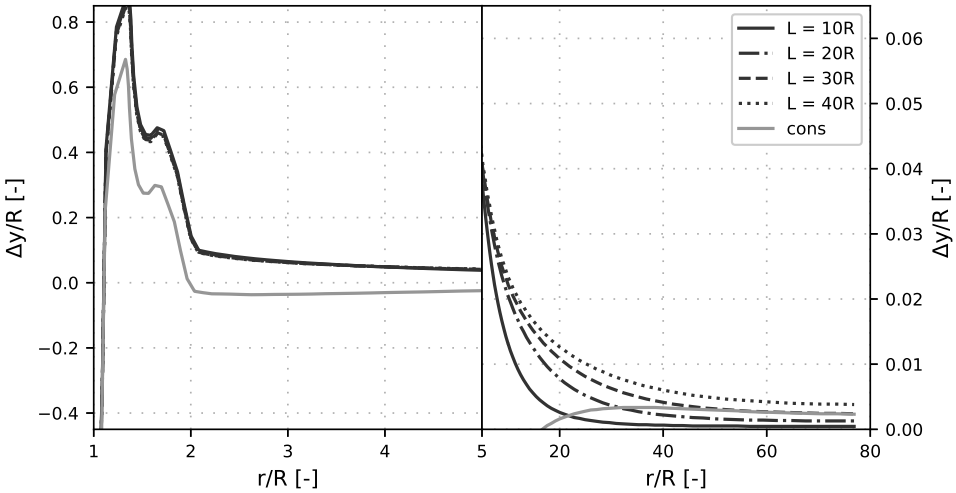

(a) *Vertical displacement*

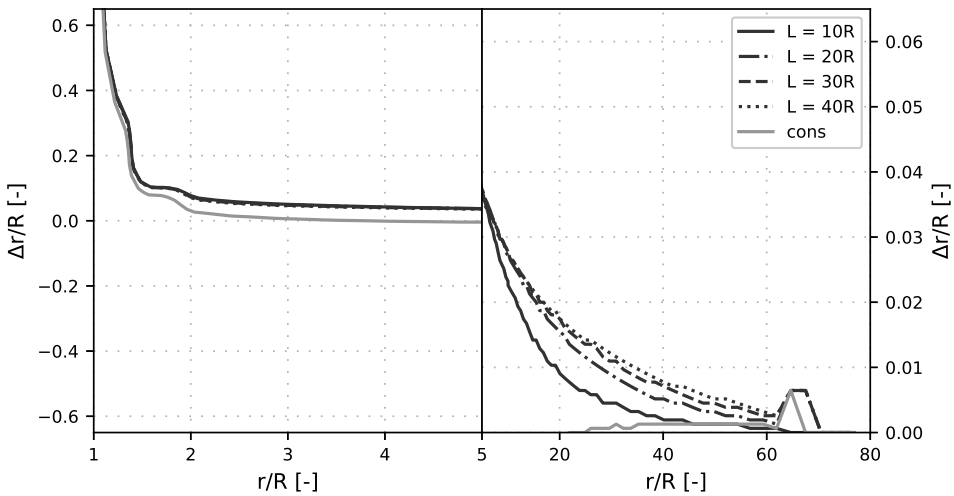

(b) *Radial displacement*

Figure 4.5: *Evolving vertical (a) and horizontal (b) displacements from pile driving and subsequent consolidation in a shallow (-**R**) horizontal cross section.*

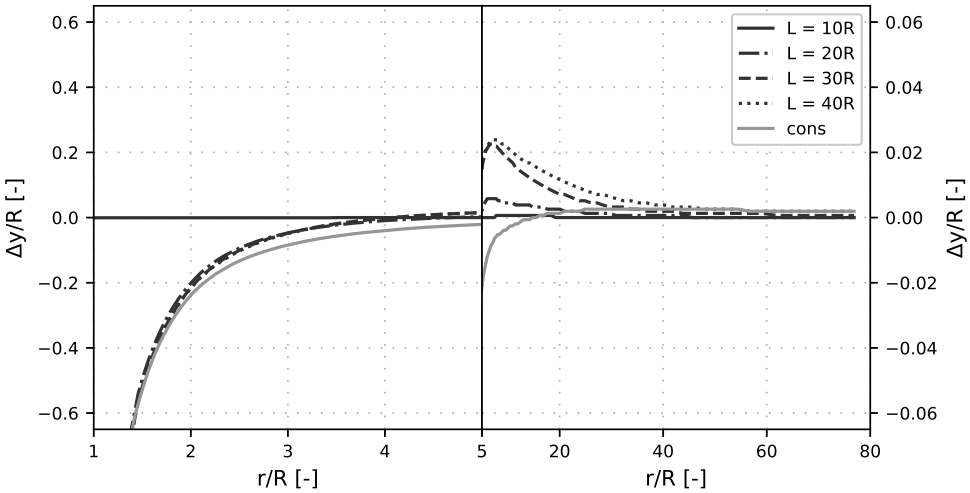

(a) *Vertical displacement*

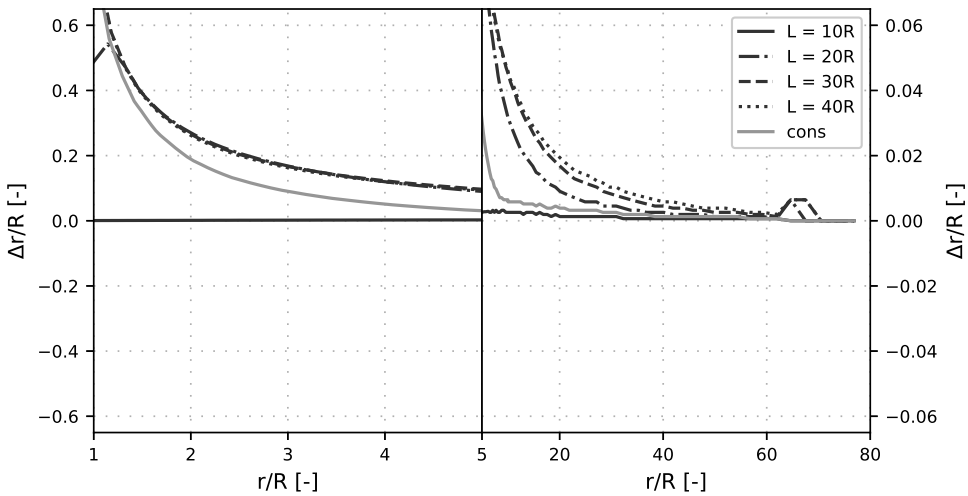

(b) *Radial displacement*

Figure 4.6: *Evolving (a) vertical- and (b) radial displacements from pile driving and subsequent consolidation in a deep (-19R) horizontal cross section.*

5 Influence of soil properties on the mass displacement due to piling in natural soft clays

This chapter investigates the impact of soft soil features, such as anisotropy and destructuration (loss of structure in sensitive clay) on the resulting mass displacement from pile installation. Initially, the sensitive and anisotropic reference case established in Chapter 4 will be compared to an isotropic and an anisotropic clay without any bonding. The latter two cases are modelled using the Modified Cam Clay model (MCC) and the SCLAY1 model. Due to the model hierarchy the parameters derived for Utby clay will be used, as the focus in this study is on the impact of anisotropy and sensitivity.

In addition, a Global Sensitivity Analysis was performed to investigate the impact of different soil properties on the resulting mass displacement directly after installation and after consolidation. The sensitivity study is performed using an experimental design with two level fractional factorial design. This ensures a reliable result with a limited number of numerical simulations.

5.1 Displacement paths

The full displacement paths during pile installation and consolidation for the three different clays are presented for 4 shallow post points (Figure 5.1) and 4 deep (Figure 5.2). Here, a large difference in response is found between the sensitive clay and the two clays without sensitivity. However, slightly further away ($>3R$) the results between the two anisotropic clays converge towards to a similar response with a slightly higher vertical upwards displacement compared to the isotropic clay. Radial movements are very similar for all three clays directly after pile installation. After consolidation, the magnitude of the displacements increased in the anisotropic clays compared to the isotropic clay, with an additional increase due to the sensitivity. The displacements in the soil deeper down in the deposit after installation are very similar directly after installation. In contrast, the consolidation movement is increasing with both anisotropy and sensitivity, which is similar to the shallow consolidation movements.

5.2 Inclinometers

Figure 5.3 shows the radial displacement in 4 vertical cross sections (inclinometer) after installation, and subsequent consolidation. At all distances from the pile, the radial movement after pile installation is very similar for all of the three clays. However, the magnitude of the consolidation movement toward the pile is differing, where the largest movement is found for the sensitive clay and the smallest for the isotropic clay. At $3R$, the radial consolidation movement for the isotropic and anisotropic nonsensitive clays are similar, while the consolidation movement for the anisotropic clay at $10R$ is considerably higher. All three clays show a similar trend in how the shape of the displacement is changed with the increasing radial distance from the pile.

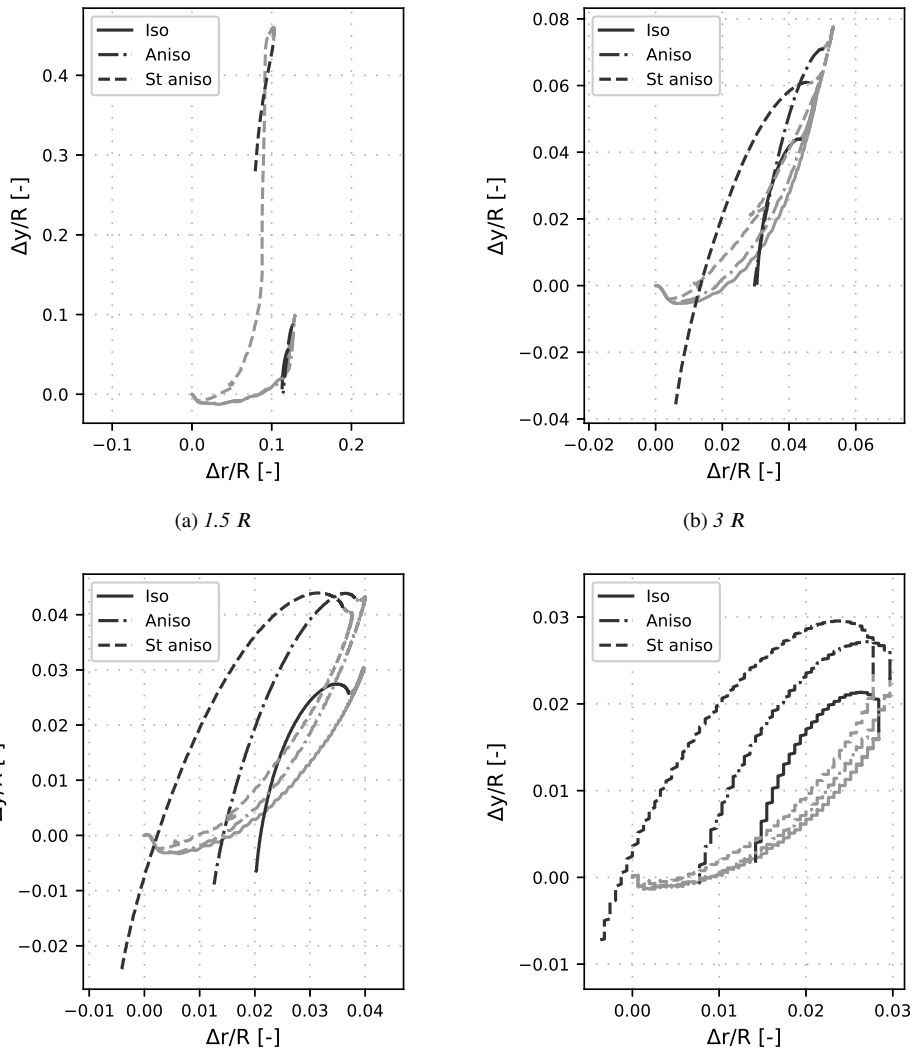

(a) *1.5 R*

(b) *3 R*

(c) *5 R*

(d) *10 R*

Figure 5.1: *Shallow displacement in the soil at a depth of R, normalised with the pile radius R, after installation (light) and consolidation (dark) for an isotropic clay (Iso), an anisotropic clay (Aniso) and a sensitive anisotropic clay (St aniso).*

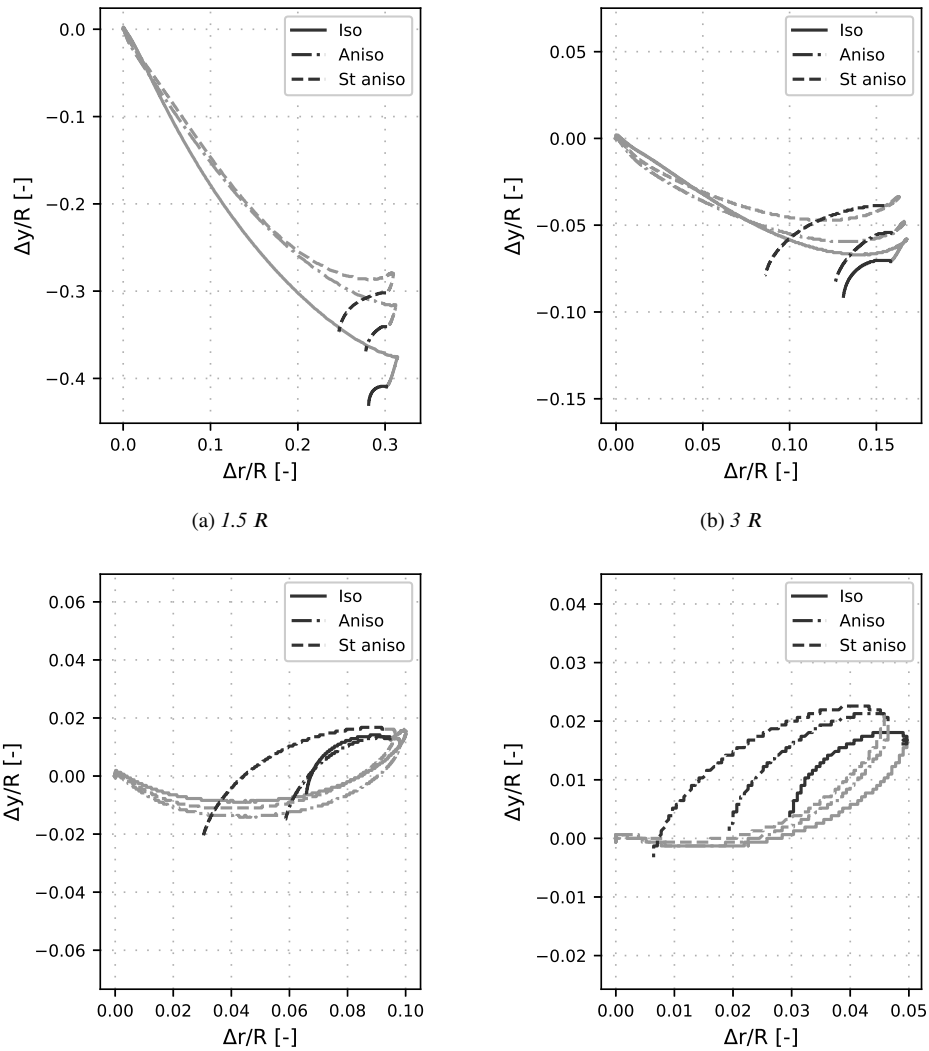

(a) *1.5 R* (b) *3 R*

(c) *5 R* (d) *10 R*

Figure 5.2: *Deep displacement in the soil at a depth of 19R, normalised with the pile radius R, after installation (light) and consolidation (dark) for an isotropic clay (Iso), an anisotropic clay (Aniso) and a sensitive anisotropic clay (St aniso).*

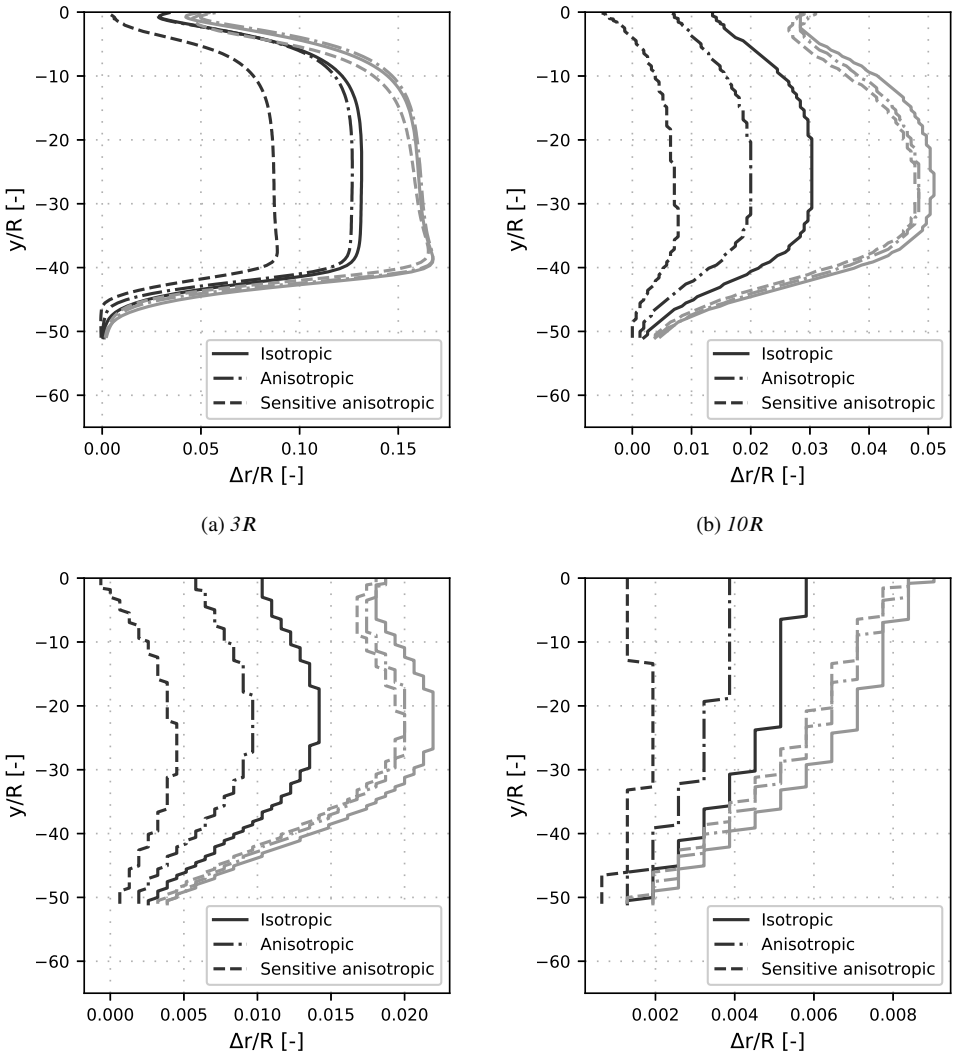

(a) *3R* (b) *10R*

(c) *20R* (d) *40R*

Figure 5.3: *Radial displacement from pile installation and subsequent consolidation for four inclinometers (vertical cross sections) located at a radial distance of respectively 3R, 10R, 20R, and 40R from the pile for an isotropic clay, an anisotropic clay and a sensitive anisotropic clay.*

5.3 Bellowhose

Vertical movement in 4 vertical cross sections (bellowhose) are presented in Figure 4.4. At distance from the pile, the vertical movement is very similar for all three clays, and in agreement with the trends found for the horizontal displacements. Closer to the pile, the vertical displacement is influenced by the difference in constitutive response in the soil, where both the consideration of anisotropy and additional sensitivity are leading to larger upward displacements in the upper part of the soil. Displacements in the soil from consolidation closer to the pile show trends in agreement with previous trends where sensitivity and anisotropy lead to larger consolidation settlements compared to the nonsensitive and isotropic counterpart.

5.4 Horizontal cross section

The radial and vertical displacements along a shallow horizontal cross section at depth R for the three different clays is presented in Figure 5.5. Similar vertical displacements are found at a distance of about $20R$ from the pile considering displacements directly after pile installation, while the upward displacement closer to the pile is larger for the two anisotropic clays when compared to the isotropic clay. The two clays considering anisotropy show a similar upward response with the exception of very close to the pile, where the sensitive soil exhibits a substantially larger vertical upward displacement. Vertical movement after consolidation is very similar in between the isotropic and anisotropic clay, while the sensitive clay show considerably larger downward movement until a radial distance from the pile of about $40R$, where all models show a similar consolidation response. The shallow radial movement after installation is very similar between the clays. However, the consolidation movement is different for all the three clays, with the largest displacements for the sensitive clay and the smallest for the isotropic clay.

The displacements for soil in a horizontal cross section located at a depth of $19R$ is found in Figure 5.3. Downward vertical displacement is appearing close to the pile and is changing to an upward direction at a distance of about $4R$ from the pile, displacement in the isotropic clay is lower when compared to the two anisotropic clays. Radial movement is very similar in between the clays before the consolidation. In contrast, the displacement after consolidation is considerably increased when considering first anisotropy followed by sensitivity. However, at a distance of $40R$ from the pile, the consolidation settlement is close to being equal for the three soils.

5.5 Remaining displacement after consolidation

Figure 5.7 shows the displacements after consolidation normalised with the displacement directly after full pile installation for a number of vertical cross sections. This gives an indication of the fraction of the initial displacements that are irreversible after consolidation for the radial and vertical displacements, respectively. A general trend, in agreement with previous results, is that the consolidation is increasing with the presence of anisotropy and additionally when sensitivity is included. However, the vertical movement far away from the pile ($40R$) shows a very similar ratio of persistent deformations for all of the three clays (soil models).

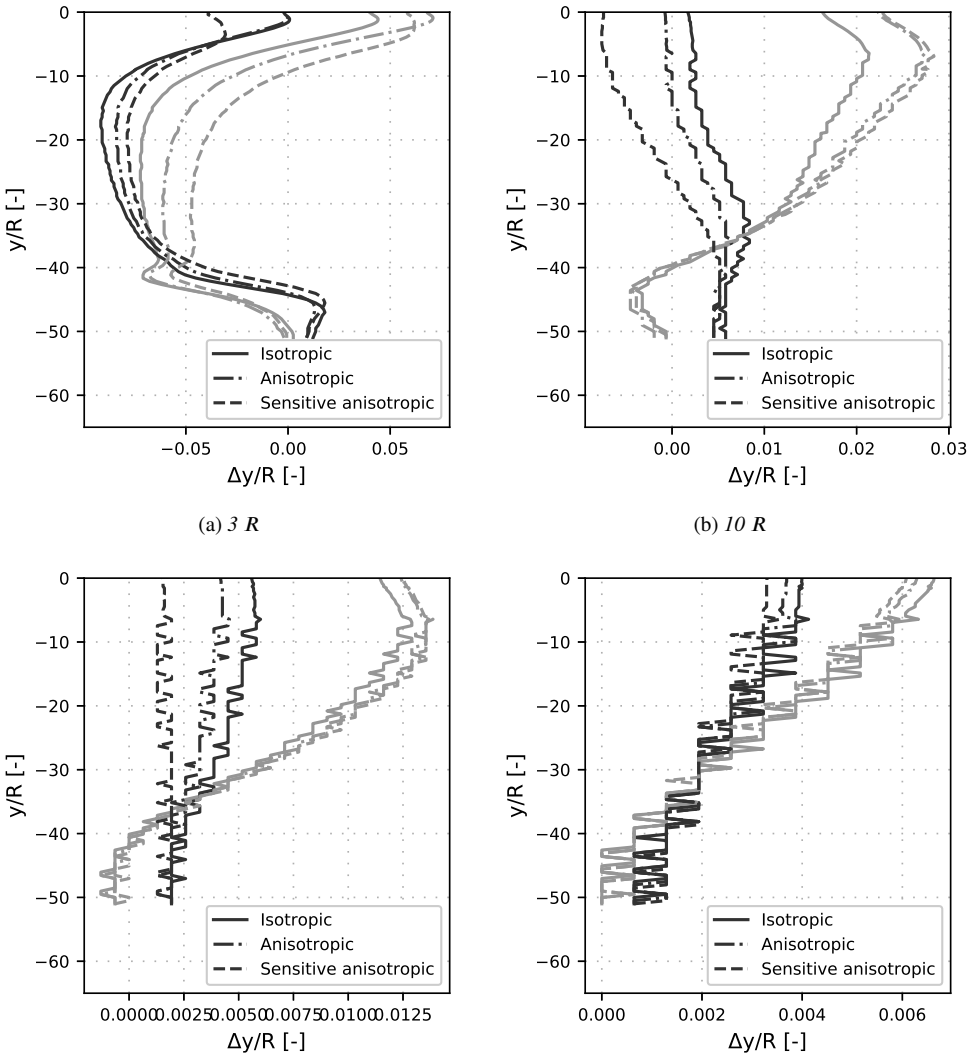

(a) *3 R* (b) *10 R*

(c) *20 R* (d) *40 R*

Figure 5.4: *Vertical displacement from pile driving and subsequent consolidation in four vertical cross sections located at a radial coordinate of 3R, 10R, 20R, and 40R for an isotropic clay, an anisotropic clay and a sensitive anisotropic clay.*

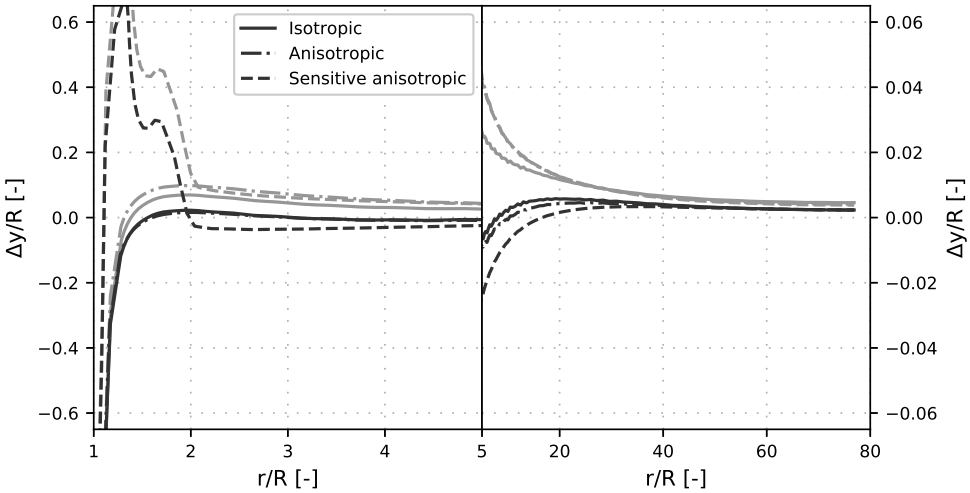

(a) *Vertical displacement*

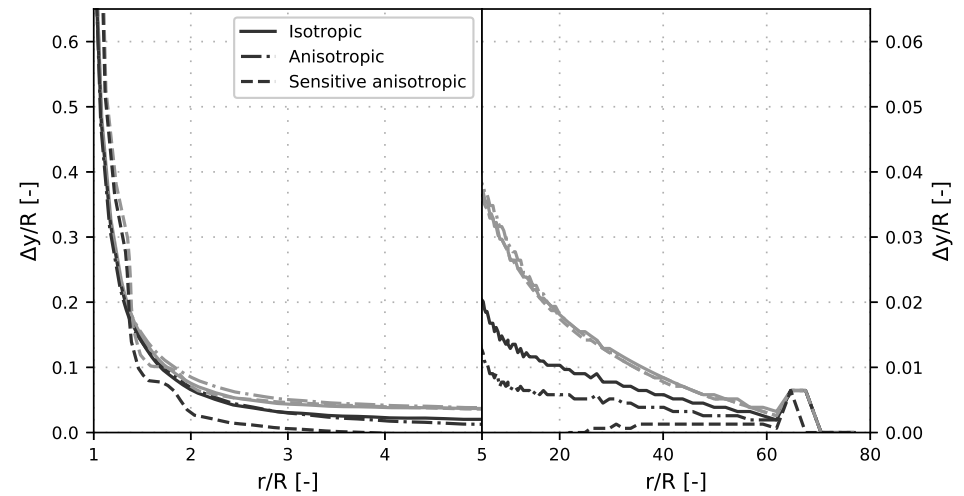

(b) *Radial displacement*

Figure 5.5: *Evolving vertical (a) and horizontal (b) displacements from pile driving and subsequent consolidation in a shallow (-**R**) horizontal cross section.*

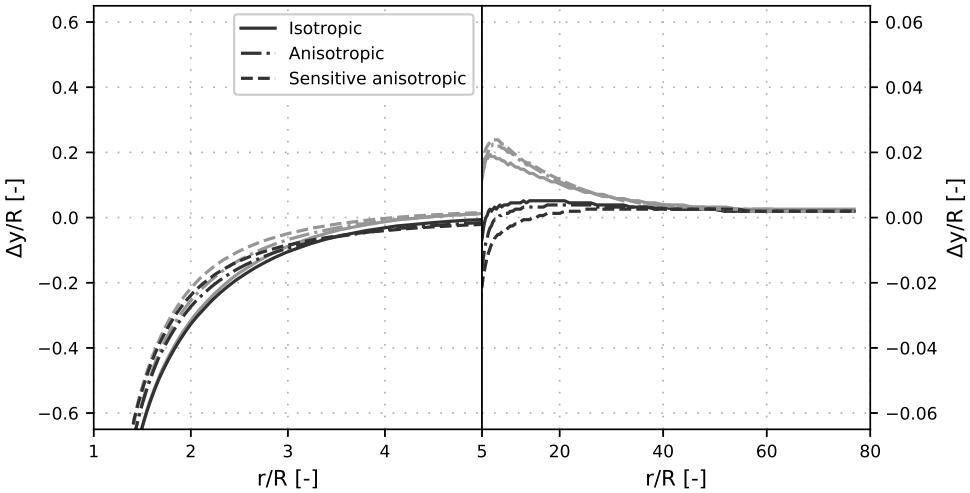

(a) *Vertical displacement*

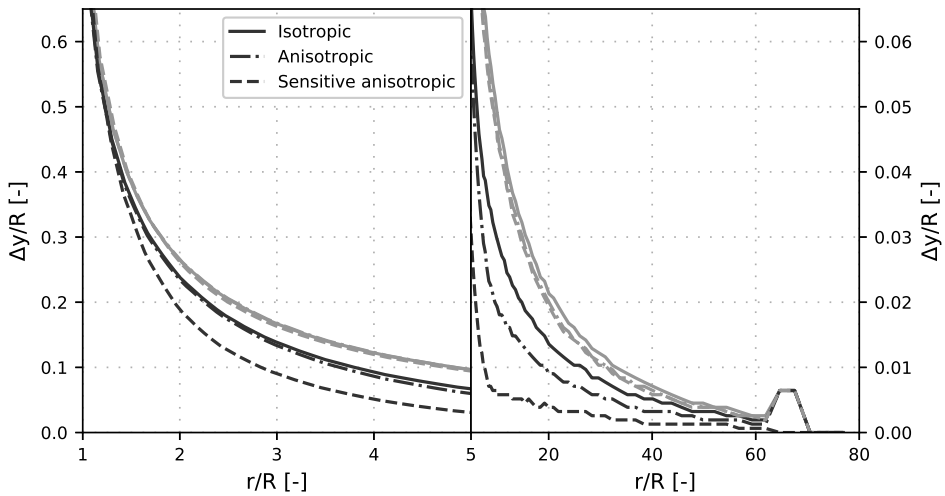

(b) *Radial displacement*

Figure 5.6: *Evolving vertical (a) and horizontal (b) displacements from pile driving and subsequent consolidation in a deep (-19R) horizontal cross section.*

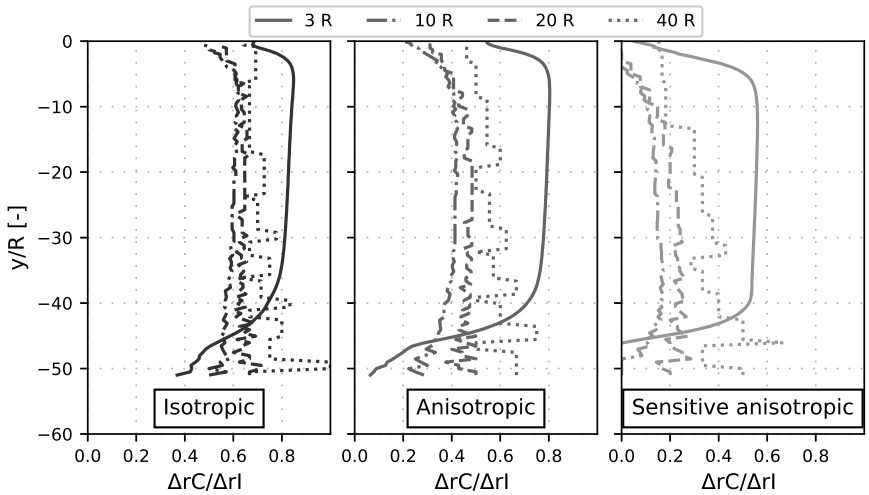

(a) *Radial*

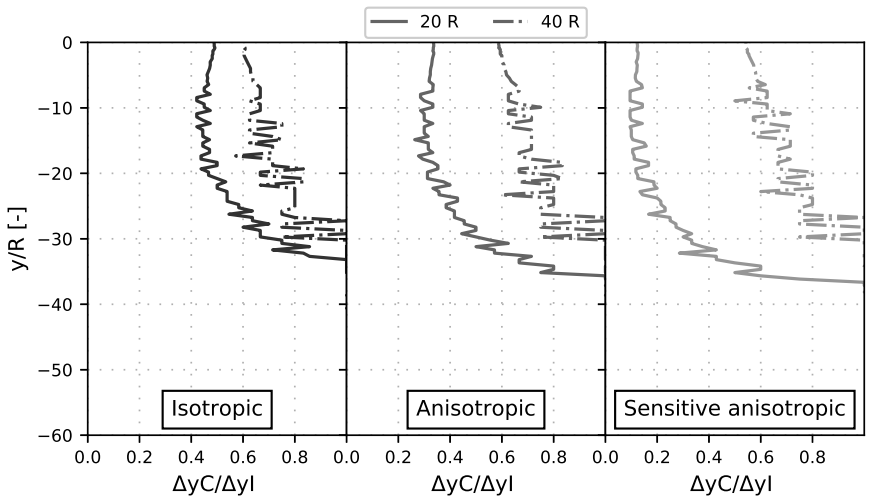

(b) *Vertical*

Figure 5.7: *Remaining radial and vertical displacement after consolidation in vertical cross sections. Displacement after consolidation is normalised with the displacement after installation*

Table 5.1: Normalised radial coordinate of where the soil volume passing through a shallow vertical cross section, at depth R, corresponds to 25% and 50% of the total installed pile volume. The total volume of soil that is displaced through the shallow vertical cross section after installation $V_{s,i}$ and consolidation $V_{s,c}$ is also included. Both volumes are normalised with the total pile volume below the cross section V_{pile}.

Analysis	25% of V_{pile} [r]	50% of V_{pile} [r]	$V_{s,i}/V_{pile}$	$V_{s,c}/V_{pile}$
Isotropic	$27.7R$	$44.7R$	0.972	0.47
Anisotropic	$22.4R$	$41.0R$	0.978	0.42
Sensitive anisotropic	$19.6R$	$39.3R$	0.985	0.36

5.6 Displaced soil volume

The vertical displacements in Figure 4.5 are recalculated into a measure of volume in the axisymmetric domain, with consideration of the fact that movement further away from the pile is corresponding to movement in a larger soil volume compared to close to the pile. The radial location of where the accumulated soil volume passing through the cross section is respectively 25% and 50% of the installed pile volume, is presented for the three different clays in Table 5.1. The normalised volume of displaced soil reaching the surface is very close to being equal to the installed pile volume, which indicates that the soil is displacing with constant volume. Remaining normalised volume after consolidation range from about 50% for the isotropic clay to about 35% for the sensitive clay. Displaced soil volumes seem to be reaching the surface closer to the pile for the sensitive clay at $19.6R$ compared to the nonsensitive clay at $27R$, with the anisotropic clay once again at in between the other two clays. This trend is observed for the radial location of where both 25% and 50% of the soil has reached the surface.

Additionally, the horizontal displacements presented in Figure 5.3 are also recalculated into a volume by again considering that the soil movement further away from the pile is corresponding to a larger volume in the axisymmetric formulation. The displaced volume, normalised with the total pile volume installed, is presented in Table 5.2 both directly after pile installation, as well as after consolidation. The difference in displaced volume directly after installation for the three clays is localised within $5R - 10R$ from the pile and remains constant at larger distances further away from the pile. The presence of anisotropy and sensitivity leads to smaller horizontal displaced soil volume compared to an isotropic (-3%) and nonsensitive clay (-8%). This finding is in line with the larger vertical displacements found close to the pile, since the soil is displaced under constant volume. The reduction of displaced soil volume due to equalisation of excess porewater pressure is smallest for the isotropic clay, followed by the anisotropic clay, and largest for the sensitive isotropic clay at all radial locations. The differences between the displaced soil volume in different clays are considerably larger after dissipation of excess porewater pressures from installation, when compared to the differences between the models directly after installation.

Table 5.2: Total soil volume displaced through a series of inclinometeres (vertical cross sections). Volumes are normalised with the total installed pile volume, V_{pile}. The results are for each cross section presented both after installation (I) and after consolidation (C).

Analysis	$3R$	$5R$	$10R$	$20R$	$40R$
	I / C	I / C	I / C	I / C	I / C
Isotropic	1.02 / 0.81	0.99 / 0.65	0.99 / 0.58	0.88 / 0.56	0.61 / 0.43
Anisotropic	1.03 / 0.78	0.98 / 0.78	0.94 / 0.37	0.82 / 0.37	0.56 / 0.31
Sensitive anisotropic	0.98 / 0.50	0.94 / 0.27	0.91 / 0.11	0.79 / 0.14	0.53 / 0.15

Table 5.3: Range of parameters used in the two level fractional factorial sensitivity analysis for the modelling of pile installation into a sensitive anisotropic clay.

Parameter	Mean	-	+
κ	0.02	0.018	0.022
λ_i	0.108	0.0972	0.1188
χ_0	5	4.5	5.5
ω	30	27	33
a	9	8.1	9.9
b	0.4	0.36	0.44
OCR	1.45	1.305	1.595
M	1.56	1.404	1.716

5.7 Sensitivity study - Design of experiments

In addition to investigating the emerging response by completely excluding or including anisotropy and sensitivity in the analysis, a Global Sensitivity Analysis (GSA) was conducted to discover the most important parameters influencing the emerging displacement from displacement piles in an anisotropic sensitive clay. The study was performed by applying the two-level fractional factorial design method described in Chapter 3. The parameters and ranges considered in the SA are presented in Table 5.3 where the - and + values will be used for the sensitivity simulations giving an indication of the response around the mean value. The Experimental design was chosen as a resolution IV fractional factorial design giving in total $2^{8-4}_{IV} = 16$ realisations. The choice of using a level IV resolution instead of the full factorial design reduce the number of simulations from 256 to 16. The combination of low and high values of the analysis for the 16 simulations is presented in Table 5.4.

A simple quantification of the mass displacement need to be used in the GSA. The first measure of the mass displacement is the radial coordinate of where the accumulated soil passing through a shallow vertical cross section corresponds to 25% and 50% of the installed pile volume, previously used in Table 5.1. Second, the mass displacement will be quantified as the volume of soil that is passing through a series of inclinometers, the quantity was previously used in Table 5.2.

Figure 5.9 shows the GSA results for the amount of soil volume normalised with the pile volume that is passing a series of vertical cross sections at a distance of ($3R$, $10R$, $20R$ and $40R$). The results are given for both directly after installation and after subsequent consolidation. The effect, *i.e.* change in response, from changing each parameter from the min to max value on the

Table 5.4: Table of contrast presenting the combination of parameters used for the 16 analyses needed for the two level fractional factorial experimental design 2^{8-4}_{IV} sensitivity analysis.

Run no.	κ	λ_i	χ_0	ω	a	b	OCR	M
1	-	-	-	-	-	-	-	+
2	+	-	-	-	+	+	-	-
3	-	+	-	-	+	-	+	-
4	+	+	-	-	-	+	+	+
5	-	-	+	-	-	+	+	-
6	+	-	+	-	+	-	+	+
7	-	+	+	-	+	+	-	+
8	+	+	+	-	-	-	-	-
9	-	-	-	+	+	+	+	-
10	+	-	-	+	-	-	+	+
11	-	+	-	+	-	+	-	+
12	+	+	-	+	+	-	-	-
13	-	-	+	+	+	-	-	+
14	+	-	+	+	-	+	-	-
15	-	+	+	+	-	-	+	-
16	+	+	+	+	+	+	+	+

response, *i.e.* amount of soil passing the cross section, is normalised with the total absolute effect for the specific study. A negative response indicates that the total volume of soil passing through a cross section is decreased when the specific parameter is changed from the - value to the + value. The total effect and the mean response is included at the top of the Figures. A general trend for all of the analyses worth highlighting is that the total effect is low after installation, in comparison to the total effect after installation, indicating that the impact of the soil behaviour, and the parameters controlling those, is strongly increasing after effective stresses start changing during the consolidation in the soil. The most influential parameters on the displacements after consolidation are κ, λ_i, OCR and M.

Figure 5.8 shows the result where the response is chosen as the radial coordinate of where the accumulated soil passing through a horizontal cross section at depth -R is equal to 25% and 50% of the pile volume below the location of the cross section. The effect can be either negative or positive, in this case corresponding to the movement of the normalised radial coordinate where 25% of the pile volume has passed the cross section. Two different pile lengths of $20R$ and $40R$ are included in the analysis. The normalised effect of each of the parameters is stable, except for the influence of M, which is strongly increasing with increased pile length and distance from the pile, *i.e.* the 50% response. The strongest influence is found for the stiffness κ in the overconsolidated (elastic) region and inclination of the critical state angle M, where the decrease in stiffness, *i.e.* increase in κ, leads to the displacement of soil further away from the pile, whilst the increase in M leads to more soil moving upwards closer near the pile.

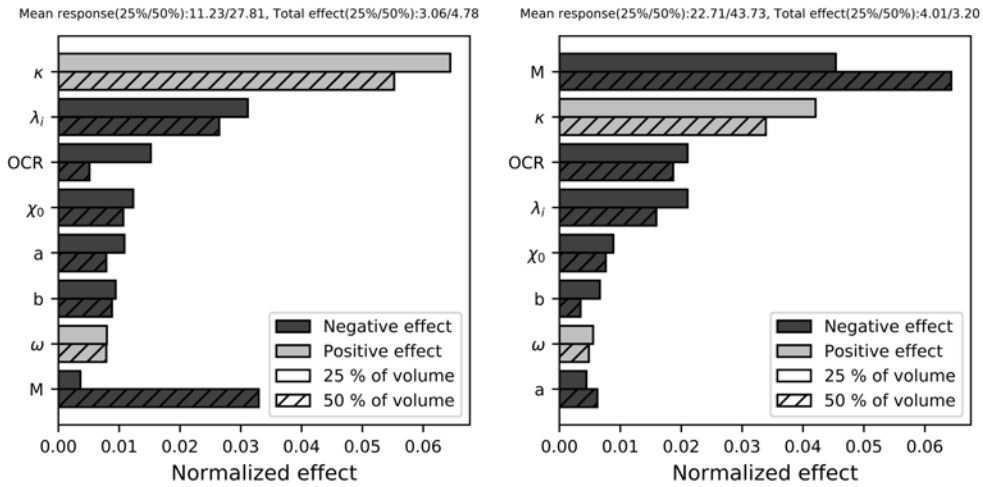

(a) $L = (20R)$ (b) $L = (40R)$

Figure 5.8: *Relative effect of parameters on the mass displacement from piling in an anisotropic sensitive clay.*

5.8 Key results

The comparison of resulting displacements from pile installation in an isotropic clay, anisotropic clay and a sensitive anisotropic clay show that both anisotropy and sensitivity are significantly affecting the response. Both anisotropy and sensitivity lead to a larger amount of the displaced soil that is reaching the surface near the pile, compared to an isotropic and nonsensitive clay. The total amount of soil displaced through a horizontal cross section is very close to the installed pile volume supporting the assumption of constant volume displacement of the soil during pile installation in natural clays with low hydraulic conductivity and with a representative penetration rate. However, the phenomena underpinning the difference in the displacements directly after pile installation are occurring within a radial distance of $10R$ from the pile. At larger distances this is stable, with only a modest difference of about 8% of the installed pile volume. In contrast, the magnitude and extent of displacements during consolidation are strongly influenced by the effective stress driven response of the clay. The sensitive and anisotropic clay shows the largest displacements during consolidation, followed by the nonsensitive anisotropic clay. The isotropic clay shows the smallest displacements due to the consolidation. The sensitivity study generalises these findings, where a considerably larger effect was found for the model parameters after consolidation compared to directly after (undrained) installation. However, the parameters controlling the amount of anisotropy and sensitivity are less influential on the response when compared to the basic parameters that describe stiffness, preconsolidation pressure and strength, *i.e.* κ, λ_i, OCR and M.

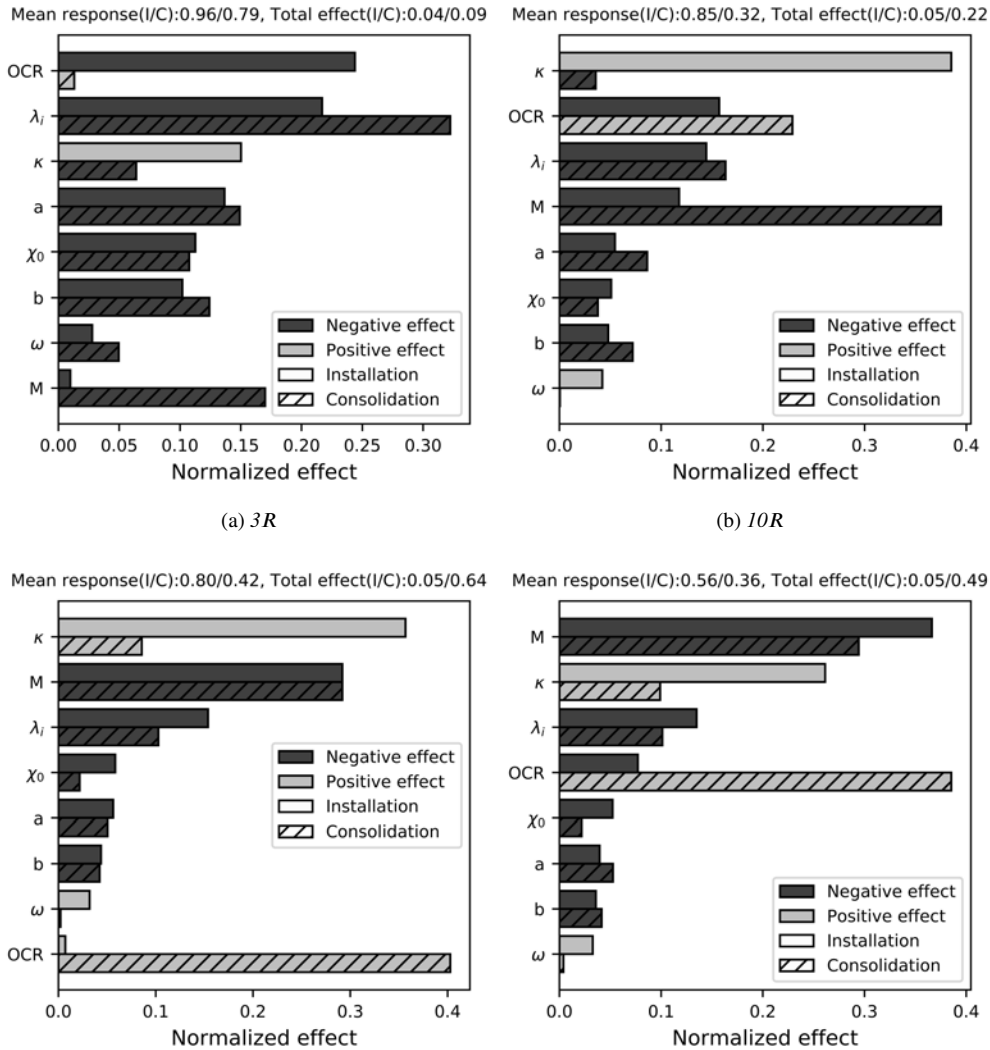

(a) *3R* (b) *10R*

(c) *20R* (d) *40R*

Figure 5.9: *Relative effect of parameters on the mass displacement from piling in an anisotropic sensitive clay.*

6 Benchmark methods for predicting mass displacements from piling

Previous chapters established an understanding of the magnitude and extent of the emerging displacements from installation of a single displacement pile in a soft sensitive clay. The impact of the important soft soil features, such as anisotropy and sensitivity on the displacements was also investigated.

However, the complexity of the numerical reference method and considerable computational effort were required for modelling the installation of a single pile using a 2D axisymmetric domain. This chapter will compare the reference modelling method used in Chapters 4 and 5 with a number of prediction methods that are less complex and not as computationally demanding. The comparison aims to establish an understanding of the results from different modelling methods and assess the merit of each individual method for the prediction of mass displacements from pile installation.

Table 6.1 presents the details of the methods that are benchmarked. The reference case, denoted as SCLAY1S V, established in Chapter 4 was compared to another FE based prediction method that uses the same constitutive model using a numerical cavity expansion method denoted SCLAY1S H. Instead of a gradual vertical penetration of the pile into the domain, the cavity expansion method is introducing the pile by a gradual horizontal displacement applied along the full pre-embedded pile length $L = 40R$. The displacement is starting from the slightly off-set axisymmetric axis and is continued until the pile is expanded to correspond to the pile radius R. Chapter 5 indicates that the impact of the constitutive response of the soil is limited during the undrained installation of a pile in clay. Therefore, two additional prediction methods were included using a total stress formulation and a Poisson's ratio ν of 0.495 to mimic an undrained incompressible behaviour using a total stress formulation, excluding the complex coupled water and soil effective stress formulation. One of the additional simulations used a linear elastic material response (LE H), while the other used a linear elastic perfectly plastic response using a Mohr Coloumb failure criterion (MC H). Two analytical methods, *i.e.* CEM and SSPM were also included to compare with the FE simulations.

Table 6.1: Overview of different modelling methods to predict the mass- displacements from pile installation into soft clay.

Method	Penetration	Stress formulation	Soil behaviour	Consolidation
SCLAY1S V	Vertical	Coupled eff. stress	SCLAY1S	Yes
SCLAY1S H	Horizontal	Coupled eff. stress	SCLAY1S	Yes
LE H	Horizontal	Total stress	LE constant volume	No
MC H	Horizontal	Total stress	LE perfectly plastic, constant volume	No
SSPM	Vertical	-	Constant volume	No
CEM	Horizontal	-	Constant volume	No

6.1 Displacement paths

The displacements paths for the analytical methods of CEM and SSPM are compared with results for SCLAY1S V and SCLAY1S H. Figure 5.1 and Figure 5.2 show the displacements for respectively a shallow and deep point in the soil at different radial distances from the pile. As CEM only considers radial displacements, the displacement path appears to be a overly simplistic as it excludes the vertical component of the displacements. Yet, CEM seems to capture the magnitude of the radial displacements well for the deeper point at all radial distances. The different methods for modelling installation in the FE calculations have a large effect on the response near the pile for all depths. The calculated response of the clay, however, converges with increasing distance from the pile. Close to the soil surface, the direction of the displacements is very similar for the two FE methods and the SSPM method, with exception of the response very close to the pile shaft. At depth, the numerical cavity expansion method predicts a constant upward movement in contrast to the SSPM, and the reference method SCLAY1 V, that both model the penetration process, where an initial downward movement is followed by an upward movement. While the SSPM gives a net upward displacement for soil located at all radial distances from the pile, the SCLAY1 V model gives a net downward movement for soil located up until a a radial distances of 2-4R. Displacements after equalisation of excess porewater pressures, consolidation in the figures, for the two FE methods show a similar displacement direction and magnitude. An unexpected initial inward and upward movement is noticed for the SSPM at larger depths.

6.2 Inclinometers

The displacement in 4 inclinometers located at radial coordinates of $3R$, $10R$, $20R$ and $40R$ are shown in Figure 6.3. In addition to the methods presented using the displacement paths, two additional FE simulations, with an elastic and elastoplastic model respectively, are also included. Initially, it should be noted that all the methods that are compared show displacements at the same magnitude at all different radial locations. The CEM, relying on the assumption that all soil displaces radially, provides an upper limit, which is confirmed from the plotted results. Focusing on the shape of the displacements curves, and excluding the straight line representing the CEM, all of the methods except the linear elastic model show a similar evolving shape with the distances form the pile. SSPM and SCLAY1 V that model the vertical penetration show a more distinct curvy shape compared to when the pile is modelled with only a horizontal expansion.

6.3 Bellowhose

The vertical displacements along 4 vertical cross sections, *i.e.* bellow hose, are presented in Figure 6.4. As seen for the predicted the radial displacements, the magnitude of the vertical displacements are in good agreement for most methods, with exception of the LE FE model. LE FE exhibits a smaller upward movement in the soil within $20R$ compared to the other FE methods. Near the surface, all of the FE models using a failure criterion show a similar response with an upward movement in contrast to the deeper soil layers where only the vertical penetration is showing a net downward movement. While at a distance from the pile of over $10R$, all of these methods show a very similar vertical displacement. SSPM is showing a similar shape as the FE models but are

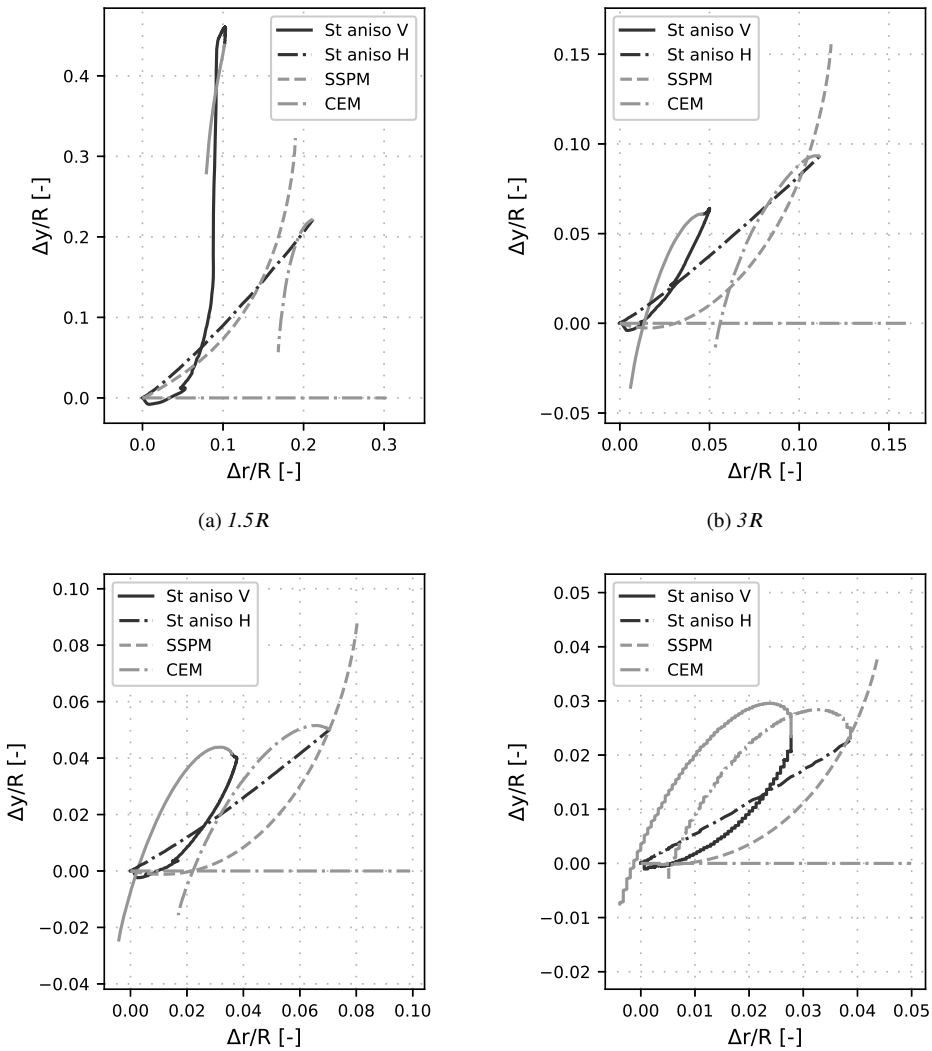

(a) *1.5R*

(b) *3R*

(c) *5R*

(d) *10R*

Figure 6.1: *Comparision of displacement paths for shallow soil at depth 1R below the surface, after installation (light) and consolidation (dark) for a sensitive anisotropic clay using vertical penetration (v) and horizontal expansion (h) compared to SSPM and CEM.*

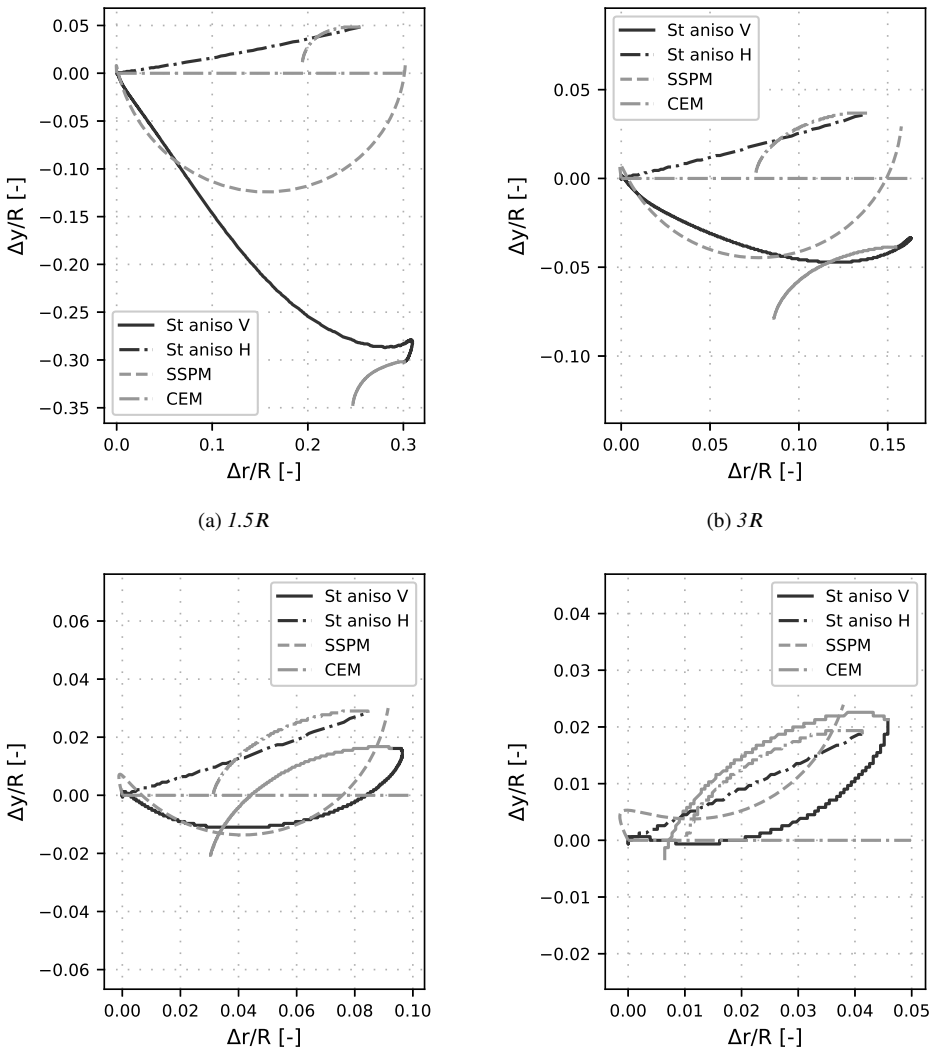

(a) *1.5R* (b) *3R*

(c) *5R* (d) *10R*

Figure 6.2: *Comparision of displacement paths for deep soil at depth 19R below the surface, after installation (dark) and consolidation (light) for a sensitive anisotropic clay using vertical penetration (v) and horizontal expansion (h) compared to SSPM and CEM.*

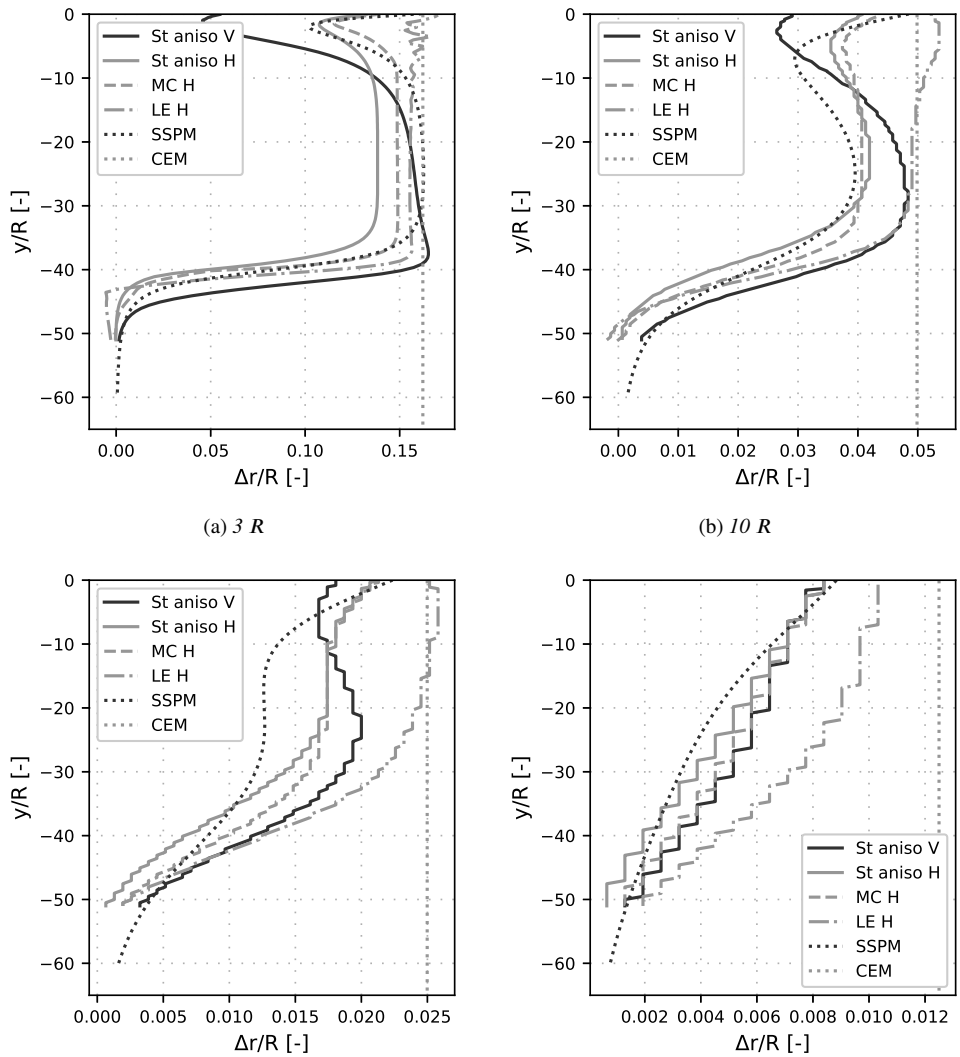

(a) *3 R*

(b) *10 R*

(c) *20 R*

(d) *40 R*

Figure 6.3: *Comparision of horizontal displacement from pile installation for four vertical cross sections located at a radial coordinate of 3R, 10R, 20R, and 40R for a sensitive anisotropic clay (St aniso) for vertical penetration (V) and horizontal expansion (H). Results from a linear elastic (LE H) and a linear elastic perfectly plastic analysis (MC H) as well as CEM and SSPM.*

tending to have a more uniform vertical displacement with depth at a distance far away from the pile in comparison with the other methods whereas an opposite relation is visible close to the pile.

6.4 Movement in horizontal cross section

Figure 6.5 shows the vertical and radial displacements in horizontal cross sections located at a depth R below the surface for all of the 5 modelling methods. The predicted vertical displacements for the FE simulations conducted with model in which the soil can yield and ultimately fail are already very similar at a distance of a few radii from the pile. However, the LE calculations show different behaviour with almost no vertical displacement close to the pile, in contrast to the far field response where the vertical displacement from the LE calculation is larger than the other methods.

The SSPM predicts a larger vertical displacement close to the pile and a smaller vertical displacement at a distance from the pile. The shallow radial displacement predicted by the different methods are showing a larger spread compared to the vertical displacements. The CEM and LE calculation provide show a very similar response until a radial distance of about $30R$, whereas only the CEM provides the upper limit for all simulations and the LE results start to converge with the other FE simulations. A lower limit is formed by the SCLAY1S models until a radial distance of about $35R$, where the results are in line with the results from the two numerical cavity expansion based pile installation methods with a failure criterion in the constitutive model. These two methods are very similar to the radial displacement predicted by SSPM at all radial coordinates.

Displacements in deep horizontal cross sections are presented in Figure 6.6. The predicted radial displacements are very uniform close to the pile for all of the methods. However, at a distance of about $10R$ the LE and CEM solutions are showing larger radial displacements, and at a distance of about $25R$ the CEM is standing out with considerably larger radial displacements compared to the other methods. The vertical displacements at depth are very similar between the different methods, with the reference FE simulation with vertical penetration that is showing a downward movement, in contrast to the upward movement predicted by the other methods. At a radial distance of about $4R$, again with the exception of the LE simulation, a similar result is found.

6.5 Consolidation displacement

In previous chapters, the displacement after pile installation was shown to be similar when considering different types of clay, in comparison to a large difference in displacement found after the excess porewater pressures generated during installation are dissipated. During this equalisation stage an increase in effective stress leads to additional deformations, a form of consolidation where both the total stress and effective stress evolve. The impact of consolidation behaviour in the soil after pile installation on the accuracy of the modelling approach is further studied. Figure6.7 shows the horizontal displacement after installation, and subsequent consolidation in a vertical cross section for the two different installation methods. The corresponding vertical movement is presented in Figure 6.8.

The resulting displacement after consolidation is similar for the two modelling methods: the differences between the methods are not increasing during consolidation when compared

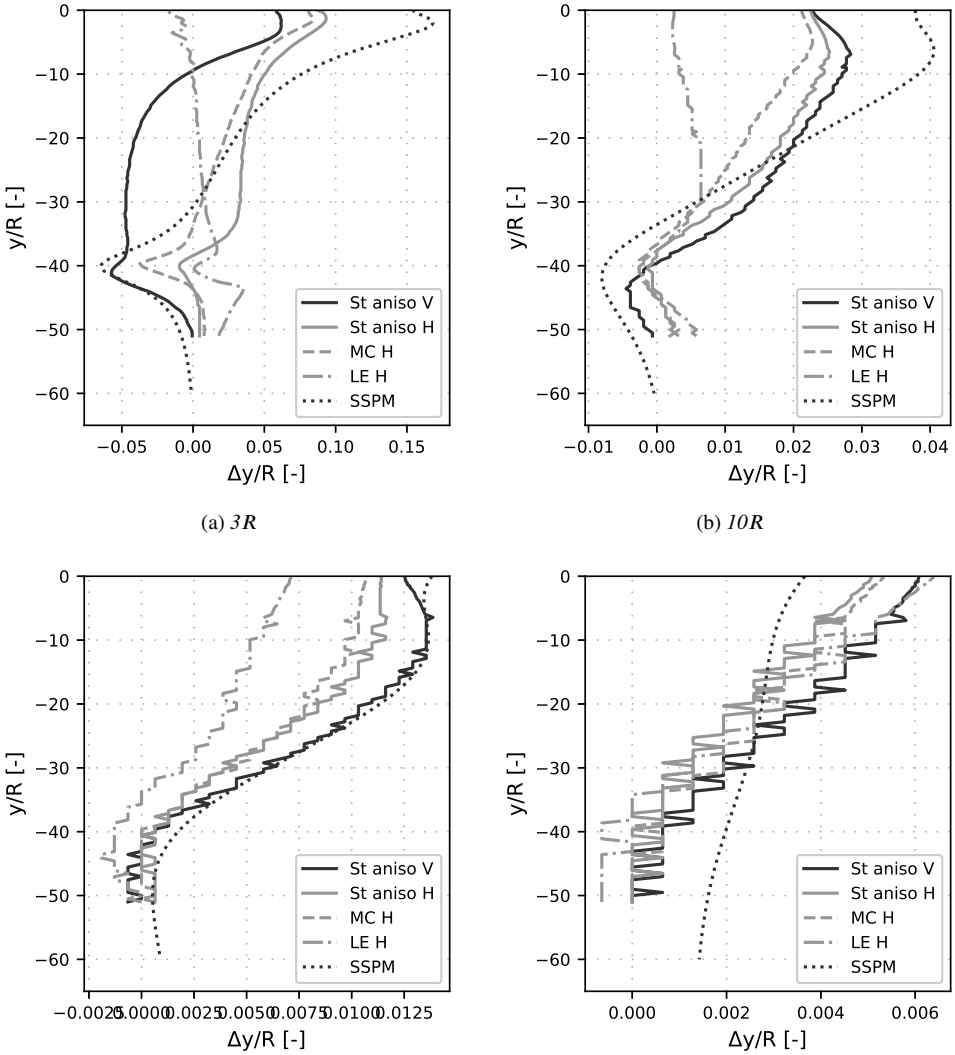

(a) *3R* (b) *10R*

(c) *20R* (d) *40R*

Figure 6.4: *Comparison of vertical displacements from pile installation for four vertical cross sections located at a radial coordinate of 3R, 10R, 20R, and 40R for a sensitive anisotropic clay (St aniso) for vertical penetration (V) and horizontal expansion (H). Results from a linear elastic (LE H) and a linear elastic perfectly plastic analysis (MC H) as well as the CEM and SSPM method are included.*

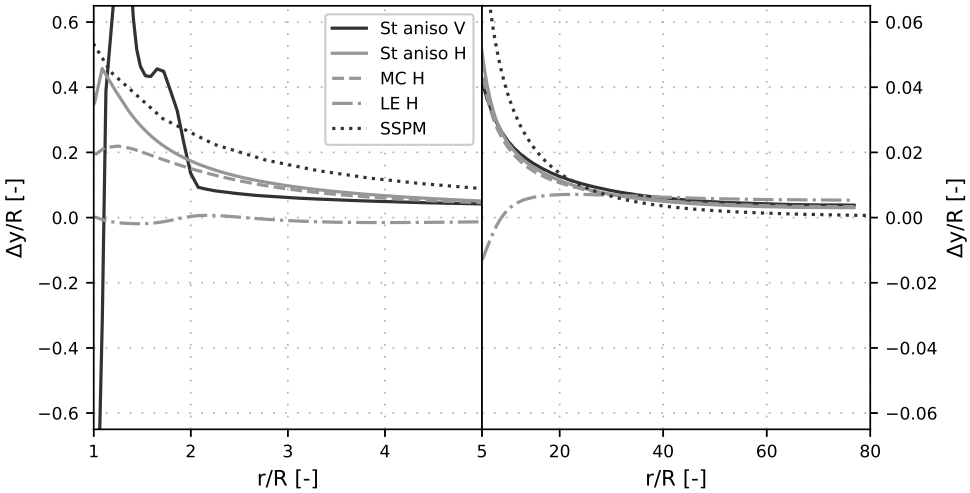

(a) *Vertical displacement*

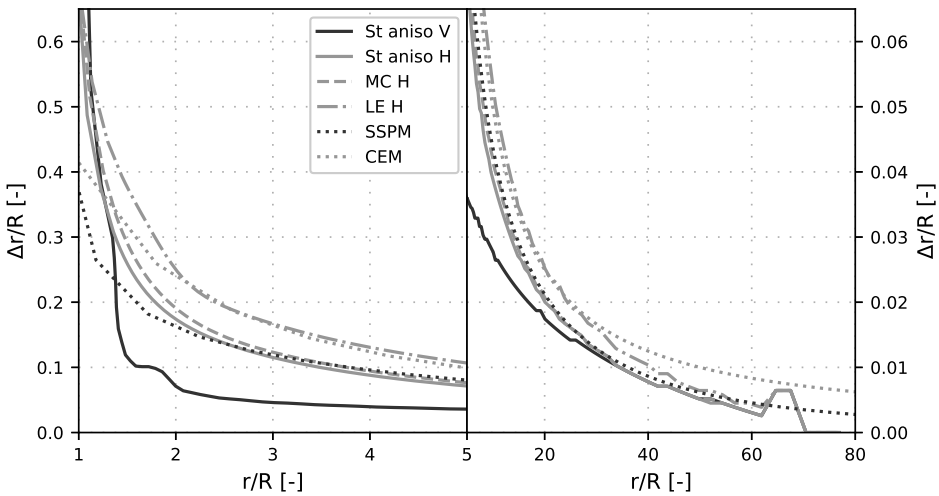

(b) *Radial displacement*

Figure 6.5: *Comparision of evolving vertical (a) and horizontal (b) displacements from pile installation and subsequent consolidation in a shallow (-**R**) horizontal cross section.*

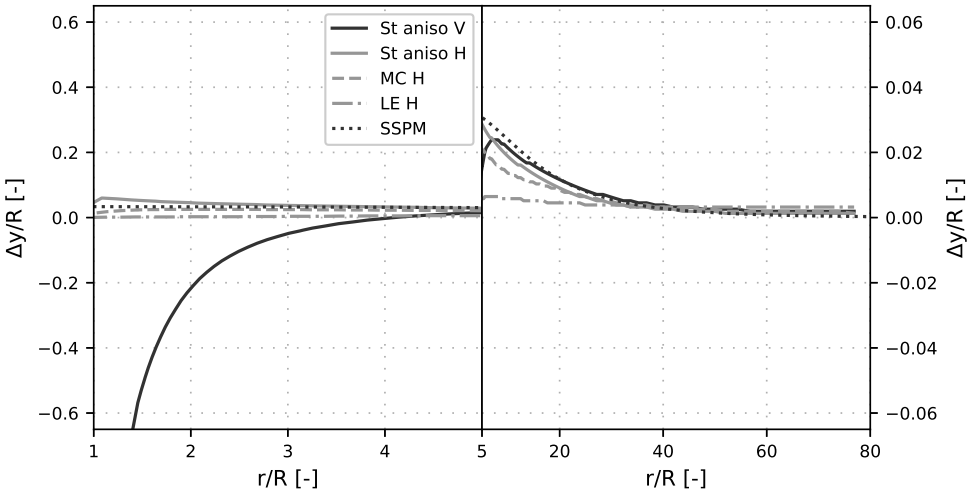

(a) *Vertical displacement*

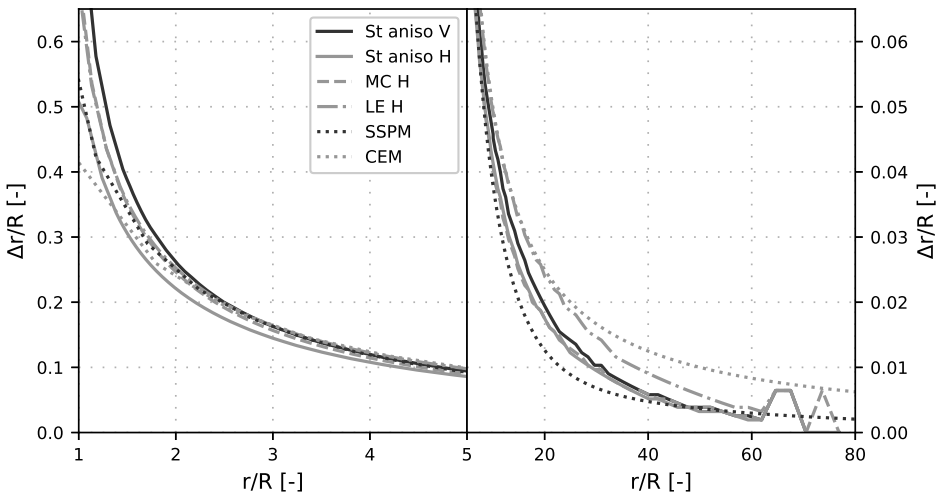

(b) *Radial displacement*

Figure 6.6: *Evolving vertical (a) and horizontal (b) displacements from pile installation and subsequent consolidation in a deep (-19R) horizontal cross section.*

to the displacements directly after pile installation finished. This strongly suggests that both models capture the consolidation process in a similar manner and that the additional displacements resulting from this phase are not significantly affected by the modelling method. The similarity in consolidation response for the two installation methods are further supported by looking at the ratio of remaining vertical and horizontal displacements after consolidation to the corresponding displacement directly after installation for a series of vertical cross sections presented in Figure 6.9. It appears that the choice of modelling method of the pile installation has limited influence on the resulting displacements from the dissipation of excess porewater pressures.

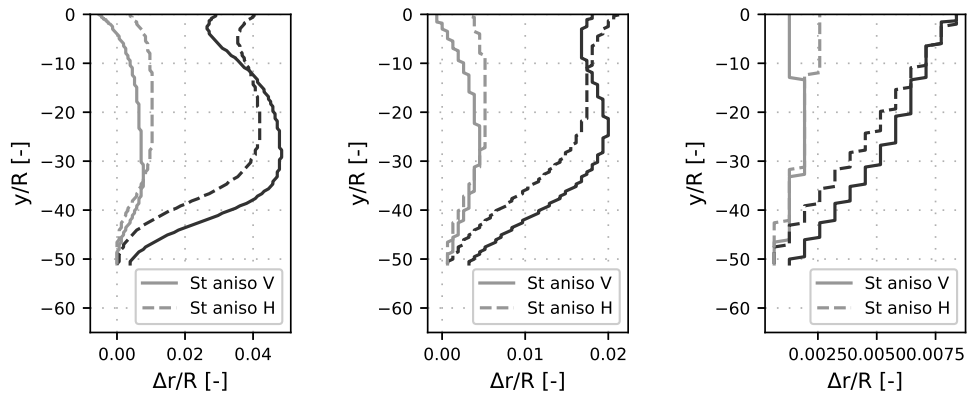

(a) *10R* (b) *20R* (c) *40R*

Figure 6.7: *Comparison of vertical displacement from pile installation four vertical cross sections located at a radial coordinate of 3R, 10R, 20R, and 40R for a sensitive anisotropic clay (St aniso) for vertical penetration (V) and horizontal expansion (H).*

6.6 Key results

The most important finding of this chapter is that all of the compared methods are predicting displacement in the same magnitude and with a similar dependency on the radius. The CEM should be considered as an upper limit for the radial displacements. At a distance far away from the pile the CEM is showing much larger radial displacements compared to the other methods. The SSPM method and the FE calculation using a vertical penetration is capturing the overall behaviour close to the pile with an initial downward movement, and subsequent following upward movement after the pile base has passed the location of the soil.

Compared to the FE calculations, the SSPM show larger vertical displacement close to the pile, and smaller further away from the pile, but generally is in reasonable agreement with the FE calculations using a failure criterion. Assuming plastic flow combined with a total stress formulation and a constant volume constraint leads to results that are comparable during the penetration phase modelled with the FE methods using a coupled effective stress formulation. However, a LE material description seems to be overly simplistic for capturing the finer aspects

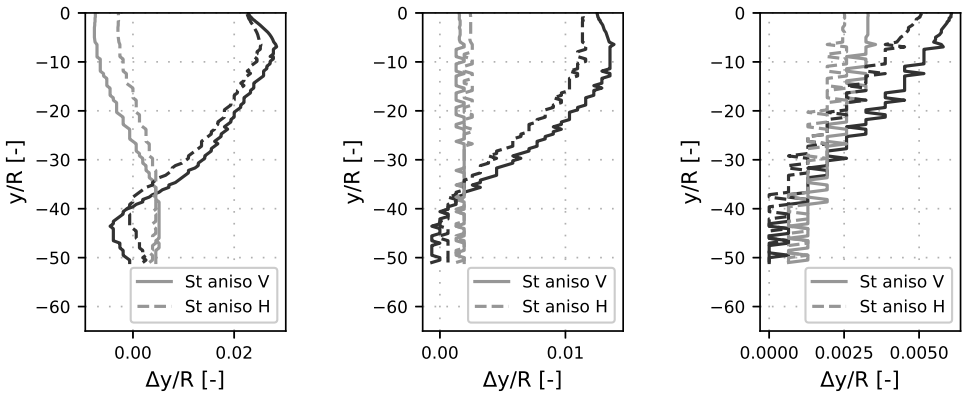

(a) *10R* (b) *20R* (c) *40R*

Figure 6.8: *Comparison of vertical displacement from pile installation four vertical cross sections located at a radial coordinate of 3R, 10R, 20R, and 40R for a sensitive anisotropic clay (St aniso) for vertical penetration (V) and horizontal expansion (H).*

related to the displacements close to the pile. The LE formulation, however, is giving results resembling the other methods further away from the pile. In general, the different methods show a larger spread in results close to the surface, in comparison to results for a soil located deeper down. The displacements after installation and after subsequent consolidation for the two methods considering the dissipation of pore pressures was similar. Although the different in displacement paths for soil located close to the pile is considerable, the two methods are capturing the consolidation process in a similar manner. If the displacements in the close vicinity of the pile are not the focus in the analysis, the (numerical) horizontal cavity expansion methods give results with sufficient accuracy for the mass displacement.

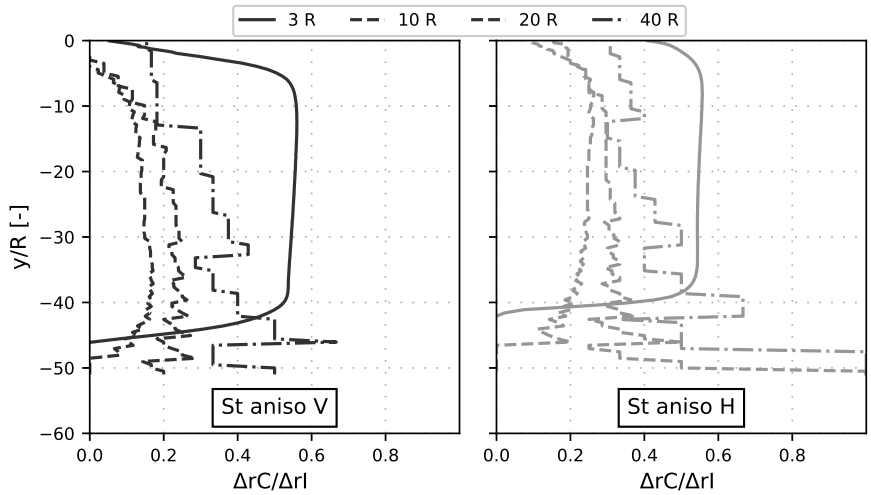

(a) *Radial*

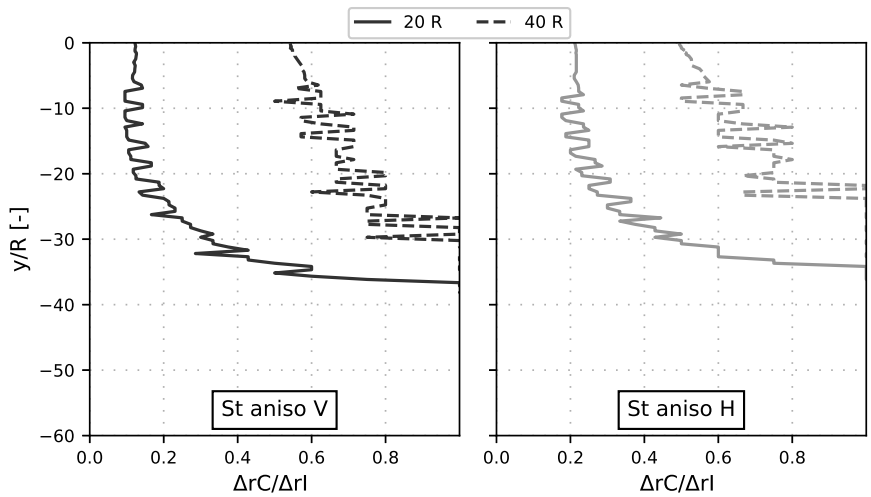

(b) *Vertical*

Figure 6.9: *Remaining displacement after consolidation for vertical cross sections. Displacement after consolidation is normalised with the displacement after installation for radial displacement (a) and vertical displacement (b).*

7 Conclusions & recommendations

7.1 Conclusions

An advanced numerical reference model was developed for the systematic investigation of mass displacements from pile installation in natural clay. The numerical model builds upon an effective stress based constitutive model that is implemented in an Eulerian Finite Element framework for modelling large deformations that also incorporates a coupled formulation for groundwater flow and dissipation of excess porewater pressures. This implementation captures the rate dependent response, *i.e.* ranging from totally undrained to fully drained, emerging from the generation and subsequent dissipation of excess porewater pressures in a deforming soil mass.

In addition to linear elasticity and Mohr-Coulomb, several more advanced constitutive models, such as Modified Cam Clay, SCLAY1 and SCLAY1S, that have increasing fidelity for capturing the behaviour of natural sensitive clay have been used. The model was successfully verified and validated against theoretical solutions, other numerical results reported in literature and experimental data from physical model tests. Furthermore, the anticipated soil behaviour agrees well with the extensive empirical data set on cone penetration testing in soft soils as condensed into the CPT classification system.

The main results focus on assessing the magnitude of mass displacements from pile installation in natural clay. Furthermore, the impact of key soft soil features, such as bonding and anisotropy on the magnitude and extent of the mass displacement was quantified. A fully coupled framework was used, consequently excess porewater pressures were generated and the volumetric response of the clay were initially under constant volume followed by a volumetric compression during the equalisation stage when excess porewater pressures have dissipated. As a result, the undrained response, *i.e.* constant volume, was emerging from the penetration rate and hydraulic properties of the clay, rather than being prescribed to the system.

A clear difference in behaviour was found between the soil movements from shallow and deep installation depths, indicating a transition from a shallow failure mechanism towards a deep mechanism that is more confined. The surface effect is especially pronounced for soil close to the pile, appearing as lower radial displacement and higher vertical displacements compared to the soil displacements at larger depths. The near-surface effect is strongly influencing the displacement patterns down to a depth of about 10 pile radii, after which the magnitude of the radial and vertical displacement is constant down to the full depth of the pile. Another factor affecting the displacement in the soil is the relative distance to the installed pile. Closer to the pile, the ongoing penetration past the depth of interest is not resulting in any additional deformations. In contrast, at a distance from the pile, the displacement is strongly linked to the penetration of additional pile length into the ground. The transition from a close to a far-field behaviour of the displacement field is appearing at a radial distance of about 20 pile radii with a tendency to occur closer to the pile for the vertical component of the displacements.

Constant volume displacement was shown for the isotropic, anisotropic and sensitive anisotropic clay where the displaced soil was equal to the installed pile volume. Increased vertical displacements, however, occurred close to the pile both due to the anisotropy and the sensitivity compared to the isotropic condition, resulting in a concentration of the displaced soil towards the pile with increasing sensitivity and anisotropy in the clay. During the consolidation stage, the dissipation of

excess porewater pressures leads to a contraction in the clay, inducing vertical downward movement and horizontal movement towards the pile, reversing the displacement paths from pile installation. The magnitude of displacements due to the dissipation of excess porewater pressures was strongly influenced by the anisotropy and sensitivity of the clay, where the largest displacements occurred in the sensitive anisotropic clay and the smallest in the isotropic clay.

Although, for the normalised penetration rate investigated, the displaced soil volume is solely controlled by the emerging undrained response of the clay, the distribution of the displaced soil volume was shown to be affected by the constitutive behaviour of the soil. A sensitivity analysis was conducted focusing on quantifying the impact from different model parameters on the distribution of displaced soil volume, both after installation and subsequent equalisation (consolidation) stage. Directly after penetration, the elastic stiffness κ and the slope of the critical state line M were shown to be the most important parameters controlling the distribution of the displaced soil volume. The overconsolidation ratio (OCR) and the intrinsic compression index λ_i also showed to be influential, especially close to the pile. After the dissipation of excess porewater pressures, the same model parameters (soil properties) were shown to be the most important with the highest impact coming from the OCR of the soil.

Two different approaches to model the pile installation using Finite Element Analysis were compared for the anisotropic sensitive clay using a fully coupled formulation. The first approach was modelled as a vertical penetration while the second simplified approach modelled the pile installation as an expanding horizontal boundary (numerical cavity expansion method). Close to the pile, *i.e.* within a distance of about 10 pile radii, the two installation methods gave different displacement patterns. At larger distances, however, the two methods were shown to give similar results indicating that the simplified numerical cavity expansion method is sufficient to predict the magnitude of the displacements at some distance from the pile. In addition, the two installation methods predicted similar displacements after dissipation of excess porewater pressures at all radial distances from the pile. It should be emphasised that the displacements in the soil due to the dissipation of excess porewater pressure can only be captured by an effective stress based model that is incorporated in a coupled hydromechanical Finite Element framework.

The Finite Element based numerical horizontal cavity expansion method was also used with a linear elastic and a linear elastic perfectly plastic soil model. The linear elastic perfectly plastic model response was shown to give good agreement both in magnitude and shape of the deformation measurements compared to the advanced model that incorporates an anisotropic model with destructuration of soil sensitivity. However, the linear elastic simulation was shown to predict larger horizontal and smaller vertical displacement compared to the other FE simulations indicating that the detailed aspects of displacements due to surface effects is not fully captured when a linear elastic response is used for the soil response.

Additionally, the results from the Shallow Strain Path Method (SSPM) and the (analytical) Cavity Expansion Method (CEM) were compared to the FE simulations. The SSPM was shown to predict similar surface dependent deformations as the FE models that have a failure criterion. In addition, the magnitude of the displacement is decreasing with distance at a similar rate as the FE calculations. The displacement path with an initial downward movement followed by an upward movement for the soil close to the pile is captured by the SSPM, although the SSPM predicts larger upward displacements compared to the FE simulation.

In contrast, the CEM which is based on radial deformations only is not suitable to use if the vertical deformations are of any interest. However, the CEM was shown to provide an upper limit

of the radial deformations predicted by the more advanced (numerical) models. In conclusion, the SSPM can be used as a simplified method to predict the undrained deformations due to the installation of piles. The analytical CEM method should be considered as an upper limit to the radial displacement due to pile installation.

7.2 Recommendations for upcoming studies

This research combines the large deformation FE framework with a coupled porewater formulation with an advanced effective stress based constitutive model to investigate the resulting mass displacement from pile installation into natural clays. Some simplifications and limitations, however, have been made along the way. The following points are recommended for further investigation on the impact of pile installation in soft soils:

- The small strain stiffness of natural soils was not considered in this work, given the strong influence of the elastic stiffness on the resulting displacement (especially at large distances from the pile) the impact of small strain stiffness on the resulting displacement fields should be investigated further.
- The impact of pile installation is only studied with respect to displacements. Due to the coupled numerical formulation with an advanced effective stress based constitutive model the change in stress state in the soil due to the pile installation is captured by the model. Further studies should focus on the impact of pile installation on the response of the pile by studying the development of effective stress by the installation, subsequent consolidation and loading of the pile.
- Piles are commonly installed in groups. The possibility to superimpose the resulting displacement field from one pile to account for the installation of pile groups should be examined further. The resulting displacement and the possibility for superposition of the resulting displacement fields from pile groups should be studied for the stage directly after pile installation has finished, as well as after consolidation.
- The driving of closely spaced piles within a pile group will lead to overlapping influence zones of disturbed regions from the individual piles. How this overlap is effecting the drainage condition, stress state and properties of the soil is not trivial and should be investigated further. The influence of the disturbance from installation of multiple piles on the response of both the single pile and the pile group should also be examined.
- Natural soft soils are rate-dependent, the impact of both creep and the intrinsic material rate dependence for larger loading rates should be further investigated.

References

Abu-Farsakh, M., Rosti, F., and Souri, A. (2015). "Evaluating pile installation and subsequent thixotropic and consolidation effects on setup by numerical simulation for full-scale pile load tests". In: *ICanadian Geotechnical Journal* 52(11), pp. 1173–1746. DOI: 10.1139/cgj-2014-0470.

Azzouz, A. S. and Morrison, M. J. (1981). "Field measurements of model pile in two clay deposits". In: *Journal of Geotechnical Engineering* 114(1), pp. 104–121.

Baligh, M. M. (1985). "Strain Path Method". In: *Journal of Geotechnical Engineering* 111.9, pp. 1108–1136. DOI: 10.1061/(ASCE)0733-9410(1985)111:9(1108).

Bergström, A., Javed, S., and Dijkstra, J. (2021). "Field test of a floating thermal pile in sensitive clay". In: *Géotechnique* 71.4, pp. 334–345. DOI: 10.1680/jgeot.19.P.094.

Bishop, R. F., Hill, R., and Mott, N. F. (1945). "The theory of indentation and hardness tests". In: *Proceedings of the Physical Society* 57.3, pp. 147–159. DOI: 10.1088/0959-5309/57/3/301. URL: https://doi.org/10.1088/0959-5309/57/3/301.

Box, G. E. P. and Draper, N. R. (2006). *Response Surfaces, Mixtures, and Ridge Analyses*. 2nd ed. John Wiley & Sons, Inc., New Jersey, USA. ISBN: 978-0-470-05357-7.

Bozozuk, M., Fellenius, B. H., and Samson, L. (1978). "Soil disturbance from pile driving in sensitive clay". In: *Canadian Geotechnical Journal* 15(3), pp. 346–361. DOI: 10.1139/t79-048.

Bui, H. H., Fukagawa, R., Sako, K., and Ohno, S. (2008). "Lagrangian meshfree particles method (SPH) for large deformation and failure flows of geomaterial using elastic-plastic soil constitutive model". In: *International Journal for Numerical and Analytical Methods in Geomechanics*, pp. 1537–1570. DOI: 10.1002/nag.688.

Castro, J. and Karstunen, M. (2010). "Numerical simulations of stone column installation". In: *Canadian Geotechnical Journal* 47(10), pp. 1127–1138. DOI: 10.1139/T10-019.

Ceccato, F., Beuth, L., Vermeer, P., and Simonini, P. (2016). "Two-phase Material Point Method applied to the study of cone penetration". In: *Computers and Geotechnics* 80, pp. 440–452.

Cooke, R. W., Price, G., and Tarr, K. (1979). "Jacked piles in London Clay: A study of load transfer and settlement under working conditions". In: *Geotechnique* 29(2), pp. 113–147.

Crosta, G. B., Imposimato, S., and Roddeman, D. G. (2003). "Numerical modelling of large landslides stability and runout". In: *Natural Hazards and Earth System Sciences* 3.6, pp. 523–538. DOI: 10.5194/nhess-3-523-2003. URL: https://nhess.copernicus.org/articles/3/523/2003/.

Crosta, G. B., Imposimato, S., and Roddeman, D. G. (2015). "Landslide Spreading, Impulse Water Waves and Modelling of the Vajont Rockslide". In: *Rock Mechanics and Rock Engineering* 49, pp. 2413–2436.

DeJong, J. and Randolph, M. (2012). "Influence of Partial Consolidation during Cone Penetration on Estimated Soil Behavior Type and Pore Pressure Dissipation Measurements". In: *Journal of Geotechnical and Geoenvironmental Engineering* 138 (7), pp. 777–788. DOI: 10.1061/(asce)gt.1943-5606.0000646.

Dijkstra, J., Broere, W., and Heeres, O. (2011). "Numerical simulation of pile installation". In: *Computers and Geotechnics* 38, pp. 612–622.

Dugan, J. P. J. and Freed, D. L. (1984). “Ground Heave Due to Pile Driving”. In: *International Conference on Case Histories in Geotechnical Engineering* 28.

Edstam, T. (2011). “Massundanträngning i samband med pålslagning i lera”. In: *SBUF. Rapport 12133*. URL: https://www.sbuf.se/Projektsida/?project=ae303727-15fd-4a7e-a794-019f5fd4fb55.

Francescon, M. (1983). “Model pile tests in clay: Stresses and displacements due to installation and axial loading”. PhD Thesis. Univ. if Cambridge, UK.

Göteborgs Stad (2022). *Översiktsplan*. https://oversiktsplan.goteborg.se/. Accessed: 2022-06-27.

Gue, S. S. (1984). “Ground heave around driven piles in clay”. PhD Thesis. Dept. Eng. Sci., university of Oxford, UK.

Hagerty, D. and Peck, R. (1971). “Heave and lateral movements due to pile driving”. In: *Proceedings of the American Society of Civil Engineers* 97(11), pp. 1513–1532.

Hall, L., Kullingsjö, A., Alheid, P., Johansson, E., and Holmberg, G. (2020). “"Piling made less boring" - Minskad omgivningspåverkan genom samverkan”. In: *Grundläggningsdagen 2020*.

Hu, Y. and Randolph, M. (1998). “A practical numerical approach for large deformation problems in soil”. In: *International Journal for Numerical and Analytical Methods in Geomechanics* 22(5), pp. 327–350. DOI: 10.1002/(SICI)1096-9853(199805)22:5<327::AID-NAG920>3.0.CO;2-X.

Huetink, H. (1986). “On the simulation of thermo-mechanical forming processes”. PhD thesis. Universiteit Twente.

Hunt, C. E., Pestana, J. M., Bray, J. D., and Riemer, M. F. (2000). “Effect of Pile Installation on Static and Dynamic Properties of Soft Clays”. In: *Innovations and Applications in Geotechnical Site Characterization*, pp. 199–212. DOI: 10.1061/40505(285)15. eprint: https://ascelibrary.org/doi/pdf/10.1061/40505%28285%2915. URL: https://ascelibrary.org/doi/abs/10.1061/40505%28285%2915.

Isaksson, J., Yannie, J., Karlsson, M., and Dijkstra, J. (2022). “Simulation of CPT penetration in sensitive clay”. In: *Cone Penetration Testing 2022 (1st ed.)* Ed. by G. Gottardi and L. Tonni. CRC Press, pp. 480–485. DOI: https://doi.org/10.1201/9781003308829.

Jardine, R. and Potts, D. (1988). “Hutton tension leg platform foundations: Prediction of driven pile behaviour”. In: *Geotechnique* 38(2), pp. 231–252.

Karlsrud, K. (2012). “Prediction of load-displacement behaviour and capacity of axially loaded piles in clay based on analyses and interpretation of pile load results”. PhD thesis. Department of Civil, Transport Engineering, Norwegian University of Science, and Technology. ISBN: 9788247134719.

Karlsson, M., Yannie, J., and Dijkstra, J. (2019). “Modeling aging of displacement piles in natural soft clay”. In: *Journal of Geotechnical and Geoenvironmental Engineering* 145.10, p. 04019070.

Karlsson, M., Emdal, A., and Dijkstra, J. (2016). “Consequences of sample disturbance when predicting long-term settlements in soft clay”. In: *Canadian Geotechnical Journal* 53.12, pp. 1965–1977. DOI: 10.1139/cgj-2016-0129.

Karstunen, M. and Amavasai, A. (2017). *BEST SOIL: Soft soil modelling and parameter determination*. CHALMERS UNIVERSITY OF TECHNOLOGY. ISBN: 978-91-984301-0-3.

Koskinen, M., Karstunen, M., and Wheeler, S. (2002). “Modelling destructuration and anisotropy of a natural soft clay”. In: *NUMGE 2002 : 5th European Conference on Numerical Methods*

in Geotechnical Engineering (NUMGE 2002). Ed. by P. Mestat. Presses de l'ENPC, Paris, pp. 11–22. DOI: https://doi.org/10.1201/9781003308829.

Lehane, B. and Gill, D. (2004). "Displacement fields induced by penetrometer installation in an artificial soil". In: *International Journal of Physical Modelling in Geotechnics* 4, pp. 25–36. DOI: 10.1680/ijpmg.2004.040103.

Lehane, B. and Jardine, R. (1994). "Displacement pile behaviour in glacial clay". In: *Canadian Geotechnical Journal* 31, pp. 79–90.

Liyanapathirana, D. S. (2009). "Arbitrary Lagrangian Eulerian based finite element analysis of cone penetration in soft clay". In: *Computers and Geotechnics* 36(5), pp. 854–860. DOI: 10.1016/j.compgeo.2009.01.006.

Mahmoodzadeh, H. and Randolph, M. (2014). "Penetrometer Testing: Effect of Partial Consolidation on Subsequent Dissipation Response". In: *Journal of Geotechnical and Geoenvironmental Engineering* 140(6), p. 04014022.

Mahmoodzadeh, H., Randolph, M., and Wang, D. (2014). "Numerical simulation of piezocone dissipation test in clays". In: *Geotéchniqe* 64 (8), pp. 657–666. DOI: 10.1680/geot.14.P.011.

Massarsch, K. R. (1976). "Soil Movements Caused by Pile Driving in Clay". Thesis in partial fulfillment of the requirements for the Degree Doctor of Engineering. Dept. Soil and Rock Mechanics, Royal Institute of Technology (KTH), Stockholm, Job-Rapport No 6, 261 p.

Massarsch, K. R. and Wersäll, C. (2013). "Cumulative Lateral Soil Displacement Due to Pile Driving in Soft Clay". In: *Sound Geotechnical Research to Practice*. Ed. by A. W. Stuedlein and B. R. Christopher. ASCE, pp. 462–479. DOI: 10.1061/9780784412770.031.

Monforte, L., Gens, A., Arroyo, M., Mánica, M., and Carbonell, J. (2021). "Analysis of cone penetration in brittle liquefiable soils". In: *Computers and Geotechnics* 134, p. 104123.

Nazem, M., Sheng, D., and Carter, J. P. (2006). "Stress integration and mesh refinement for large deformation in geomechanics". In: *International Journal for Numerical Methods in Engineering* 65, pp. 1002–1027. DOI: 10.1002/nme.1470.

Ni, Q., Hird, C., and Guymer, I. (2010). "Physical modelling of pile penetration in clay using transparent soil and particle image velocimetry". In: *Géotechnique* 60.2, pp. 121–132. DOI: 10.1680/geot.8.P.052.

Pålkommisionen (2022). *Pålstatistik for Sverige 2021*. http://www.palkommissionen.org/. Accessed: 2022-06-27.

Pestana, J. M., Hunt, C. E., and Bray, J. D. (2002). "Soil deformation and excess pore pressure field around a closed-ended pile". In: *Journal of Geotechnical and Geoenvironmental Engineering* 128.1, pp. 1–12. DOI: 10.1061/(ASCE)1090-0241(2003)129:7(669).

Phoon, K.-K. and Kulhawy, F. H. (1999). "Characterization of geotechnical variability". In: *Canadian Geotechnical Journal* 36(4), pp. 612–624.

Pucker, T. and Grabe, J. (2012). "Numerical simulation of the installation process of full displacement piles". In: *Computers and Geotechnics* 45, pp. 93–106. DOI: 10.1016/j.compgeo.2012.05.006.

Randolph, M. and Gouvernec, S. (2011). *Cavity Expansion Methods in Geomechanics*. Spon Press, USA. ISBN: 9780415477444. URL: https%20://books.google.se/books?id=qI8xPQAACAAJ.

Randolph, M., Steenfelt, J. S., and P., W. C. (1979). "The effect of pile type on design parameters for driven piles". In: *Proceedings VII ECSMFE 1979, Brighton,* 2, pp. 107–114.

Rehkopf, J. C. (2001). “PREDICTION AND MEASUREMENT OF GROUND MOVEMENTS DUE TO PILE DRIVING IN CLAY: A CASE STUDY IN EAST BOSTON”. matheses. Civil and environmental engineering, Massachusetts Institute of Technology.

Robertson, P. (1990). “Soil classification using the cone penetration test”. In: *Canadian Geotechnical Journal* 27, pp. 151–158. DOI: 10.1139/t90-014.

Roddeman, D. G. (2022). *TOCHNOG PROFESSIONAL User’s manual, June 22*. https://www.tochnogprofessior Accessed: 2022-06-23.

Roy, M., Blanchet, R., Tavenas, F., and La Rochelle, P. (1981). “Behaviour of a sensitive clay during pile driving.” In: *Canadian Geotechnical Journal* 18, pp. 67–85.

Sagaseta, C. and Whittle, A. (2001). “Prediction of ground movements due to pile driving in clay”. In: *Journal of Geotechnical and Geoenvironmental Engineering* 127.1, pp. 55–66. DOI: https://doi.org/10.1061/(ASCE)1090-0241(2001)127:1(55).

Sagaseta, C., Whittle, A., and Santagata, M. (1997). “Deformation analysis of shallow penetration in clay”. In: *International Journal for Numerical and Analytical Methods in Geomechanics* 21.10, pp. 687–719. DOI: 10.1002/(SICI)1096-9853(199710)21:10<687::AID-NAG897>3.0.CO;2-3.

Schneider, J., Lehane, B., and Schnaid, F. (2007). “Velocity effects on Piezocone measurements in normally and over consolidated clays”. In: *International Journal of Physical Modelling in Geotechnics* 7, pp. 23–34.

Schneider, J., Randolph, M., Mayne, P., and Ramsey, N. (2008). “Analysis of Factors Influencing Soil Classification Using Normalized Piezocone Tip Resistance and Pore Pressure Parameters”. In: *Journal of Geotechnical and Geoenvironmental Engineering* 134(11), pp. 1569–1586. DOI: 10.1061/(asce)1090-0241(2008)134:11(1569).

Sheil, B. B., McCabe, B. A., Hunt, C. E., and Pestana, J. M. (2015). “A practical approach for the consideration of single pile and pile group installation effects in clay: Numerical modelling”. In: *Journal of Geo-Engineering Sciences* 2, pp. 119–142. DOI: 10.3233/jgs-140027.

Tahershamsi, H. and Dijkstra, J. (2022). “Using Experimental Design to assess rate-dependent numerical models”. In: *Under review at Soils and Foundations*.

Trafikkontoret, G. S. (2021). “Hisingsbron, Projektsamarbete i samband med byggande i anslutning till Götaälvbron”. In: URL: https://stadsutveckling.goteborg.se/siteassets/hb-erfarenhetsrapport----version-a.pdf5.

van den Berg, P. (1994). “Analysis of soil penetration”. PhD Thesis. Delft University, Netherlands.

Vytiniotis, A., Casey, B., and Sykora, D. W. (2018). “Lateral Soil Movements Due to Pile Driving: A Case Study in Soft Clays”. In: *IFCEE 2018*, pp. 113–128. DOI: 10.1061/9780784481622.010.

Yu, H. (2000). *Cavity Expansion Methods in Geomechanics*. Springer, Netherlands. ISBN: 9780412799907. URL: https://books.google.se/books?id=Qp3RMF1h9NUC.

Part I
Appended Paper A

Paper A

Simulation of CPT penetration in sensitive clay

Cone Penetration Testing 2022 – Gottardi & Tonni (eds)

Simulation of CPT penetration in sensitive clay

J. Isaksson
Chalmers University of Technology, Sweden
NCC AB, Sweden

J. Yannie
NCC AB, Sweden

M. Karlsson & J. Dijkstra
Department of Architecture and Civil Engineering, Chalmers University of Technology, Sweden

ABSTRACT: This paper presents the results from numerical simulations of CPTu penetration in a natural clay combining the SCLAY1S constitutive model with a large deformation Finite Element framework including a coupled deformation and porewater pressure formulation. The hierarchical model formulation of SCLAY1S captures many features of a natural sensitive clay, such as the evolving anisotropic strength-stiffness response, as well as the degradation of the initial bonding. A sensitivity analysis is performed varying the overconsolidation ratio (*QCR*), bonding and anisotropy, also the hydraulic conductivity (hence, c_v) of the clay. The findings indicate that some soil properties (the c_v and *OCR*) impact both the normalised cone resistance Q_t and the generation of excess porewater pressures. In contrast the sensitivity S_t of soft soils primarily affects Q_t. In the current work it seems that the effects of the inherent and stress induced (from CPT penetration) anisotropy is not detected using these normalised plots.

1 INTRODUCTION

The cone penetration test is a widely used method to perform geotechnical site investigation, by continuous measuring of the cone resistance, the sleeve friction, and in case of the piezocone (CPTu) the generated excess porewater pressures, during the penetration into a soil. This allows the mapping of a deposit to be performed in a time-effective manner with a high resolution (Lunne et al. 1997). Further soil characterisation can be performed using classification systems based on statistical correlations of normalised CPTu results against borehole data, see e.g. Robertson (2016) and Schneider et al. (2008). Due to the continuous measurement of the soil response, the CPTu is a great tool to detect differences in the response between and within soil layers by relying on a contrast in hydro-mechanical properties, e.g a change in hydraulic conductivity, overconsolidation ratio or sensitivity (brittleness).

Another approach to establish the relation between soil properties and CPTu response is to use numerical modelling where a prescribed change of a model parameter of a given constitutive model leads to a change in CPTu response. This approach is becoming increasingly more attainable with the ongoing developments for numerical analyses. Three modelling aspects that are necessary for accurate simulation of CPTu penetration are (i) the capability of the Finite Element (FE) code to deal with large deformations (ii) the adequate coupling of deformations and the generation/dissipation of excess porewater pressures (iii) a constitutive model that incorporates the complex features of natural soils.

A number of numerical methods able to simulate the kinematics of CPTu penetration in FE have been reported, among others the Arbitrary Lagrangian Eulerian method (Berg et al. 1996, Walker & Yu 2006), Material Point Method (Ceccato et al. 2016), Geotechnical Particle Finite Element Method (Hauser & Schweiger 2021, Monforte et al. 2021), and remeshing procedures (Hu & Randolph 1998, Orazalin & Whittle 2018, Mahmoodzadeh et al. 2014). In some cases the effects of CPT penetration are captured in an Updated Lagrangian framework (Yi et al. 2012, Konkol & Bałachowski 2018, Mahmoodzadeh et al. 2014).

Some of the studies (Ceccato et al. 2016, Monforte et al. 2021, Yi et al. 2012, Konkol & Bałachowski 2018, Mahmoodzadeh et al. 2014, Orazalin & Whittle 2018) also incorporates a coupled stress formulation enabling the study of partial drainage during penetration. Constitutive models able to describe advanced soil features such as brittleness (Monforte et al. 2021) and anisotropy (Hauser & Schweiger 2021, Orazalin & Whittle 2018) has also been incorporated to simulate CPTu penetration.

DOI: 10.1201/9781003308829-67

This paper builds upon those previous studies by implementing SCLAY1S in a fully coupled Eulerian Finite Element (FE) framework. Subsequently, the relation between the CPTu response and different soil properties is investigated. The model parameters varied, include the hydraulic conductivity (k), the sensitivity of the soil (S_t), the fabric anisotropy and the overconsolidation ratio (OCR).

2 NUMERICAL MODEL

Natural features of soft clay, such as breakage of initial bonding and fabric anisotropy, are captured by the SCLAY1S constitutive model (Koskinen et al. 2002) and (Karstunen et al. 2005). The elasto-plastic model originates from the Modified Cam Clay (MCC) constitutive model (Roscoe & Burland 1968), in addition to the volumetric hardening of MCC, SCLAY1S also incorporates rotational hardening and gradual degradation of bonding due to plastic strains in the soil. In short, the evolution of the initial anisotropy and degradation of strength is controlled by volumetric plastic strains and deviatoric plastic strains in the hardening law. The model is hiearchical, i.e. an appropriate choice of model parameters leads to the (de-) activation of the model features that capture (evolution of) anisotropy and destructuration. Hence, in its simplest form the model formulation becomes identical to MCC.

For the current work, the SCLAY1S model was implemented in the Tochnog Professional (Roddeman 2021) finite element framework that is able to handle large deformations by using an Eulerian description with a fixed mesh, where the solution fields for the stress, material velocity and other state variables of the calculation are advected through the domain. Penetration of the CPTu into the soil is performed with the moving boundary method proposed by Dijkstra et al. (2011). Initially, the cone is considered to be outside of the calculation domain, i.e. above the soil surface, and the desired stress state and other state variables required for the model are prescribed to establish the initial state in the model. The numerical penetration is then performed by defining a geometric entity representing the CPTu and prescribing the penetration velocity v to all nodes in this geometry while simultaneously expanding the geometry downwards with the same penetration velocity.

The axisymmetric nature of the problem is exploited using a 2D simplification where the horizontal soil movement and groundwater flow is prevented perpendicular to the axis of symmetry. The geometry and boundary conditions of the numerical model are presented in Figure 1. The initial stress state is prescribed by the vertical effective stress (σ_v'), initial porewater pressure (u_0) and the initial earth pressure coefficient (K_0). Horizontal movement is prevented at the far right boundary while keeping the porewater pressure constant to u_0, hence allowing for groundwater flow across the boundary. At the bottom boundary, vertical groundwater flow and soil movement is prevented. The top boundary of the domain is modelled with a prescribed vertical load that is in equilibrium with the total vertical stress (σ_v) and is equal to the sum of σ_v' and the initial porewater pressure u_0. The increase in stress due to the weight of the soil in the domain is set to be zero to create a uniform soil domain.

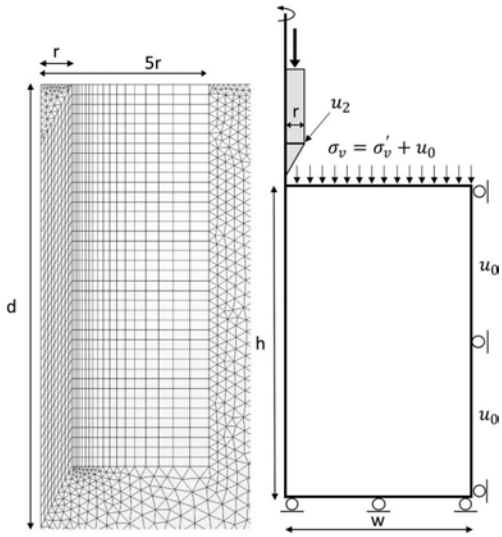

Figure 1. Boundary conditions and mesh in the region close to the penetrating CPTu.

All simulations presented in the study were performed using a 60 cone with a diameter (d) of 0.036 m corresponding to a radius (r) of 0.018 m. The height of the domain h was set to two times the penetration depth and the width w was set to $40r$, to prevent numerical disturbance related to boundary effects. A structured quadrilateral mesh (see Figure 1) was required in the location of the penetrating cone to ensure geometrical compatibility between the mesh and the penetrating cone that is prescribed with a geometry entity. Quadrilateral elements were used in a region extending 5 cone radii (r) from the axis of symmetry. The rest of the domain is filled with unstructured triangular elements. In total, the model contains 1789 quadrilateral elements and 3579 triangular, both with first order shape functions. All simulations in this paper were performed with a penetration rate v of 0.02 m/s down to a final penetration depth of $20d$. The porewater pressure presented in this study was extracted from a position right above the cone shoulder corresponding to the u_2 position. The cone resistance q_c was calculated from the total force needed to push the inclined cone tip downwards divided by the area of the cone. The net

cone resistance q_{net} was calculated by subtracting the initial vertical stress σ_{v0} from the cone resistance q_c.

Table 1. Model parameters used to investigate the effect of drainage conditions on the CPTu response.

Symbol	Parameter	Value
σ_v'	Vertical effective stress [kPa]	109
u_0	Initial porewater pressure [kPa]	70
$K0$	Initial earth pressure coefficient [-]	0.61
OCR	Overconsolidation ratio [-]	1.02
e_0	Initial void ratio [-]	1.41
λ	Virgin compression index [-]	0.205
κ	Swelling/recompression index [-]	0.044
ν	Poisson's ratio	0.3
M	Slope of CSL line [-]	0.9
χ_0	Initial amount of bonding [-]	0
a	Rate of destructuration [-]	0
b	Rate of destructuration due to to deviator strain [-]	0
α_0	Initial anisotropy [-]	0
ω	Rate of rotation [-]	0
ω_d	Rate of rotation due to deviator strain [-]	0

3 VARIATION OF HYDRAULIC CONDUCTIVITY

Initially, the effect of the drainage conditions on the CPTu response was studied using a MCC model formulation, by varying the hydraulic conductivity k in the range 5.510^{-3} m/s and 1.110^{-8} m/s. An isotropic hydraulic conductivity was used in all performed simulations. All the model parameters used in the numerical study are presented in Table 1 and are based on those derived for kaolin clay, as used for the numerical studies of the CPTu in Mahmoodzadeh et al. (2014). The normalised penetration velocity V is used to define the current drainage conditions for quasi-static penetration problems, as it enables the comparison between various test conditions. V is defined as:

$$V = \frac{vd}{c_v} \tag{1}$$

where v is the penetration rate, d is the diameter of the CPT cone and c_v is the vertical consolidation coefficient of the soil.

$$c_v = \frac{k_v(1+e_0)\sigma'_{v0}}{\lambda\gamma_w} \tag{2}$$

The normalised penetration velocity helps to correct for experimental scaling conditions by linking the penetration velocity and size of the object and soil volume (drainage lengths) to the properties of the soil such as the vertical effective stress σ'_{v0}, initial void ratio e_0, stiffness λ and the hydraulic conductivity (via the vertical consolidation coefficient c_v).

DeJong & Randolph (2012) proposed a backbone curve of both the net cone resistance and excess porewater pressure normalised with the corresponding undrained value based on the result from seven different studies investigating the change in response for the CPTu under different drainage conditions and confining stress p. Mahmoodzadeh & Randolph (2014) also proposed a backbone curve based on a series of centrifuge test of CPTu penetration in kaolin clay. The net cone resistances are normalised with the results from the undrained penetration simulation and are presented in Figure 2. Whereas, the results for the normalised excess porewater pressure are presented in Figure 3. Both figures also show the two proposed backbone curves.

The transition of the simulated net cone resistance from the undrained to the intermediate and drained state are in good agreement with both backbone curves. The relative magnitude of the net cone resistance in the drained state, however, is considerably larger when compared to the proposed backbone curves. As this study is with equal strength in the soil as in the element near the interface, the contact between the CPTu and the soil can be considered rough. Monforte et al. (2021) performed an additional sensitivity study on the impact of the interface roughness on the CPTu simulations. The normalised net cone resistance for the rough interface (ϕ = 19) increased with about 40 % from the smooth interface (included in Figure 2). In contrast, the normalised excess porewater pressure response is not greatly affected by the interface formulation. Looking at Figure 2 the results from this study fit in between the smooth and the rough interface response reported by Monforte et al. (2021).

The normalised excess porewater pressure from this study is slightly shifted compared to the other studies (Figure 3). This is due to the presence of some numerically locked-in porewater pressures in a single element near the cone shoulder, i.e. at the u_2 position and is most prominent for very low hydraulic conductivities corresponding to a practically undrained state with normalised penetration velocities above 50. The porewater pressure presented herein, are unsmoothed and taken from the u_2 position and is considered to be accurate when looking at the relative change in response between the analyses in the sensitivity study.

4 CPTU IN SOFT CLAYS

The numerical investigation into the impact of soil properties on the CPTu penetration in soft (sensitive) clays was performed starting from a normally consolidated and isotropic reference state without

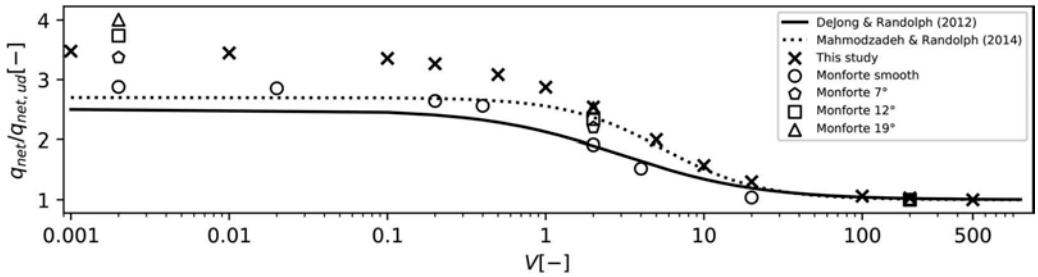

Figure 2. Normalised cone resistance over normalised penetration rate. Comparison between results from this study and Mahmoodzadeh & Randolph (2014) and DeJong & Randolph (2012). Results from Monforte et al. (2021) is included to indicate the effect of interface properties on the CPTu response.

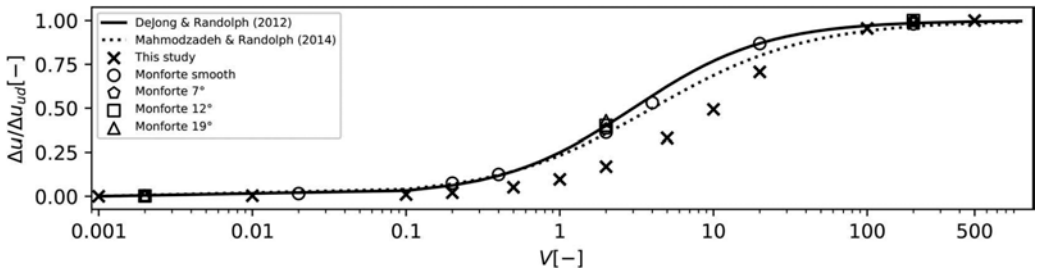

Figure 3. Normalised excess porewater pressure over normalised penetration rate. Comparison between results from this study and Mahmoodzadeh & Randolph (2014) and DeJong & Randolph (2012). Results from Monforte et al. (2021) is included to indicate the effect of interface properties on the CPTu response.

Table 2. Parameters used for investigation of the CPTu response in soft clays.

Symbol	Parameter	Value
OCR	Overconsolidation ratio [-]	1.2, 1,5, 1,8
χ_0	Initial amount of bonding [-]	2, 5, 10, 20, 50
a	Rate of destructuration [-]	6
b	Rate of destructuration due to deviator strain [-]	0.4
α_0	Initial anisotropy [-]	0.352
ω	Rate of rotation [-]	10
ω_d	Rate of rotation due to deviator strain [-]	0.374

initial bonding, using a normalised penetration velocity of V= 200 for the CPTu. First, the impact of OCR on the soil response was investigated by increasing the OCR in three increments from 1.02 to 1.8. The brittleness of the soil was also investigated by varying the SCLAY1S state parameter for destructuration χ_0 between 0 (no initial structure) and 50 (clay with a high sensitivity). Although this parameter is closely related to the sensitivity of the soil it should not be considered to be similar. Finally, the impact of fabric anisotropy on the CPTu response was studied by introducing an initially inclined yield surface, that evolves with deviatoric and volumetric strains, in the model formulation. Table 2 presents the range of the SCLAY1S parameters used. The rate parameters and anisotropy α_0 are assumed based on Gras et al. (2017) for natural clays, whilst keeping the original parameters from the kaolin clay. This ensures consistency of model parameters between simulations. Although this approach captures the soft soil features found in natural clays, the dataset does not represent a natural clay deposit.

Robertson (1990) proposed a classification system based on the normalised cone resistance Q_t and pore pressure ratio B_q, where

$$Q_t = \frac{q_{net}}{\sigma'_{v0}} \tag{3}$$

$$B_q = \frac{\Delta u}{q_{net}} \tag{4}$$

The Q_t is the relation between the net cone resistance from the CPTu measurements and the initial effective vertical stress. B_q is the excess porewater

pressure divided by the net cone resistance. This classification system is shown in Figure 4 with the results from the present numerical study. The arrows that annotate the data points correspond to each model parameter and are showing the direction of the normalised CPT response when the parameter is increased in the numerical analysis. Distinct trends for each parameter are clearly identified and are in good agreement with trends proposed by Robertson (1990), for both S_t and OCR.

The numerical results are also presented in the classification chart (Figure 5) originally proposed by Schneider et al. (2008), which is based on Q_t and the excess porewater pressure (Δu) normalised with the initial vertical effective stress (σ'_{v0}). The impact of changing S_t, OCR and c_v indicates clear trends that are in good agreement with the response suggested by Schneider et al. (2008). The effect of fabric anisotropy α only shows limited impact on the results. The results only slightly changed, due to the lower Q_t and excess porewater pressures when compared to the isotropic model results.

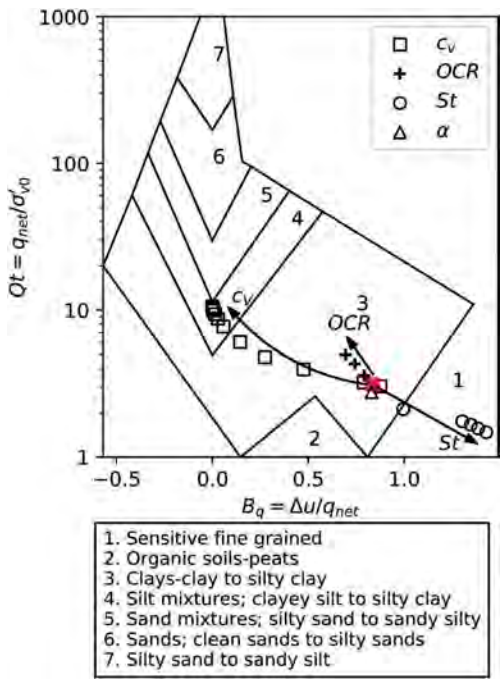

Figure 4. The effect on CPTu response from changing the consolidation coefficient c_v; overconsolidation ratio OCR; sensitivity S_t and considering fabric anisotropy α in the characterisation chart for CPTu proposed by Robertson (1990).

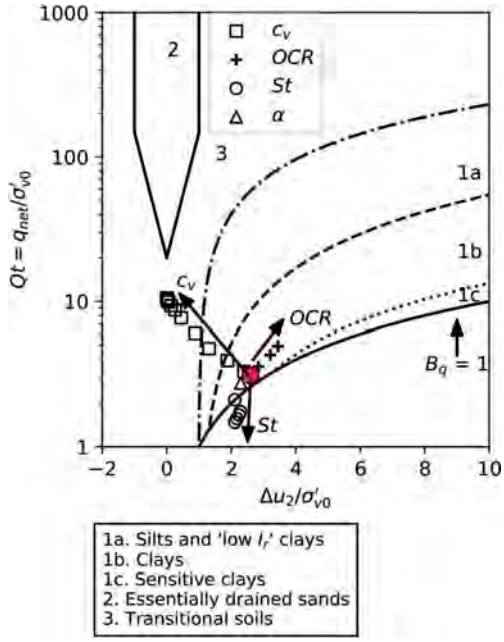

Figure 5. The effect on CPTu response from changing consolidation coefficient c_v; overconsolidation ratio OCR; sensitivity S_t and considering fabric anisotropy α in the charaterisation chart for CPTu proposed by Schneider et al. (2008).

5 CONCLUSIONS

This paper presents the results from a series of CPTu simulations using a large deformation Finite Element framework in which partial consolidation during penetration is considered by linking the material deformations to the coupled response of porewater flow. An Eulerian framework, in which the mesh is fixed and the soil is able to move independently of the mesh, has been used, to avoid mesh distortions from large deformations associated with the CPTu penetration. The SCLAY1S model is implemented for these analyses, as it captures the evolving anisotropic strength-stiffness response, as well as the degradation of the initial bonding present in natural sensitive clays.

In the first part of the paper the effect of different drainage conditions is quantified and the overall trend compares well with prior work. Further studies need, however, to be conducted to improve the accuracy of the calculated porewater pressures at the shoulder of the CPTu. Extending the study to also include the response on the friction sleeve of the CPTu could further expand the conclusions of this study.

The impact of features that are fundamental to soft soils, i.e. hydraulic conductivity, OCR, sensitiv-

ity and anisotropy, on the CPTu response have been investigated in a hierarchical manner. The following can be concluded after integrating the results in the CPTu classification charts:

- Increasing the hydraulic conductivity leads to an increase in normalised penetration resistance while the normalised excess porewater pressure is decreasing.
- Increasing the OCR is associated with an increase in both the normalised cone resistance and the normalised excess porewater pressure.
- Increasing S_t leads to a considerable decrease in the normalised cone resistance while leaving the normalised excess porewater pressure nearly unaffected
- The simulated CPTu response is practically unaffected by soil anisotropy.

The conclusions of this study are in good agreement with suggestions from Robertson (1990) and Schneider et al. (2008) for the anticipated response from a change in c_v, OCR and S_t. Hence, the results of this study contribute to the interpretation of the widely used classification charts, by linking it to the fundamental features of natural soils.

The extensive empirical evidence used to establish the relation between CPT and soil characteristics is in good agreement with the numerical results, increasing the confidence in the ability to accurately simulate penetration into soft soils with the proposed numerical method. Finally, the numerical simulations should be validated further against in-situ CPTu data.

ACKNOWLEDGEMENTS

The authors acknowledge the financial support provided by SBUF (Development fund of the Swedish construction industry, grant 13614) and BIG (Better Interaction in Geotechnics, grant A2019-19, from the Swedish Transport Administration)

REFERENCES

Berg, P., R. Borst, & H. Huétnik (1996). An eulerean finite element model for penetration in layered soil. *International Journal for Numerical and Anaylytical Methods in Geomechanics 20*, 865–886.

Ceccato, F., L. Beuth, P. Vermeer, & P. Simonini (2016). Two-phase material point method applied to the study of cone penetration. *Computers and Geotechnics 80*, 440–452.

DeJong, J. & M. Randolph (2012). Influence of partial consolidation during cone penetration on estimated soil behavior type and pore pressure dissipation measurements. *Journal of Geotechnical and Geoenvironmental Engineering 138 (7)*, 777–788.

Dijkstra, J., W. Broere, & O. Heeres (2011). Numerical simulation of pile installation. *Computers and Geotechnics 38*, 612–622.

Gras, J., N. Sivasithamparam, M. Karstunen, & J. Dijkstra (2017). Strategy for consistent model parameter calibration for soft soils using multi-objective optimisation. *Computers and Geotechnics 90*, 164–175.

Hauser, L. & H. Schweiger (2021). Numerical study on undrained cone penetration in structured soil using g-pfem. *Computers and Geotechnics 133*, 104061.

Hu, Y. & M. Randolph (1998). A practical numerical approach for large deformation problems in soil. *International Journal for Numerical and Analytical Methods in Geomechanics 22*, 327–350.

Karstunen, M., H. Krenn, S. Wheeler, M. Koskinen, & R. Zentar (2005). Effect of anisotropy and destructuration on the behavior of murro test embankment. *International Journal of Geomechanics 5(2)*, 87–97.

Konkol, J. & L. Baachowski (2018). Large deformation modelling of cpt probing in soft soil—pore water pressure analysis. In M. A. Hicks, F. Pisanò, and J. Peuchen (Eds.), *Proceedings of the 4th International Symposium on Cone Penetration Testing (CPT'18)*, London, pp. 371–376. CRC Press.

Koskinen, M., M. Karstunen, & S. Wheeler (2002). Modelling destructuration and anisotropy of a natural soft clay. In Mestat (Ed.), *Proc., 5th European Conf. Numerical Methods in Geotechnical Engineering*, Paris, pp. 11–20. Presses de l'ENPC/LCPC.

Lunne, T., P. Robertson, & J. Powell (1997). *Cone penetration testing in geotechnical practice*. New York: E & FN Spon/ Routledge.

Mahmoodzadeh, H. & M. Randolph (2014). Penetrometer testing: Effect of partial consolidation on subsequent dissipation response. *Journal of Geotechnical and Geoenvironmental Engineering 140 (6)*, 04014022.

Mahmoodzadeh, H., M. Randolph, & D. Wang (2014). Numerical simulation of piezocone dissipation test in clays. *Geotéchniqe 64 (8)*, 657–666.

Monforte, L., A. Gens, M. Arroyo, M. Mánica, & J. Carbonell (2021). Analysis of cone penetration in brittle liquefiable soils. *Computers and Geotechnics 134*, 104123.

Orazalin, Z. & A. Whittle (2018). Realistic numerical simulations of cone penetration with advanced soil models. In M. A. Hicks, F. Pisanò, and J. Peuchen (Eds.), *Proceedings of the 4th International Symposium on Cone Penetration Testing (CPT'18)*, London, pp. 483–489. CRC Press.

Robertson, P. (1990). Soil classification using the cone penetration test. *Canadian Geotechnical Journal 27*, 151–158.

Robertson, P. (2016). Cone penetration test (cpt)-based soil behaviour type (sbt) classification system — an update. *Canadian Geotechnical Journal 53*, 1910–1927.

Roddeman, D. (2021). Tochnog professional user's manual, october 21. https://www.tochnogprofessional.nl/manuals/user/user.pdf. Accessed: 2021- 10-21.

Roscoe, K. & J. Burland (1968). On the generalized stress-strain behaviour of wet clay. In *Engineering plasticity*, Cambridge Univ. Press, Cambridge U.K., pp. 553–609.

Schneider, J., M. Randolph, P. Mayne, & N. Ramsey (2008). Analysis of factors influencing soil classification using normalized piezocone tip resistance and pore pressure parameters. *Journal of Geotechnical and Geoenvironmental Engineering 134(11)*, 1569–1586.

Walker, J. & H. S. Yu (2006). Adaptive finite element analysis of cone penetration in clay. *Acta Geotechnica 1*, 43–57.

Yi, J. T., S. H. Goh, F. Lee, & M. Randolph (2012). A numerical study of cone penetration in fine-grained soils allowing for consolidation effects. *Geotéchniqe 62 (8)*, 707–719.